

ADAPTIVE CONTROL STRATEGIES FOR
LOWER-LIMB EXOSKELETONS TO ASSIST GAIT

By Safoura Sadegh Pour Aji Bishe

A Dissertation

Submitted in Partial Fulfillment
of the Requirements for the Degree of
Doctor of Philosophy
in Bioengineering

Northern Arizona University

December 2021

Approved:

Zachary F. Lerner, Ph.D., Chair

Kiisa Nishikawa, Ph.D.

Tarang Kumar Jain, Ph.D.

Kyle Winfree, Ph.D.

ABSTRACT

ADAPTIVE CONTROL STRATEGIES FOR LOWER-LIMB EXOSKELETONS TO ASSIST GAIT

SAFOURA SADEGH POUR AJI BISHE

Walking is a critical mode of transportation during everyday life. As a result, gait impairments can greatly affect the quality of life and personal independence of those who are affected. About 15% of people in the world have some type of physical disability, and that population is increasing rapidly. One type of disability that refers to a group of conditions that affect movement control is Cerebral Palsy (CP). Exoskeletons may help patients with CP extend their lower limb joints during walking by providing assistance and helping them walk more efficiently. Alternatively, the strategy of this assistance may vary depending on the type and severity of crouch gait.

In this dissertation, we worked on four different adaptive control strategies for lower-limb exoskeletons capable of providing assistance during walking on different terrains for unimpaired individuals and individuals with CP. In the first chapter of this doctoral dissertation, we describe an adaptive control strategy development of a light-weight ankle exoskeleton based on the biomechanics of walking and how the ankle plantarflexion assistance provided based on this strategy improved the walking performance of unimpaired individuals and individuals with CP. The second chapter describes the development of a user-adaptive control strategy of a light-weight hip exoskeleton. Then the assistance provided by this control strategy is evaluated on unimpaired individuals during level and incline treadmill, as well as one individual with CP walking during level treadmill walking. In chapter three, we describe the development of a coordinated ankle-knee control strategy of a lightweight unilateral ankle-knee exoskeleton based on the biomechanics of

walking and validation of this control strategy on an unimpaired individual. The fourth chapter describes a bioinspired ankle joint torque simulation method based on the Winding Filament Muscle model with the potential to control the ankle joint of commercialized exoskeletons. A conclusion of these four control strategies is provided in the final chapter of this doctoral dissertation.

Acknowledgments

This project would not have been possible without the support of many people. Many thanks to my adviser, Dr. Zachary Lerner, for his patience, guidance, and mentorship. Also, thanks to my dissertation committee members, Dr. Kiisa Nishikawa, Dr. Tarang Jain, and Dr. Kyle Winfree, for their advice and wisdom.

Dr. Kiisa Nishikawa not only advised on the technical aspect of this project, she provided much needed moral support throughout this journey. I gratefully recognize the help of Ying Fang, Leah Liebelt, and other members of the Biomechatronics lab at NAU, who provide me valuable input during the course of this study.

I am grateful for my parents, whose constant love and encouragement kept me motivated and confident. Finally, I owe my deepest gratitude to Omid, who is my love. I am forever thankful for the unconditional love and support throughout the entire dissertation process and every day.

Table of Contents

ABSTRACT	ii
Acknowledgments.....	iv
Table of Contents	v
List of Tables	vii
List of Figures	viii
I. Adaptive Ankle Exoskeleton Control: Validation Across Diverse Walking	
Conditions	1
I.1. Introduction	1
I.2. Methods.....	3
I. 2. 1. Motivation.....	3
I. 2. 2. Ankle moment estimation model.....	7
I. 2. 3. Ground reaction force estimation	10
I. 2. 4. Closed-loop control algorithm	11
I. 2. 5. Electromechanical exoskeleton system	12
I. 2. 6. Validating design overview	14
I. 2. 7. Protocol for exoskeleton controller validation.....	15
I. 2. 8. Clinical feasibility analysis.....	17
I. 2. 9. Data processing.....	17
I. 2. 10. Simulated open-loop controller comparison	19
I.3. Results	20
I. 3. 1. Controller validation with unimpaired.....	20
I. 3. 2. Comparison to the simulated open-loop controller.....	25
I. 3. 3. Clinical feasibility testing outcomes.....	26
I.4. Discussion	27
I.5. Conclusion.....	34
II. A Low-Profile Hip Exoskeleton for Pathological Gait Assistance: Design and Pilot Testing	
Testing	36
II.1. Introduction	36
II.2. Methods.....	39
II. 2. 1. Electro-Mechanical Design.....	39

II. 2. 2.	Control Overview and Theory	42
II. 2. 3.	High-Level Controller Validation	44
II. 2. 4.	Low-Level Controller Validation.....	44
II. 2. 5.	Unimpaired Walking Performance Validation.....	44
II. 2. 6.	Unimpaired Walking Performance Validation.....	45
II. 2. 7.	Data Processing	48
II.3.	Results	49
II. 3. 1.	High-Level Controller Validation	49
II. 3. 2.	Low-Level Controller Validation.....	49
II. 3. 3.	Walking Performance Outcomes	51
II.4.	Discussion	51
III.	Developing a Synergistic Control Strategy for Knee and Ankle Exoskeleton Assistance	55
III.1.	Introduction	55
III.2.	Method.....	57
III. 2. 1.	Ground Reaction Forces.....	57
III. 2. 2.	Ankle Moment Estimation	59
III. 2. 3.	Knee Moment Estimation	61
III. 2. 4.	Experiment Design.....	64
III. 2. 5.	Experiment Design.....	64
III.1.	Results and Discussion.....	66
IV.	Simulating Ankle Torque during Walking Using a new Bioinspired Muscle Model with Application for Controlling a Powered Exoskeleton.....	70
IV.1.	Introduction	70
IV.2.	Method.....	71
IV. 2. 1.	The Winding Filament Muscle Model	72
IV. 2. 2.	Model Configuration and Implementation.....	76
IV.3.	Result and Discussion.....	77
V.	Conclusions and Future Work	79

List of Tables

Table 1. CONTRIBUTION OF THE NORMAL GRF TO THE BIOLOGICAL ANKLE MOMENT DURING INCLINE AND DECLINE WALKING	7
Table 2. PARTICIPANT INFORMATION	13
Table 3. DETAILED RESULTS OF PRESCRIBED AND MEASURED TORQUE PROFILES	14
Table 4. POST-HOC COMPARISON BETWEEN OUR CLOSED-LOOP CONTROLLER AND THE ADAPTIVE OPEN-LOOP (FEED-FORWARD) CONTROLLER	21
Table 5. CLINICAL FEASIBILITY TESTING RESULTS	27
Table 6. UNEVEN TERRAIN TESTING RESULTS.....	35
Table 7. PARTICIPANT INFORMATION	40
Table 8. HIGH-LEVEL CONTROLLER ACCURACY.....	49
Table 9. COORDINATED CONTROLLER ACCURACY.....	68
Table 10. WFM MODE PARAMETERS, USING PARTICLE SWARM OPTIMIZATION	76
Table 11. THE ROOT MEAN SQUARE ERROR BETWEEN BIOLOGICAL MOMENT AND WFM.....	77

List of Figures

Figure 1. Ankle moment estimation approach and assumptions. A) Schematic depicting ankle moment contributions, primary regions of foot contact, and model assumptions. B) Plot showing the contributions to the biological ankle moment.....	4
Figure 2. Scatter plot reporting the relationship between the moment produced by the forefoot normal force and the total biological ankle moment.	5
Figure 3. Contribution of normal and tangential ground reaction forces to the biological ankle moment during incline and decline walking at 15°.	8
Figure 4. Overview of the closed-loop control system. A) Schematic depicting the custom embedded foot sensor design used for estimating the biological ankle moment and prescribing proportional exoskeleton torque. B) Schematic of the real-time exoskeleton control loop.....	11
Figure 5. Ankle exoskeleton and experimental setup depicting the walking conditions for controller validation.....	12
Figure 6. Closed-loop controller accuracy for each walking condition. Accuracy was calculated as 100 minus the RMSE between the prescribed torque output and the biological ankle moment. The blue bars represent the mean accuracy across the 6 unimpaired participants for the main validation experiment. The gray bars represent the average trial accuracy for the participant with CP (CP1) that completed all of the validation conditions. Error bars represent ± 1 standard deviation.....	18
Figure 7. Time series comparison of biological moment, prescribed torque, and the measured torque across the validation conditions for one representative participant. The biological ankle moment was normalized by the average peak moment during calibration, while the exoskeleton torque was normalized by the nominal torque setpoint; perfect accuracy would result in complete overlap of the torque and moment profiles. The stair ascent plot depicts a trial in which the left leg	

strikes the ground level, while the stair descent plot depicts a trial in which the right leg strikes the ground. 22

Figure 8. Time series comparison of biological moment, controller-specified torque, and the measured torque across the validation conditions for the participant with cerebral palsy (CP1) that completed all of the validation tasks. The biological ankle moment was normalized by the average peak moment during calibration, while the exoskeleton torque was normalized by the nominal torque setpoint; perfect accuracy would result in complete overlap of the torque and moment profiles. The stair ascent plot depicts a trial in which the left leg strikes the ground level, while the stair descent plot depicts a trial in which the right leg strikes the ground. 23

Figure 9. Time series comparison of biological moment, controller-specified torque, and the measured torque across the validation conditions for the participants with cerebral palsy CP2, CP 3, and CP 4. The biological ankle moment was normalized by the average peak moment during calibration, while the exoskeleton torque was normalized by the nominal torque setpoint; perfect accuracy would result in complete overlap of the torque and moment profiles. 24

Figure 10. The normalized moment arm between the forefoot and the ankle joint center of rotation across the walking conditions for (A) the unimpaired validation cohort and (B) the clinical case study. The forefoot moment arm was evaluated to test our analytical model assumption that the moment arm between the forefoot and ankle is nearly constant across the stance phase. The values in the legend for each condition indicate the mean \pm SD of the relative moment arm across stance phase. 25

Figure 11. Results from our clinical feasibility tests reporting the change in metabolic cost, averaged over the final 2 minutes of 6-minute steady-state walking trials with the adaptive closed-loop ankle exoskeleton controller for three participants with cerebral palsy (CP2-CP4)..... 28

Figure 12. Pictures of the heel on board (A), toe on board (B) and soft foam (C) experimental pilot tests of uneven terrain.	32
Figure 13. Plots depicting the comparison between the prescribed torque and biological ankle plantarflexor moment for walking over a hard plate with pressure under the midfoot.	34
Figure 14 . Pictures of our hip exoskeleton.	38
Figure 15. 3D CAD model of the hip exoskeleton components. Purple arrows show the passive DOFs and the green arrow shows the active joint	39
Figure 16. Schematics of our hip exoskeleton control strategy.	41
Figure 17 . Desired torque and torque sensor data of one unimpaired participant in real time during walking over treadmill at different speeds with 8 Nm extension and 5 Nm flexion assistance ...	45
Figure 18 . Desired torque and torque sensor data of three unimpaired participants in real time during walking level ground.	46
Figure 19 . Desired torque and torque sensor data of three unimpaired participants in real time during walking level ground	47
Figure 20. Average metabolic energy consumption reduction of 3 unimpaired subjects during level and incline walking at their preferred speed.	48
Figure 21. Data of one CP subject at her preferred speed during level walking: A) Biological moment, desired torque and torque sensor data average versus percent gait. B) Average of hip joint angle.....	50
Figure 22. normalized EMG of rectus femoris and semitendinosus of one CP subject at her preferred speed during level walking.....	52
Figure 23. metabolic energy consumption of one CP subject at her preferred speed during level walking on 10 gait cycles with and without hip exoskeleton.	53

Figure 24. Rolling friction coefficient of unimpaired individual during level walking with preferred speed on 5 gait cycles.....	58
Figure 25. Contribution of mass, horizontal, and vertical ground reaction force to the ankle moment.	59
Figure 26. Schematic of ground reaction force and foot force to the ground during level ground walking.....	60
Figure 27. Contribution of mass, horizontal, and vertical ground reaction force to the knee moment.	62
Figure 28. Scatter plot of knee moment versus $Gx \times MAKGx$	63
Figure 29. $MAKGx$ over gait cycle during level ground walking.....	64
<i>Figure 30. The schematic of our biomechanical model of foot-shank, the control strategy based on this model, and the ankle-knee exoskeleton designed in NAU Biomechatronic Lab.</i>	<i>65</i>
Figure 31. Normalized ankle joint moment estimated by Opensim in compare to the coordinated controller and a reference controller during stance phase.	66
Figure 32. Normalized knee joint moment estimated by Opensim in compare to the coordinated controller and a reference controller during stance phase.	67
Figure 33. Maximum (a) plantarflexion ankle and (b) knee extension angle during stance phase for zero moment, reference controller and coordinated controller assistance.	68
Figure 34. Metabolic cost of walking for zero moment, reference controller and coordinated controller assistance.	69
Figure 35. Schematic of the Winding Filament Muscle (WFM) model. The contractile element (CE) represents the myosin cross-bridges, the actin filament is represented by a pulley, the titin	

protein is represented by a spring-damper element, and the tendon is represented by a spring in series with the pulley. 71

Figure 36. The bio-inspired WFH algorithm uses a pair of antagonistic virtual muscles (m_A = anterior muscles and m_P = posterior muscle) to control ankle torque. L_{m_A} and L_{m_P} represent the lengths of the anterior and posterior muscles, respectively. 72

Figure 37. (A) Translational Balance, (B) Rotational Balance..... 73

I. Adaptive Ankle Exoskeleton Control: Validation Across Diverse Walking Conditions

I.1. Introduction

Lower-limb wearable assistive devices are widely researched for their potential to augment human ability for a range of locomotor tasks [1]. Areas of growing interest include walking performance augmentation during extended or challenging walking terrain, load carriage for military and industry applications [2], [3], and mobility assistance for the elderly and people with physical disabilities [4]–[7]. Depending on their intended function, powered lower-limb exoskeletons can be designed to provide assistance across multiple or individual joints [8]–[11]. Wearable exoskeletons used for mobility augmentation and rehabilitation frequently include providing assistance at the ankle joint because of the ankle’s outsized role in efficient bipedal locomotion [12]–[15]. The need for exoskeletons to effectively augment ankle plantar-flexion has led to research on a wide variety of control systems. However, the majority of research on exoskeleton control systems has focused on providing finely tuned assistance during level treadmill walking [13], [14], [16], [17].

It is critical that control strategies can appropriately adapt to, and transition between, different environmental and locomotor demands when assisting individuals with and without disabilities. We are not aware of any practical ankle exoskeleton controllers that have been validated for all of the primary types of terrain encountered in free-living environments [18]. Exoskeletons can be controlled using high-level open-loop or closed-loop control schemes. Here, we define high-level closed-loop control as a controller that responds in real-time to deliver torque that instantaneously adapts a physiological input from the user; alternatively, high-level open-loop control provides a pre-determined torque signal that is not adjusted directly from a physiological input from the user.

Torque profiles from human-in-the-loop optimizers utilizing physiological measurements (e.g., metabolic cost) [13] are great for steady-state walking tasks. However, because they prescribe assistance that does not adapt in real-time, they are not designed to respond to instantaneous changes in demand, like transient walking speeds, perturbations, or terrain and gait transitions. In theory, high-level controllers, like intent recognition, fall detectors, and locomotor condition classifiers [19], [20], could be used in conjunction with optimized feed-forward torque profiles to adjust assistance to different environmental factors. However, these types of high-level classification controllers may require individualized calibration procedures or large training datasets because of wide variations in gait speed and walking patterns observed across user ages, body types, and physical or neuromuscular impairments. Misclassification could have disastrous effects, like an exoskeleton failing to appropriately modulate torque for stair descent and causing a fall.

High-level closed-loop exoskeleton control systems may be well-suited for intuitively adapting assistance across variable terrain and have the added benefit of responding to user intention, which seems to be a critical factor in the adoption of powered assistive devices [21]. Control systems leveraging the user's own muscle activity, like proportional myoelectric control [17], [22], have been successfully used in research for a variety of assistive devices and walking conditions [17], [23]. However, electrode-related interface and signal reliability challenges currently limit their practicality for extended use outside of controlled laboratory environments. Additionally, non-volitional or deficient muscle activity exhibited by some individuals with neuromuscular disabilities make myoelectric exoskeleton control unsuitable for some clinical patient populations.

The overarching objective of this work was to validate a robust yet realistic ankle exoskeleton control strategy capable of seamless operation across walking conditions encountered during daily life for unimpaired individuals and impaired individuals with some independent walking capacity. The specific goals of the present paper were to (1) develop an analytical ankle joint moment estimation model that could be reliably recreated from custom embedded sensors, and (2) validate the ability of a closed-loop exoskeleton control system based on the estimation model to accurately adapt assistance proportional to the biological ankle plantar-flexor moment during (a) level, (b) incline, and (c) decline walking, each at multiple speeds; (d) stair ascent; (e) stair descent; and (f) 90° turning while walking over-ground. We completed validation experiments in six unimpaired individuals and four individuals with cerebral palsy (CP) for a clinical feasibility analysis. Validation testing was completed on an untethered robotic ankle exoskeleton to confirm our ability to accurately estimate the biological ankle moment in real-time while the device provided assistive torque to the user. To the best of our knowledge, this is the first study to validate a functioning ankle exoskeleton control system for all-terrain walking.

I.2. Methods

I. 2. 1. Motivation

Adjustments to the timing and magnitude of assistance are necessary to safely and effectively control an exoskeleton when completing, and transitioning to, variable walking conditions. For example, without adjustment, a torque profile optimized to level, preferred-speed walking would be dangerous for an individual stepping off a curb or taking the first step down a staircase because the assistance level relative to the demand on the ankle plantar-flexors would be elevated and could dangerously destabilize the user. Techniques to adjust high-level open-loop control schemes (e.g.,

an optimized torque profile) by definition, are not able to adjust assistance immediately, resulting in inherent delays and a reliance on complex walking condition sensing and classification.

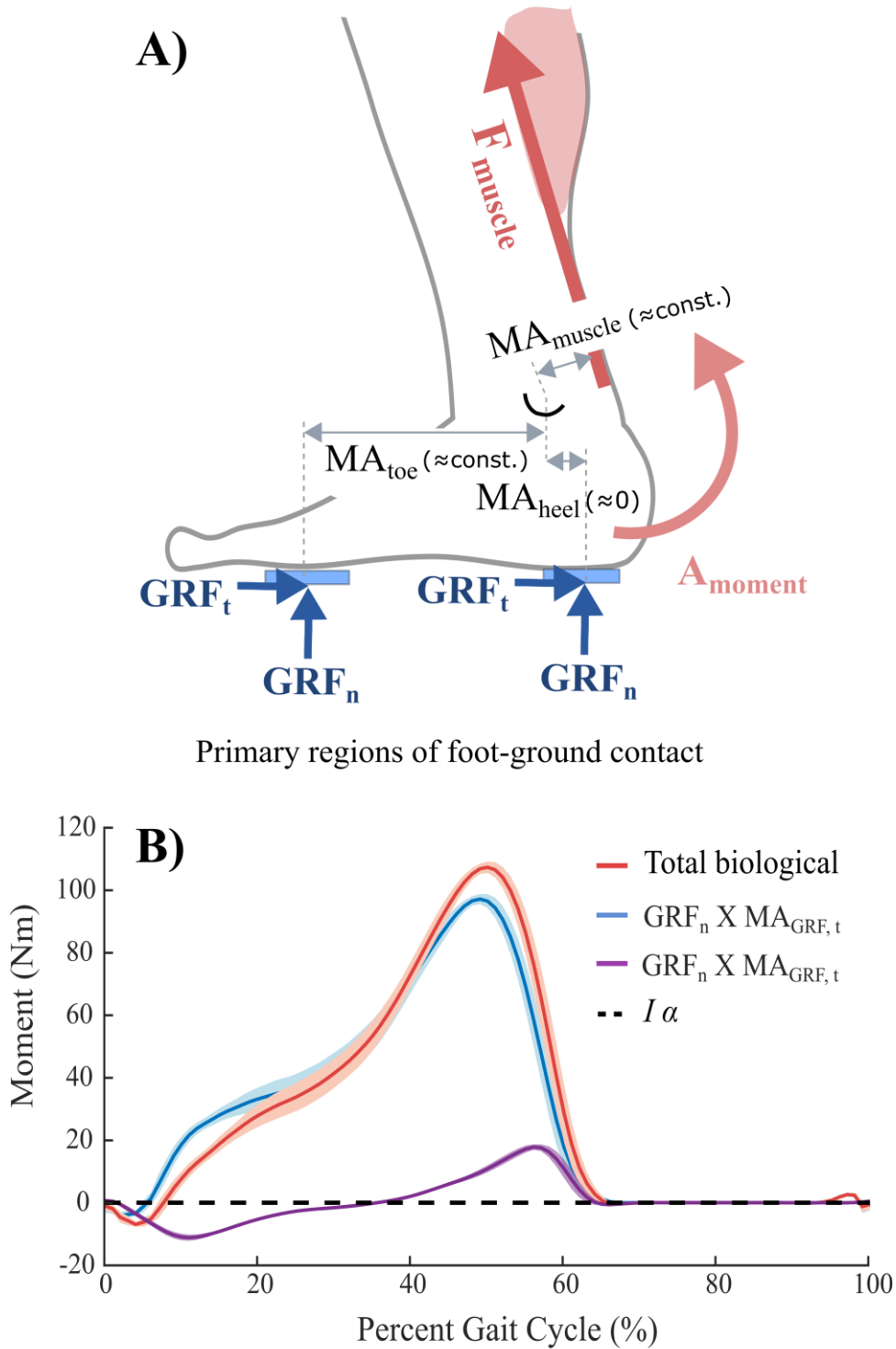


Figure 1. Ankle moment estimation approach and assumptions. A) Schematic depicting ankle moment contributions, primary regions of foot contact, and model assumptions. B) Plot showing the contributions to the biological ankle moment.

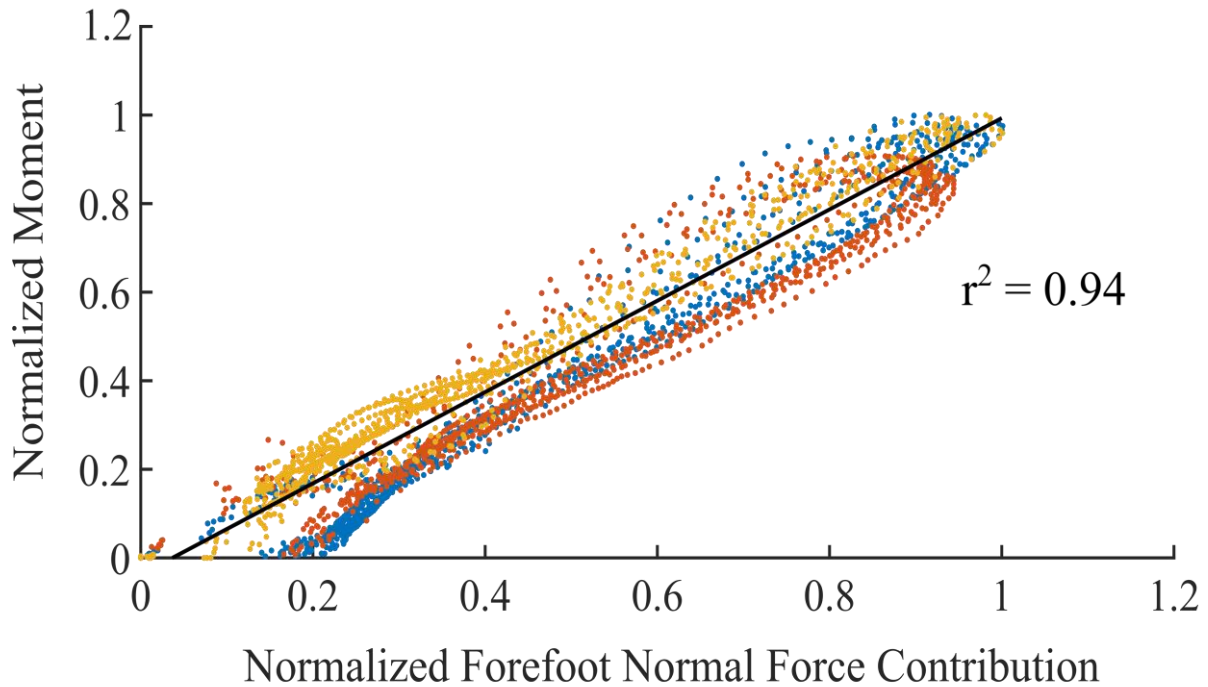


Figure 2. Scatter plot reporting the relationship between the moment produced by the forefoot normal force and the total biological ankle moment.

To address the need for a control scheme that can seamlessly and safely adjust assistance, we sought to develop an ankle exoskeleton control strategy that would instantaneously adjust assistance provided to the user. Intended for able-bodied individuals and impaired individuals with some independent walking capacity, the goal was for the controller to account for each individual's gait pattern, step-to-step variability, gait transitions, and different walking terrains encountered during daily life. Similar to proportional myoelectric control but without the need for muscle electrodes, our approach was to quantify the net demand placed on the ankle plantar-flexor muscles (the biological joint moment) in real-time, and then provide assistance proportional to that demand (i.e., proportional to the joint moment) so that the relative assistance level remained the same across all walking conditions. Not reliant on applying a “typical” ankle moment pattern, this approach would automatically adjust to the biomechanics of each user, regardless of their gait function. This type of closed-loop design also eliminates the potential for ambulatory condition misclassification

and temporal delay issues with transitions. Based on promising indications from proportional myoelectric control [7], [24], we believe there is a strong rationale for the approach of providing assistance as a fixed proportion of the biological ankle moment; it provides continuity and consistency across all modes of walking for the user's neuromuscular system, which can reliably expect the same relative amount of assistance on any terrain. In the case of abnormal walking patterns, torque provided proportional to the biological moment should (1) automatically account for differences between individuals, limbs and strides [24], and (2) appropriately and automatically adapt to changes in gait mechanics (e.g., reduced crouch) as a result of the provided torque [25].

An underlying goal of our control scheme was to provide assistance proportional to the force produced by the ankle plantar-flexor muscles during stance phase. An assumption of our approach was therefore that the biological ankle moment is proportional to the plantar-flexor muscle force. For this assumption to be reasonable, the influence of variation in Achilles tendon moment arm and co-contraction on the muscle moment production must be small. Dynamic ultrasound imaging indicates that the Achilles tendon moment arm varies 2-3 mm over the portion of stance phase during which the plantar-flexor muscles are active [26]. Analyzing the sensitivity of our model, a 2.5mm change in Achilles tendon moment arm would elicit a 5.7% change in the relationship between biological ankle moment and muscle load. Ankle muscle co-contraction is generally consistent and varies between 10% to 30% across stance phase [27]. Given the considerable difference in force production capability (~6.4 times greater [28]) for the primary agonists, the gastrocnemius and soleus, versus the primary antagonist, the tibialis anterior, while also accounting for their moment arms and relative activation during walking, a 20% change in co-contraction would result in a 6.2% change in the relationship between biological ankle moment and plantar-flexor muscle load.

Table 1. CONTRIBUTION OF THE NORMAL GRF TO THE BIOLOGICAL ANKLE MOMENT DURING INCLINE AND DECLINE WALKING

Walking	Condition	Prediction Accuracy (%)	Correlation Coefficient (R)
	15°	0.98 ± 0.001	0.99 ± 0.002
Incline	10°	0.97 ± 0.006	0.99 ± 0.001
	5°	0.96 ± 0.006	0.99 ± 0.002
	15°	0.92 ± 0.003	0.97 ± 0.002
Decline	10°	0.92 ± 0.006	0.97 ± 0.006
	5°	0.93 ± 0.002	0.98 ± 0.004
Average		0.95 ± 0.02	0.99 ± 0.01

I. 2. 2. Ankle moment estimation model

The ankle joint estimation model and exoskeleton control strategy focused on the stance phase because the ankle joint during stance phase is the largest contributor to walking efficiency (50%) and forward propulsion (80%) [12]. The theoretical starting point in deriving our analytical ankle moment estimation model was that the ankle moment (A_m) can be estimated using an inverse dynamics torque balance during walking as in Equation (1):

$$A_m = I\alpha - (GRF_t \times MR_{GRF_t}) - (GRF_n \times MR_{GRF_n}) \quad (1)$$

where I is the mass moment of inertia of the foot, α is the angular acceleration of the foot, GRF_t and GRF_n are the tangential and normal ground reaction forces, respectively, and MR_{GRF_t} and MR_{GRF_n} are the normal and tangential distance between the foot center of pressure and the ankle joint (i.e., moment arms of GRF_t and GRF_n), respectively.

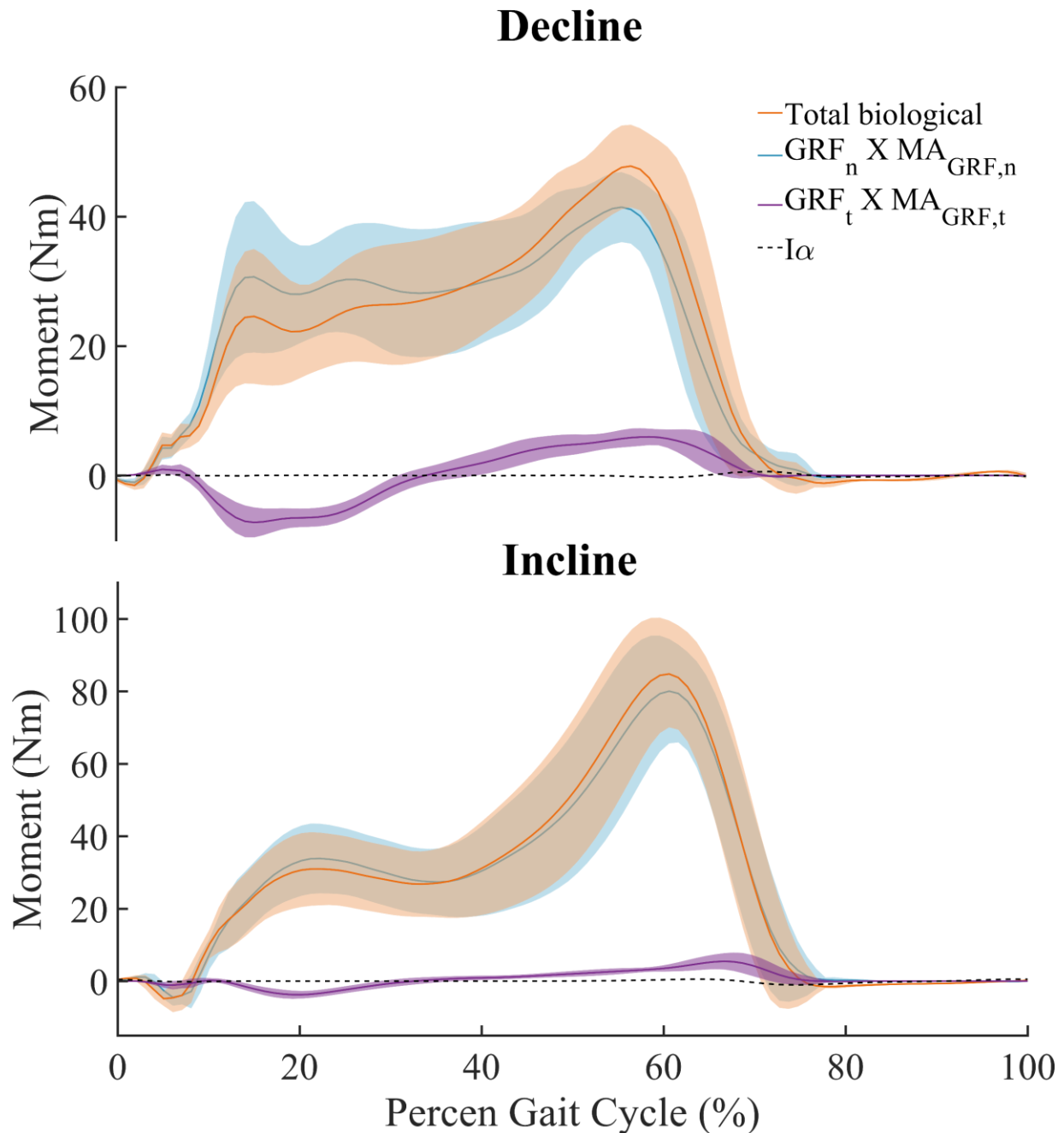


Figure 3. Contribution of normal and tangential ground reaction forces to the biological ankle moment during incline and decline walking at 15°.

We analyzed the primary contributions to the external biological ankle moment during walking from gait biomechanics data collected during level treadmill walking in 8 unimpaired individuals using the same data collection and processing approach outlined below. The moment contributed by the normal ground reaction force (GRF_n) predicted the biological ankle moment with 97%

accuracy during level and incline walking up to 15°, and more than 92% to the ankle moment during decline walking up to 15° (Table 1, Figure 3); over the stance phase, the contribution from GRF_t was < 3%, while the contribution from the foot’s inertial properties ($I\alpha$) was <0.001%. Using the forefoot sensor described below in early testing, we found that the normal force under the forefoot accounted for 94% of stance-phase ankle moment variability (Figure 2). The primary concentration of foot-ground contact occurs beneath the forefoot and heel because the arch of the foot prevents mid-foot force localization [29], [30]. During early-mid stance, the location of heel center of pressure is closely aligned with the ankle joint center of rotation (i.e., the moment arm for the heel contact location is close to zero). During late stance, the heel comes off the ground and the heel reaction force is zero. Therefore, much like computing the moment about one of two supports of a beam, the moment contribution produced by the total normal ground reaction force (GRF_n) and average center of pressure can be computed as in Equation (2):

$$A_{m,est} = GRF_{n,forefoot} \times MR_{GRF_{n,forefoot}} \quad (2)$$

where $GRF_{n,forefoot}$ is the normal ground reaction force applied to the forefoot and $MR_{GRF_{n,forefoot}}$ is the tangential distance between the forefoot and ankle. Our goal was to calculate the real-time ankle moment relative to the peak ankle moment during walking at preferred speed for which assistive torque can be finely tuned. We purposefully maximized the simplicity of the control system, electing to forego foot-ground angle sensing required to calculate the change in moment arm. With the assumption that the moment arm between the forefoot and ankle is nearly constant across the stance phase (we assess this assumption in the Results section), that term cancels (i.e., is present in both the numerator and denominator) and we can compute the relative estimated ankle moment ($A_{m,rel}$) as in Equation (3):

$$A_{m,rel} = \frac{GRF_{n,forefoot,inst}}{GRF_{n,forefoot,peak}} \quad (3)$$

where $GRF_{n,forefoot,inst}$ is the instantaneous normal ground reaction force applied to the forefoot during any ambulatory task and $GRF_{n,forefoot,peak}$ is the peak normal ground reaction force applied to the forefoot during walking at preferred speed.

I. 2. 3. Ground reaction force estimation

To estimate the forefoot GRF, and therefore the relative biological ankle moment, we developed an embedded custom force sensor mechanism that spanned the entire forefoot (Figure. 2A). A high-fidelity force sensitive resistor (FlexiForce A502, Tekscan) was embedded within a custom-designed sensor cover that localized the force underneath the head of the first metatarsal. The FlexiForce sensors were selected due to their (manufacturer-reported) performance relative to typical “Shunt Mode” FSRs on several important metrics, including loading linearity, drift, dynamic measurement calibration, and dynamic range. The custom sensor was placed on a carbon fiber footplate to provide a rigid platform for which ground reaction forces were distributed to the forefoot sensor; seeking to account for uneven surfaces, the footplate provided structural rigidity necessary for reliable forefoot contact. The instantaneous relative biological ankle moment (M_{rel}) was estimated as in Equation (4):

$$M_{rel} \approx \frac{f_{inst}}{f_{cal}} \quad (4)$$

where f_{inst} was the instantaneous forefoot sensor force, and f_{cal} was the stance-phase average peak forefoot sensor force established across 3 strides during a ~3-second calibration period at each user’s preferred walking speed.

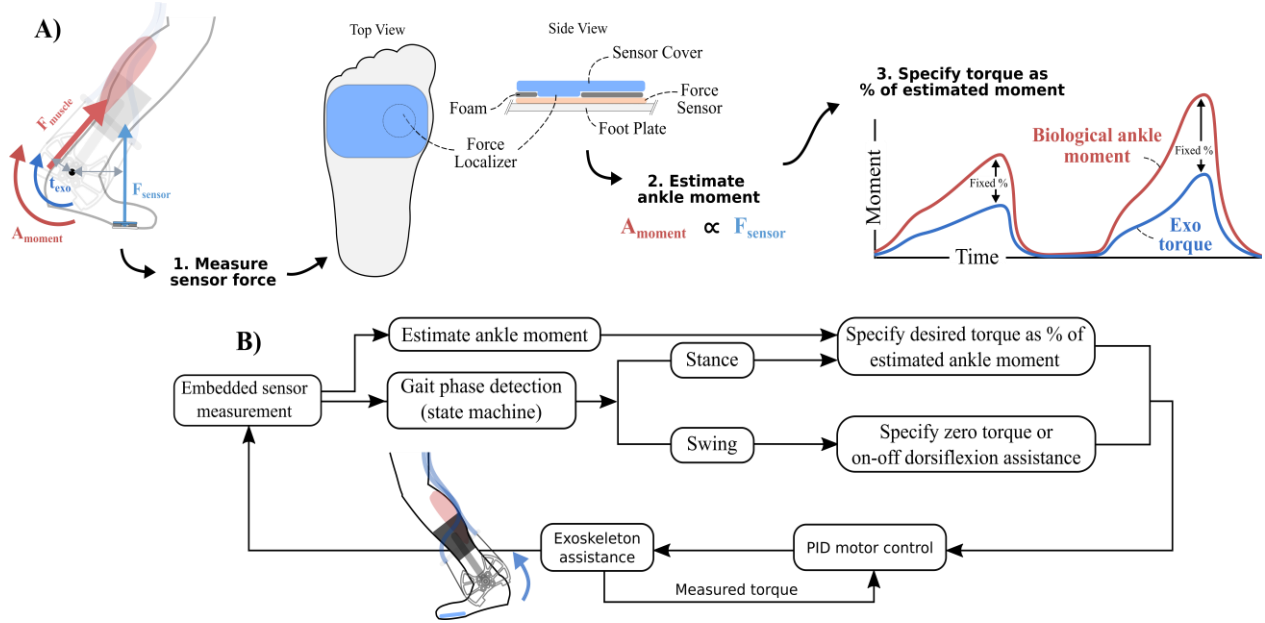


Figure 4. Overview of the closed-loop control system. A) Schematic depicting the custom embedded foot sensor design used for estimating the biological ankle moment and prescribing proportional exoskeleton torque. B) Schematic of the real-time exoskeleton control loop.

I. 2. 4. Closed-loop control algorithm

The real-time exoskeleton control scheme incorporated joint moment estimation for torque prescription, a finite state machine for gait phase detection, and low-level torque-feedback for motor control (Figure. 2B). The controller-specified exoskeleton torque (T) during stance phase was calculated as in Equation (5):

$$T = t_{set} M_{rel} \quad (5)$$

where t_{set} was the nominal peak torque setpoint established at the user's preferred walking speed and M_{rel} was the estimated relative ankle moment that acts to scale the torque setpoint. The estimated ankle moment (M_{rel}) and therefore torque setpoint (T) both vary with time; t_{set} remained constant. The calibration procedure takes place on each limb individually, which allows customization of assistance magnitude across limbs for individuals with more and less affected sides. As a result, the control system allows for the application of an appropriate assistance magnitude across individuals and limbs of varying function.

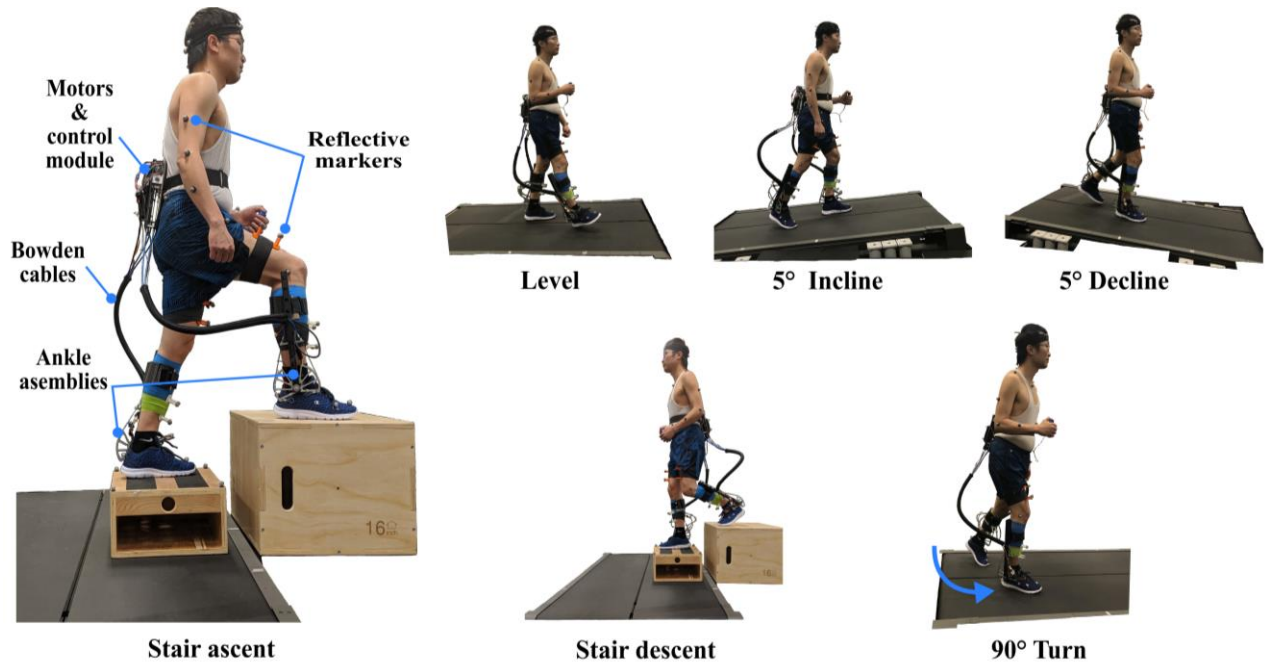


Figure 5. Ankle exoskeleton and experimental setup depicting the walking conditions for controller validation.

A finite state machine was used to define stance and swing phases of walking or stepping (Figure. 3B). Transitions to and from stance phase were triggered when the embedded force sensor readings exceeded or fell below 15% of the walking calibration peak value, respectively. The desired instantaneous torque profile was implemented using a low-level proportional-integral-derivative (PID) torque feedback motor controller.

I. 2. 5. Electromechanical exoskeleton system

Our control scheme was implemented on an untethered (i.e. battery-powered and wireless) ankle exoskeleton that was similar in design to the work in [8], [31]. In short, waist-mounted motors (EC-4pole, Maxon) were used to drive Bowden cables that actuated pulleys on bilateral ankle assemblies (Figure. 5). Each ankle assembly consisted of a carbon fiber insole that bi-directionally articulated in the sagittal plane about the ankle joint, carbon fiber uprights, molded carbon fiber

Table 2. PARTICIPANT INFORMATION

Participant	Walking Ability	Age (yrs)	Gender	Height (m)	Body Mass (kg)	Nominal Torque Setpoint (Nm)
1	Unimpaired	39	M	1.66	63.4	15.8
2	Unimpaired	23	F	1.60	60.9	15.2
3	Unimpaired	22	F	1.60	51.3	12.8
4	Unimpaired	29	F	1.68	60.0	15.0
5	Unimpaired	20	M	1.63	63.3	15.8
6	Unimpaired	20	F	1.68	58.3	14.6
CP1	GMFCS Level II	31	M	1.70	56.8	14.2
CP2	GMFCS Level III	25	F	1.47	47.4	16.6
CP3	GMFCS Level I	15	M	1.65	57.2	20.0
CP4	GMFCS Level I	11	M	1.50	48.4	16.9

Participants CP1-CP4 had mild-to-severe walking impairment from cerebral palsy, gross motor function classification score (GMFCS) level I-III.

cuffs for attachment to the shank, a torque sensor, a torque transmission pulley, and Bowden cable attachment points. The motor and transmission configuration used in this study was designed to provide up to 24 Nm of peak torque.

The control module, attached to the waist-mounted motor assembly, included a custom PCB control board that consisted of a micro-controller, motor drivers, signal processing components, and Bluetooth module. An on-board lithium polymer (Li-Po) battery (910 mAh) powered the system and motors. The micro-controller, a 32-bit ARM microprocessor (Teensy 3.6, TJRC), implemented our real-time control algorithm operated at 500 Hz. Forefoot force sensor data were collected at 12-bit resolution and filtered using a 10-sample moving average. With feedback from the torque sensors mounted to the ankle joint, a low-level PID motor controller was used to track the desired torque profile resulting from the control strategy. We used a graphical user interface (GUI) in MATLAB to remotely operate the exoskeleton via Bluetooth, and display and record data.

Table 3. DETAILED RESULTS OF PRESCRIBED AND MEASURED TORQUE PROFILES

Walking Condition	Average Prescribed Accuracy (%)	Torque Tracking Accuracy (%)	Averaged Measured Accuracy (%)
Level	Fast	86.7 ± 4.6	81.7 ± 5.7
	Med	90.4 ± 3.9	86.9 ± 3.8
	Slow	89.6 ± 4.3	87.7 ± 4.1
Incline	Fast	88.0 ± 2.6	84.3 ± 4.1
	Med	87.3 ± 3.7	87.0 ± 3.3
	Slow	87.2 ± 5.1	85.7 ± 5.8
Decline	Fast	89.0 ± 1.9	83.1 ± 4.0
	Med	90.9 ± 2.4	85.1 ± 6.5
	Slow	90.3 ± 3.6	85.3 ± 5.0
Stepping	Ascent	82.9 ± 5.1	78.3 ± 6.3
	Descent	82.6 ± 5.2	75.9 ± 12.4
90° Turn		87.6 ± 3.9	84.2 ± 5.0
Average	87.7 ± 2.7	90.3 ± 3.0	83.8 ± 3.6

I. 2. 6. Validating design overview

This protocol was approved by the Northern Arizona University Institutional Review Board. We designed an experiment to test the ability of the exoskeleton controller to appropriately adjust plantar-flexor torque for level, incline, and decline walking at multiple speeds, stair ascent and descent, and making 90° left and right turns (Figure. 3). Using a motion capture laboratory with an in-ground split-belt force-measuring treadmill, we recorded the kinematic and kinetic data needed to calculate biological joint moments.

We recruited 10 individuals to validate the control system (Table 2). The first 6 participants to complete the protocol were unimpaired individuals, enrolled to evaluate performance for

unimpaired applications. To evaluate the ability of the control system to function appropriately for individuals with walking disorders, we completed a clinical feasibility analysis with 4 individuals who had neurological impairment caused by cerebral palsy (CP).

I. 2. 7. Protocol for exoskeleton controller validation

Our control scheme was After fitting and donning the exoskeleton, reflective motion capture markers were placed on the feet, shanks, thighs, pelvis, torso, arms, and head of the participant according to recommended standards [32]. Each participant completed a standing marker calibration trial, and then walked on the treadmill for about 3-5 seconds at their preferred speed to calibrate the controller (f_{cal}). Participants walked for several minutes to acclimate to the device and assistance; walking speed was set to 1 m/s unless the participant requested a different speed, at which point the speed was incrementally adjusted (Table 3).

The first validation task was level walking at three speeds that encompassed the range often reported for individuals with neuromuscular impairment (~0.8-1.2 m/s [33]). The three speeds were the acclimation speed (“medium”, ~1.0 m/s), and 25% above (“fast”) and below (“slow) the acclimation speed (~1.25 m/s and ~0.75 m/s, respectively) (Figure 5). The second and third validation tasks were 5° incline and then 5° decline walking at the acclimation speed, and 25% and 50% below the acclimation speed (~0.75 m/s, and ~0.50 m/s, respectively). The incline/decline angle, based on American Disability Act (ADA) guidelines, was selected because it is likely the most common ramp angle encountered during daily life. Marker and ground reaction force data

were recorded for the final 10-15 seconds (a minimum of 10 gait cycles) during each of the two-minute steady-state walking trials. The fourth and fifth validation tasks were up-stair stepping (ascent) and down-stair stepping (descent). Wooden steps, isolated from one another, were placed perpendicular to the treadmill so that we could record individual ground reaction forces for the bottom step and the transition to/from the bottom step [34]. There was a 0.2 m rise each step. Assessment of controller accuracy for stair ascent and descent included the gait cycle during the transition at the bottom of the first step. Participants completed 3 trials leading with each leg (6 trials total) for both ascent and descent. The final validation task was a walking trial that involved a 90° turn. Participants approached the treadmill from the side, placed their leading limb on the first treadmill belt, pivoted and placed their trailing limb on the second belt, and then continued walking in line with the treadmill such that the next step resulted in their leading limb striking the first treadmill belt again. Participants completed 3 trials leading with each leg (6 trials total) for both left and right turning.

More than five strides [7] were processed for each condition and participant. For each task, marker trajectories were recorded at 120 Hz by 10 motion capture cameras (Vicon Motion Systems, Oxford, UK) and low-pass filtered at 6 Hz. Individual limb ground reaction forces were recorded at 960 Hz from the force plates under each treadmill belt (Bertec, Columbus, OH) and low-pass filtered at 12 Hz. Data were recorded and synchronized in Vicon Nexus. A 5V trigger was used to synchronize the experimental motion capture with the desired and measured exoskeleton torque.

I. 2. 8. Clinical feasibility analysis

A physical exam was completed by a licensed physical therapist prior to involvement from the 4 participants with CP (Table 2). These individuals had mild-to-severe walking impairment, and gross motor function classification score levels of I-III. Each participant provided written informed consent.

One individual (CP1) completed all of the validation tasks indicated above, while three additional individuals with (CP2-4) completed controller validation and steady-state metabolic testing during 5 °incline and stair walking (StairMaster Sm3 Stepmill), the two main challenging and energetically expensive ambulatory conditions encountered during daily life. Metabolic data from a wearable system (Cosmed K5) was collected to evaluate the physiological benefit of the control strategy during these two conditions to complement our prior level overground walking results [35]. Net metabolic rate, averaged over the last 2-minutes of each 6-minute trial, was compared between adaptive assistance and shod walking conditions as in [35].

I. 2. 9. Data processing

We computed the biological contribution to the ankle joint moment for comparison to the prescribed exoskeleton torque. First, we scaled a generic OpenSim (Stanford, CA, [36]) musculoskeletal model to each participant using marker positions from the standing calibration trial. Next, inverse kinematics and inverse dynamics analyses in OpenSim were used to calculate joint angles and joint moments, respectively, for each trial [31]. The ankle joint moment obtained from the inverse dynamics analysis included the user's biological and exoskeleton contributions. Therefore, the biological contribution (i.e. the joint moment produced by the muscles crossing the

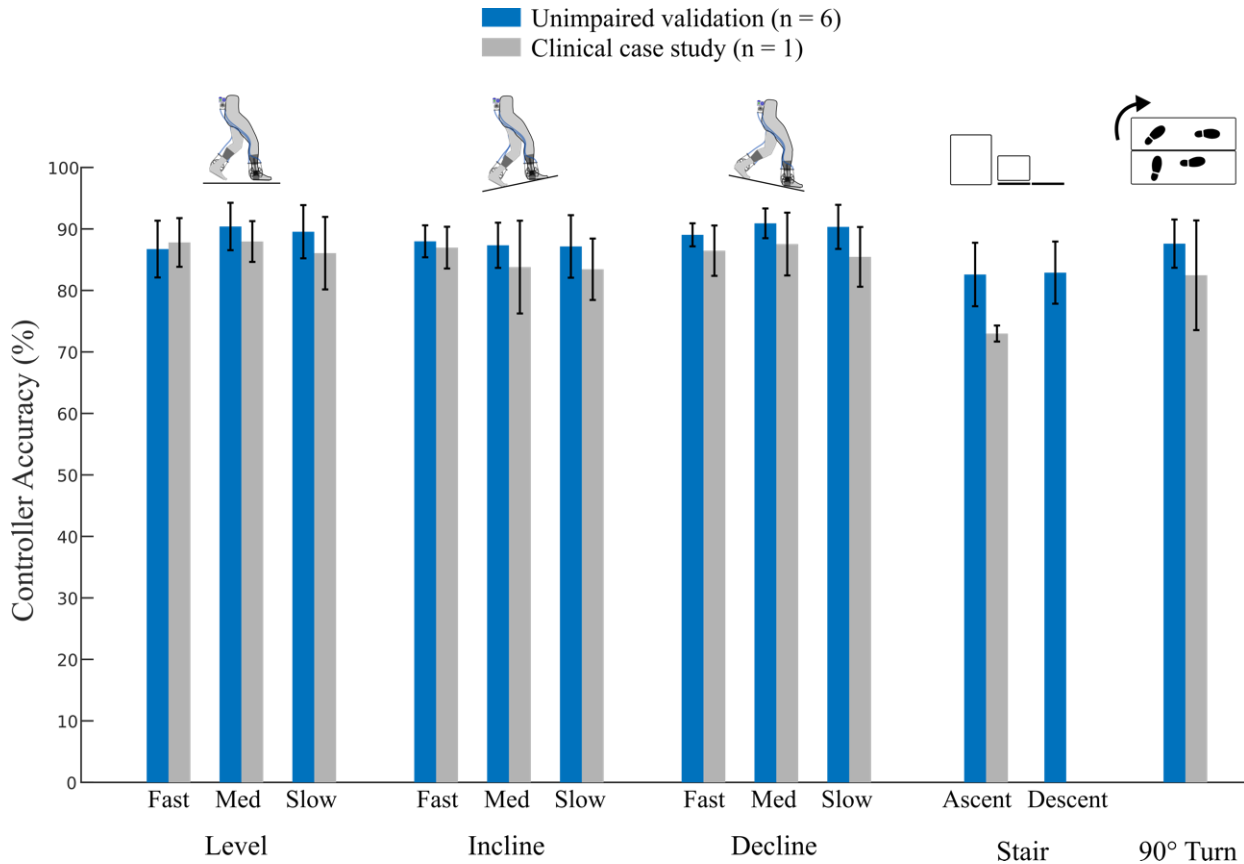


Figure 6. Closed-loop controller accuracy for each walking condition. Accuracy was calculated as 100 minus the RMSE between the prescribed torque output and the biological ankle moment. The blue bars represent the mean accuracy across the 6 unimpaired participants for the main validation experiment. The gray bars represent the average trial accuracy for the participant with CP (CP1) that completed all of the validation conditions. Error bars represent ± 1 standard deviation.

ankle) was calculated by subtracting off the measured exoskeleton torque [22], [37]. The short custom staircase was constructed from isolated steps allowing for independent stair-step reaction forces to be recorded from the force plates embedded within the instrumented treadmill. The ground reaction force vector and center of pressure measured from the force plates were appropriately transformed relative to the global motion capture reference frame for the sloped walking and stair stepping trials.

We assessed the accuracy of the proportional joint-moment control scheme by calculating the average and peak root-mean-squared-error (RMSE) between the prescribed and measured exoskeleton torque and measured biological ankle moment across the stance phase for every stride; prescribed and measured exoskeleton torque was normalized by the nominal torque setpoint (t_{set}) while the biological ankle moment was normalized by the average peak moment during the calibration. “Prescribed” torque or assistance refers to the controller-specified control signal, while “measured” torque or assistance refers to the torque delivered to the user as assessed via the torque sensor at the ankle joint. Accuracy was computed by subtracting the RMSE expressed as percent of the biological ankle moment from 100%. Our goal was for the control scheme to have an average accuracy greater than 85%. This was based on the rationale that a 15% error would only result in a 2.5-3.75% peak difference in applied torque relative to the biological ankle moment during ambulatory tasks. We also quantified the Pearson’s product moment correlation coefficient (R) between the normalized biological ankle moment and normalized prescribed exoskeleton torque. With coefficients greater than 0.9 indicating a very high correlation [38], our goal was to fall at or above this value, which would indicate that the controller was responding almost completely directly to ankle muscle output.

I. 2. 10. Simulated open-loop controller comparison

To provide additional context on the importance of the adaptive nature of our closed-loop estimation scheme for these walking tasks, we completed a post-hoc analysis of a speed and gait-phase adaptive open-loop (i.e., feed-forward) control signal based on the stance-phase average estimated ankle moment established at each user’s preferred walking speed. We re-sampled the moment profile to the time duration of each preceding stance phase prior to computing accuracy. To account for anticipated changes in the peak biological ankle moment with gait speed for the

open-loop control signal, we established a speed adjustment factor by taking the ratio between speed vs. peak biological ankle moment and speed vs. estimated biological ankle moment ($M_{,rel}$) regression equations for the level, incline, and decline walking trials. This was done to mimic a reasonable implementation of an open-loop controller that accounts for speed variation during walking, similar to [7]. We computed the average stance-phase RMSE between the open-loop control signal and the biological ankle moment across all of the walking conditions, employing the same normalization technique as described above. A paired two-tailed t-test was used to determine if the accuracy was significantly different between the adaptive and non-adaptive prescribed ankle torque. Significance was set at $p < 0.05$. Lastly, we computed the moment-arm between the forefoot and ankle joint across all of the validation tasks for one participant to test our assumption that it was nearly constant across the stance phase.

I.3. Results

I. 3. 1. Controller validation with unimpaired

There were no adverse events or falls during walking with the adaptive closed-loop controller. The force sensor design was effective in eliminating the need for customize sensor placement; once placed on the exoskeleton footplate, no adjustments were made to the sensor location. The prescribed and measured exoskeleton torque was responsive to user input and closely matched the pattern of the stance-phase biological ankle moment across all of the ambulatory conditions (Figure 6 & 7). The moment arm between the forefoot and ankle joint across the walking conditions indicated that the distance varied less than $2.0 \pm 0.04\%$, on average, across the stance phase, and $\sim 2.3 \pm 1.6\%$ around the portion of stance phase where the peak ankle moment occurred (Figure. 8). The average accuracy of prescribed exoskeleton plantar-flexor assistance relative to

Table 4. POST-HOC COMPARISON BETWEEN OUR CLOSED-LOOP CONTROLLER AND THE ADAPTIVE OPEN-LOOP (FEED-FORWARD) CONTROLLER

Walking Condition		Closed-Loop Accuracy (%)	Open-Loop Accuracy (%)
Level	Fast	86.7 ± 4.6	82.7 ± 4.1
	Med	90.4 ± 3.9	83.5 ± 5.0
	Slow	89.6 ± 4.3	83.0 ± 4.1
Incline	Fast	88.0 ± 2.6	77.6 ± 8.0
	Med	87.3 ± 3.7	81.1 ± 6.7
	Slow	87.2 ± 5.1	79.9 ± 6.0
Decline	Fast	89.0 ± 1.9	78.2 ± 7.9
	Med	90.9 ± 2.4	78.0 ± 9.0
	Slow	90.3 ± 3.6	78.4 ± 6.9
Stepping	Ascent	82.9 ± 5.1	54.6 ± 7.0
	Descent	82.6 ± 5.2	62.3 ± 6.5
90° Turn		87.6 ± 3.9	78.1 ± 3.5
Average		87.7 ± 2.7%	76.5 ± 8.8%

Accuracy refers to the prescribed torque accuracy averaged over the stance phase. The open-loop controller adapted to speed (when applicable) and gait phase.

the biological ankle moment was $87.7 \pm 2.7\%$ across all of the validation conditions. Controller accuracy was generally similar across level, incline, and decline walking (between 86.7-90.9%, Figure. 4); changes in accuracy due to variation in walking speed was minimal ($< 3.7\%$). The least accurate locomotor conditions were stair ascent and descent ($82.6 \pm 5.2\%$, and $82.9 \pm 5.1\%$, respectively), followed by fast level walking (86.7%). There was a very strong relationship ($R = 0.96 \pm 0.01$) between the controller-specified torque and the biological ankle moment across all of the validation conditions. The low-level motor controller and mechanical system provided reliable assistance across the testing conditions (Figure 7). The average accuracy of measured exoskeleton

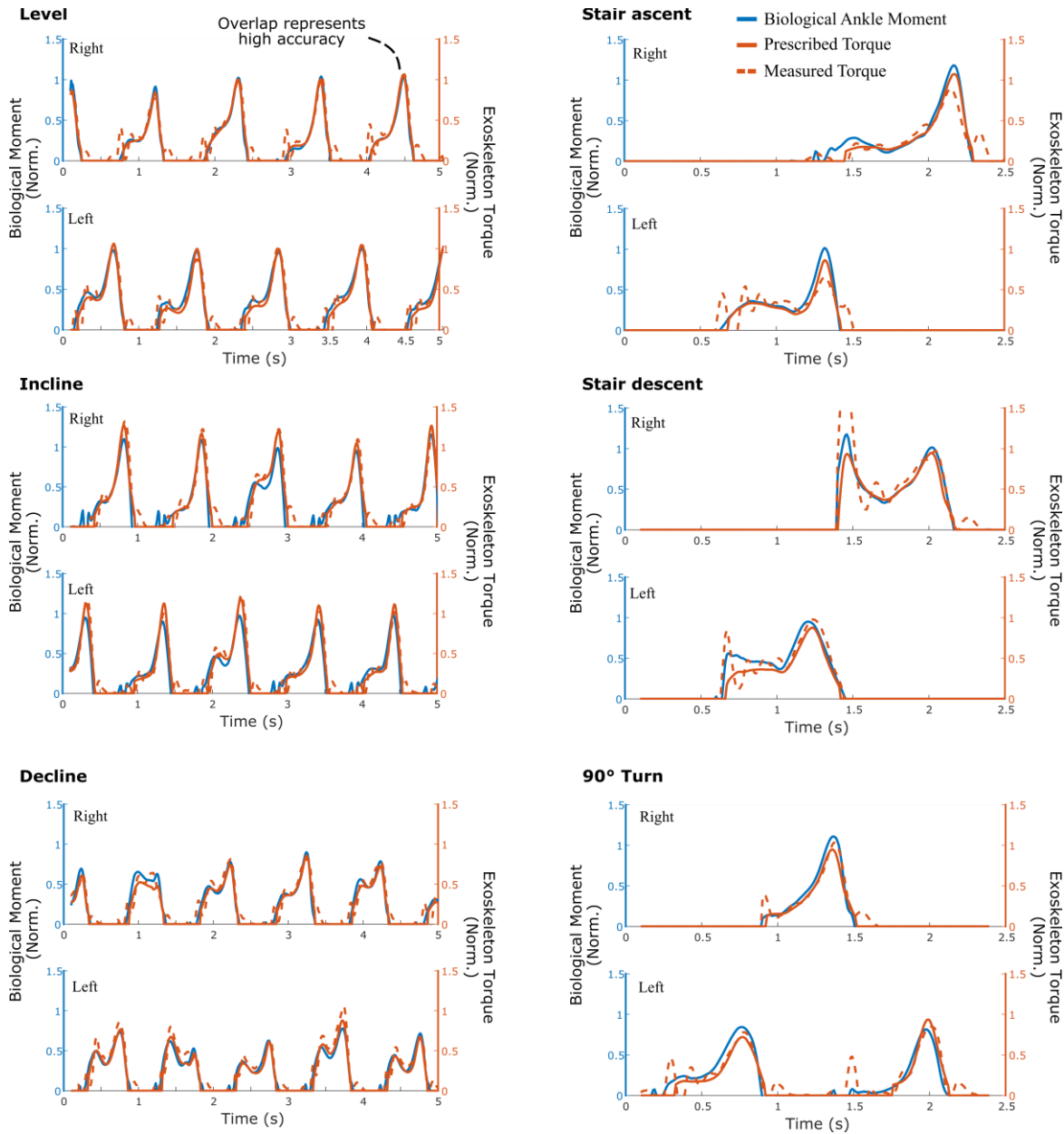


Figure 7. Time series comparison of biological moment, prescribed torque, and the measured torque across the validation conditions for one representative participant. The biological ankle moment was normalized by the average peak moment during calibration, while the exoskeleton torque was normalized by the nominal torque setpoint; perfect accuracy would result in complete overlap of the torque and moment profiles. The stair ascent plot depicts a trial in which the left leg strikes the ground level, while the stair descent plot depicts a trial in which the right leg strikes the ground.

plantar-flexor assistance relative to the biological ankle moment was $83.8 \pm 3.6\%$ across all of the validation conditions (Table 3). The average torque tracking accuracy was $90.3 \pm 3.0\%$. Torque

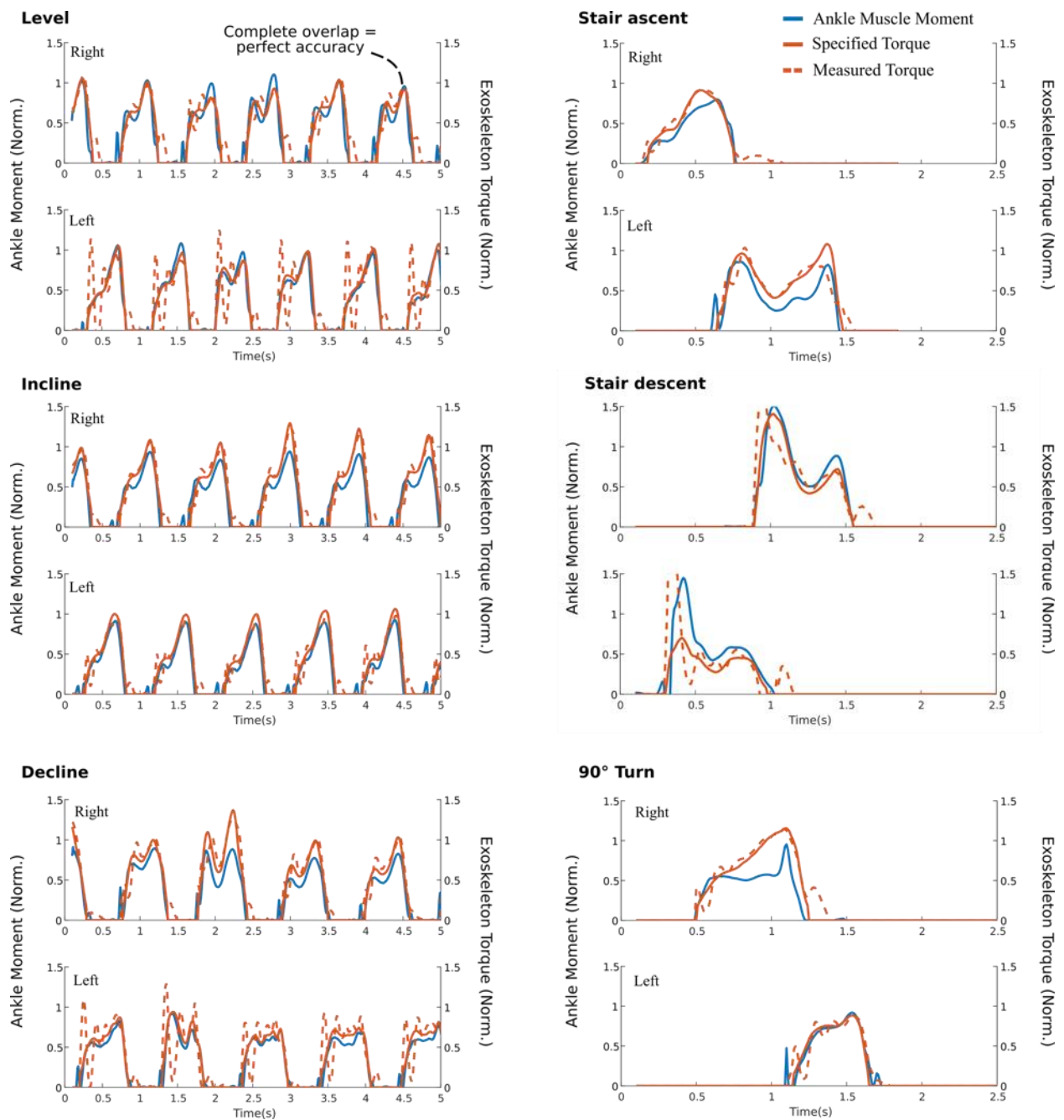


Figure 8. Time series comparison of biological moment, controller-specified torque, and the measured torque across the validation conditions for the participant with cerebral palsy (CP1) that completed all of the validation tasks. The biological ankle moment was normalized by the average peak moment during calibration, while the exoskeleton torque was normalized by the nominal torque setpoint; perfect accuracy would result in complete overlap of the torque and moment profiles. The stair ascent plot depicts a trial in which the left leg strikes the ground level, while the stair descent plot depicts a trial in which the right leg strikes the ground.

tracking accuracy was greatest at the slow steady-state walking speeds ($94.1 \pm 1.3\%$), and lowest

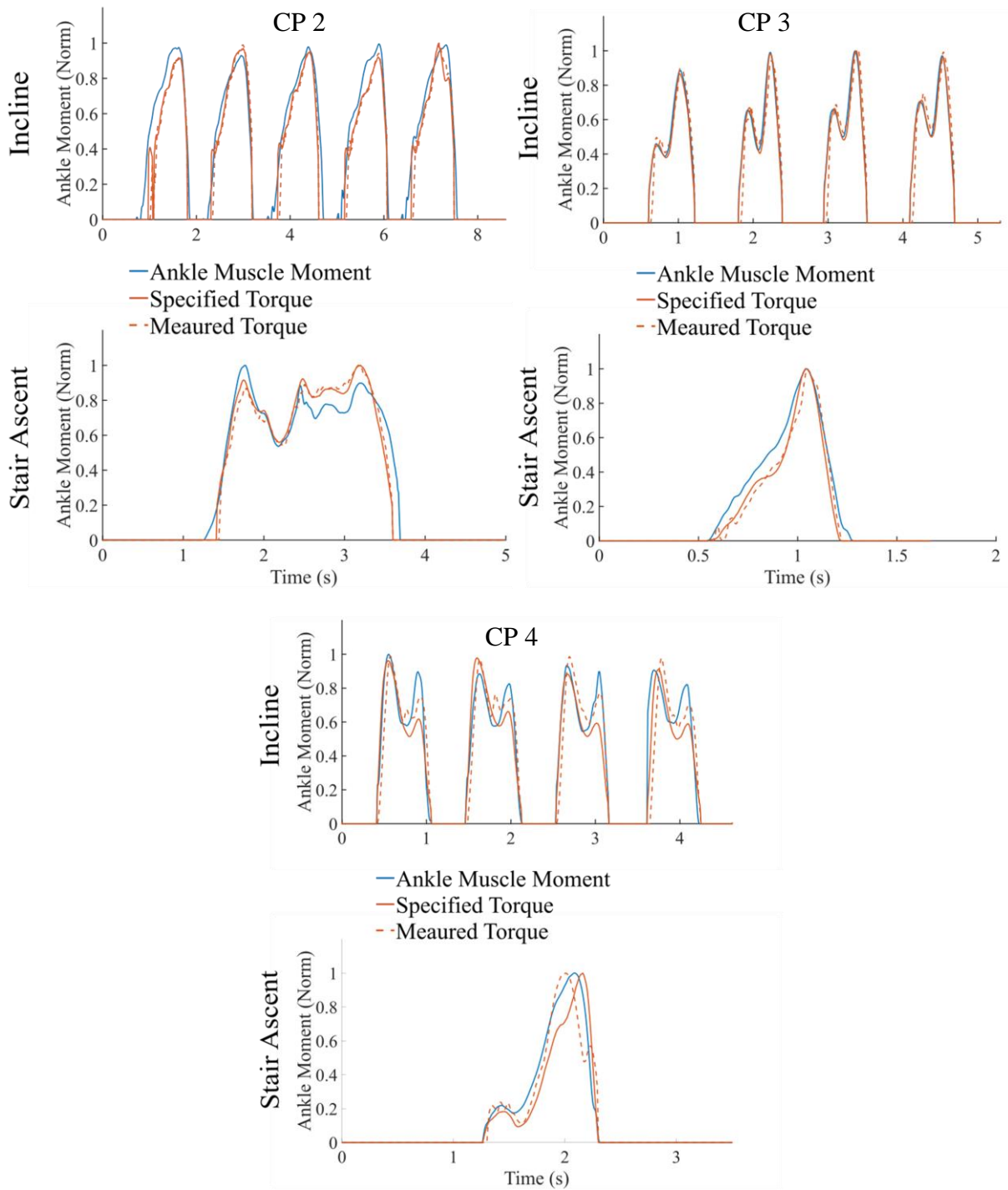


Figure 9. Time series comparison of biological moment, controller-specified torque, and the measured torque across the validation conditions for the participants with cerebral palsy CP2, CP 3, and CP 4. The biological ankle moment was normalized by the average peak moment during calibration, while the exoskeleton torque was normalized by the nominal torque setpoint; perfect accuracy would result in complete overlap of the torque and moment profiles.

during stair descent ($83.5 \pm 11.6 \%$). exoskeleton torque.

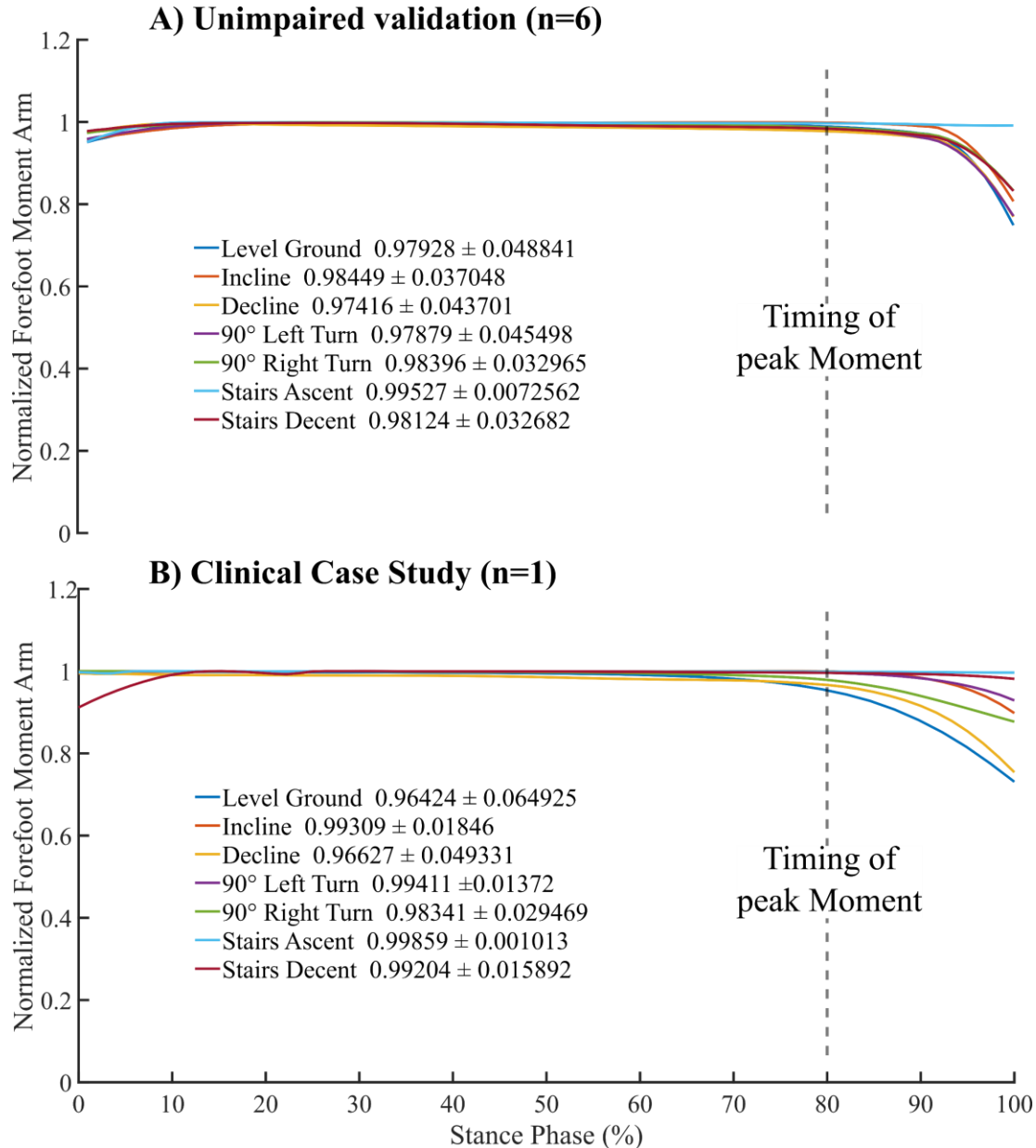


Figure 10. The normalized moment arm between the forefoot and the ankle joint center of rotation across the walking conditions for (A) the unimpaired validation cohort and (B) the clinical case study. The forefoot moment arm was evaluated to test our analytical model assumption that the moment arm between the forefoot and ankle is nearly constant across the stance phase. The values in the legend for each condition indicate the mean \pm SD of the relative moment arm across stance phase.

I. 3. 2. Comparison to the simulated open-loop controller

In our post-hoc controller analysis, we found that the simulated speed and gait-phase adaptive open-loop controller was $\sim 2X$ less accurate compared to our closed-loop control scheme ($23.5 \pm$

8.8% vs. $12.3 \pm 2.7\%$ error, $p < 0.001$, Table 4). Every walking condition had reduced accuracy for the adaptive open-loop controller relative to our closed-loop controller, with stair ascent ($54.6 \pm 7.0\%$) and descent ($62.3 \pm 6.5\%$) among the least accurate.

I. 3. 3. Clinical feasibility testing outcomes

Participant CP1 was able to safely complete all validation tasks without hand-held assistance with the exception of stair descent because they were unable to do so in a controlled, safe manner (both with and without the exoskeleton). For this participant, the moment arm between the forefoot and ankle joint across the walking conditions indicated that the distance varied less than $2.0 \pm 0.03\%$, on average, across the stance phase, and $\sim 4 \pm 2.2\%$ around the portion of stance phase where the peak ankle moment occurred (Figure. 10B). The average stance-phase accuracy of the controller-specified torque relative to the biological ankle moment was $85.1 \pm 4.3\%$ across all of the validation conditions, and there was a very strong relationship between the controller-specified torque and the biological ankle moment across all of the validation conditions ($R = 0.94 \pm 0.06$). Similar to the unimpaired participants, controller accuracy relative to the biological ankle moment was generally similar across level, incline, and decline walking (between 83.4-88.0%, Figure 6), while the least accurate locomotor conditions were stair ascent ($73.0 \pm 1.3\%$), followed by 90° turning ($82.5 \pm 8.9\%$) (Figure 8).

Participants CP2-4 safely completed incline and stair walking controller validation and metabolic testing. For these participants, the average accuracy of the prescribed and measured exoskeleton plantar-flexor assistance relative to the biological ankle moment across stair and

Table 5. CLINICAL FEASIBILITY TESTING RESULTS

Walking Condition		Average Accuracy (%)	Correlation Coefficient (R)	Metabolic Cost Reduction (%)	Torque Tracking (RMSE, %)
Incline	CP2	89.8 ± 3.7	0.96 ± 0.030	13.0	9.14 ± 2.30
	CP3	94.3 ± 4.0	0.98 ± 0.02	9.6	6.63 ± 3.78
	CP4	87.6 ± 1.8	0.94 ± 0.01	29.5	9.88 ± 4.42
Stepping	CP2	89.8 ± 3.7	0.96 ± 0.03	29.5	5.08 ± 2.75
	CP3	91.6 ± 2.7	0.97 ± 0.02	13.0	6.63 ± 2.78
	CP4	94.4 ± 2.0	0.98 ± 0.01	40.9	9.00 ± 7.30
Average		91.6 ± 3.5	0.97 ± 0.02	22.6 ± 12.5	7.75 ± 3.54

incline walking was $91 \pm 2.7\%$ and $89.6 \pm 3.8\%$, respectively. The average improvement in metabolic cost of transport was $17.4 \pm 10.6\%$ for incline walking and $27.8 \pm 14.0\%$ for stair walking (Figure 11, Figure 9, Table 6).

I.4. Discussion

The primary goal of this study was to validate a practical ankle exoskeleton control scheme that automatically and appropriately adjusts assistance during walking across variable terrain for unimpaired individuals and impaired individuals with some independent walking capacity. We believe this to be a critical first step before designing a study to evaluate the performance benefits of the controller on the variable terrain. Results from our validation experiment indicate that the controller was responsive to the mechanical output from the user's neuromuscular control,

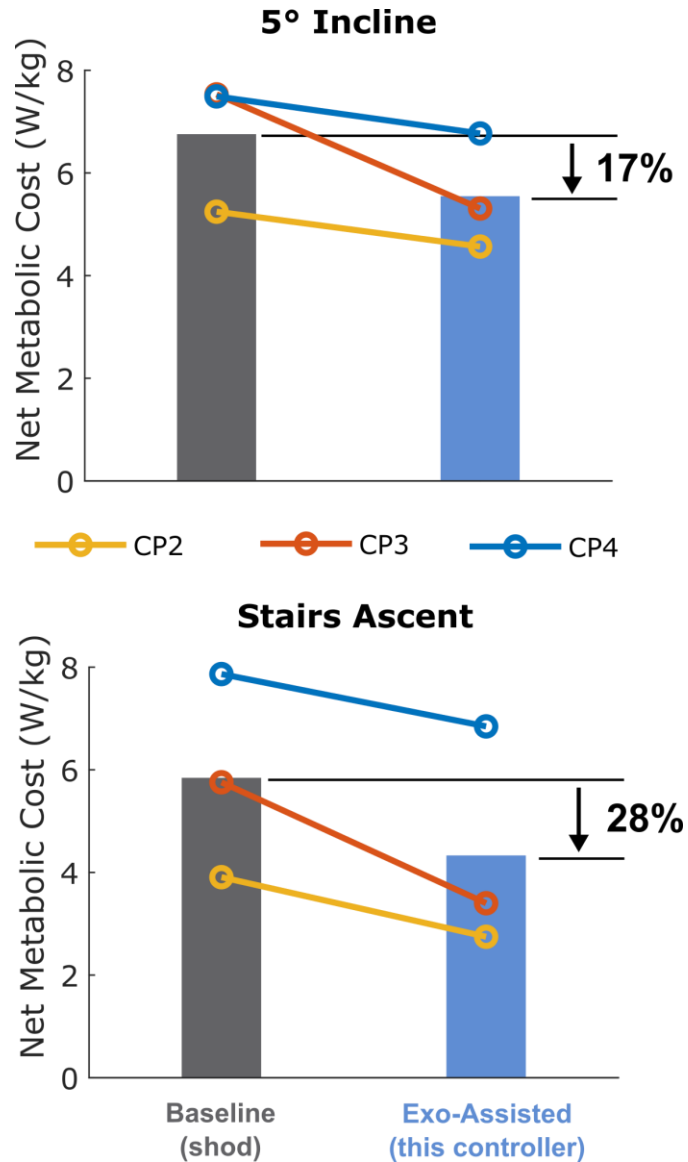


Figure 11. Results from our clinical feasibility tests reporting the change in metabolic cost, averaged over the final 2 minutes of 6-minute steady-state walking trials with the adaptive closed-loop ankle exoskeleton controller for three participants with cerebral palsy (CP2-CP4).

providing appropriate assistance for all evaluated modes of ambulation. Across all participants (unimpaired and CP), we observed high accuracy (87.3%) and a very strong relationship ($R = 95.4$) between the prescribed plantar-flexor torque and the measured biological ankle moment, achieving our goal of an average accuracy greater than 75% and an average correlation coefficient within or above 0.8- 0.9 across the validation tasks. For the unimpaired validation, we achieved our goal of

accuracies greater than 75% and correlation coefficients greater than 0.9 for all tasks. Our clinical feasibility testing results in the 4 individuals with CP suggest that the controller can accurately provide assistance proportional to the biological ankle moment for incline and stair walking, and that doing so may have a metabolic benefit. The controller accuracy outcomes reported in the manuscript reflect the intended use case because the moment prediction accuracy was maintained when torque was actually being provided to the user. Our finding of significantly greater moment estimation accuracy from the post-hoc assessment of adaptive vs non-adaptive control signals highlights the benefits of real-time proportional control.

To the best of our knowledge, this is the first study to report on the development or accuracy of an implemented ankle exoskeleton control strategy across level, sloped, stair, and turn walking in unimpaired individuals or individuals with impaired walking ability. The lack of studies in the literature speak to the difficulty of this task. While controller accuracy was generally similar across all of the conditions, stair ascent and descent were slightly more challenging for the control system (Figure 6). The steps used in this study had a slightly larger rise (0.2 m) than that of the typical step rise (0.18 m), so the stepping accuracy results reported here are likely worse than what would be experienced during normal stair navigation. The individual with CP was not able to safely descend stairs even without the exoskeleton because hand support was not allowed during the validation experiments due to the need to accurately measure the ground reaction forces. While

controller validation data for this task was therefore available, the participant could safely descend stairs with the presented system with hand support.

The analytical model presented in this paper addressed three primary issues with our prior work. First, the regression equation in [39] was developed using a different sensor array. In short, multiple smaller sensors were used across the forefoot. That sensor configuration was time consuming to place for each user and less accurately captured the ground reaction force, therefore necessitating the crude “black box” regression equation approach. Second, the regression equation in [39] was created from a single unimpaired subject walking on level ground, preventing accurate predictions for individuals with impairment and different walking conditions. Lastly, the regression equation had a non-zero y-intercept, which caused an erroneous step-like response at the beginning/end of each stride.

This controller was designed to maximize its practicality for use in real-world scenarios. Over the course of this validation experiment, we found that the simplicity of the control system made donning the exoskeleton quick and easy. The embedded foot sensor design did not require custom placement and was not susceptible to interface degradation or continuity issues – issues that can affect skin electrodes required for controllers dependent upon muscle activity measurement. Our validation measurements were completed without sensor re-calibration over the course of roughly 120 minutes per participant. Assessment of controller accuracy between the conditions at the

beginning and end of the experiment suggest that sensor drift was not an issue over this timer period.

This control system likely has applications for augmenting both unimpaired and impaired walking performance. For unimpaired individuals, this controller may benefit users during challenging locomotor tasks, like extended walking on challenging terrain. For individuals with impairment, the controller is not explicitly intended to “fix” or “correct” an abnormal gait pattern, but rather to support the extensor moment (plantar-flexor moment) during the stance phase (Figure 4A) to reduce the muscular effort and improve walking economy. In a prior study, we demonstrated that providing assistance proportional to the biological ankle moment can reduce the metabolic cost of transport for individuals with cerebral palsy as they walked over-ground around a level oval track. That cohort included individuals with severe walking impairment (Gross Motor Function Classification System Level III) [35]. In the present study, our clinical feasibility testing results showed that improvements in energy cost during incline and stair walking are possible (Figure. 7). Furthermore, we also qualitatively assessed the mechanical power delivered from the exoskeleton relative to the biological ankle power for one unimpaired participant (P1) and the participant with CP (CP1) and found good agreement in application of the exoskeleton’s positive mechanical power during late stance. This approach may be extendable to providing proportional exoskeleton assistance to other joints, including the knee [40].

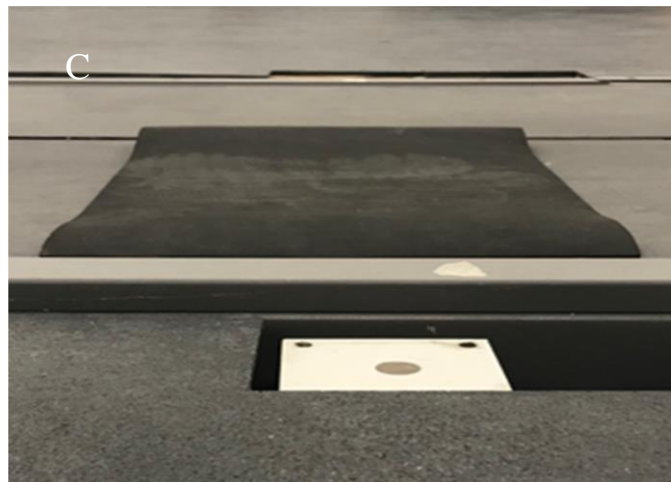


Figure 12. Pictures of the heel on board (A), toe on board (B) and soft foam (C) experimental pilot tests of uneven terrain.

A limitation of this study was that we did not focus on swing phase control and additional work

would be necessary to determine the feasibility of a closed-loop scheme during the swing phase based on the same principle of providing assistance as a percentage of the biological moment. However, this controller can function during the swing phase for all of the presented walking conditions that, at a minimum, mimics the individual's baseline swing-phase ankle function. For unimpaired individuals, zero torque during swing phase allows the user to perform the same swing phase ankle motions as during unassisted walking. For individuals with disabilities, we typically provide a small, nominal amount of dorsi-flexor assistance to mimic their AFOs. Therefore, this controller provides the benefit of powered assistance during stance phase and mimics baseline function during the swing phase. Adaptive swing phase is a focus of future work.

Another limitation of this study was that we assumed the moment arm between the forefoot and the ankle joint remained constant. While we confirmed this assumption was reasonable for the activities reported in this manuscript through analysis of the moment arms and resulting model accuracy, there remains the possibility of reduced accuracy for motions involving both large foot-ground angles and larger ground reactions forces. Future work will investigate accuracy during walking on steeper inclines/declines, and the inclusion of foot angle sensing for further improvements in controller robustness. While preliminary evidence suggests that the carbon fiber footplate distributes loads to the forefoot sensor and allows for maintained controller accuracy when walking on uneven surfaces (Figures 12 and 13, Table 6), additional testing may be necessary.

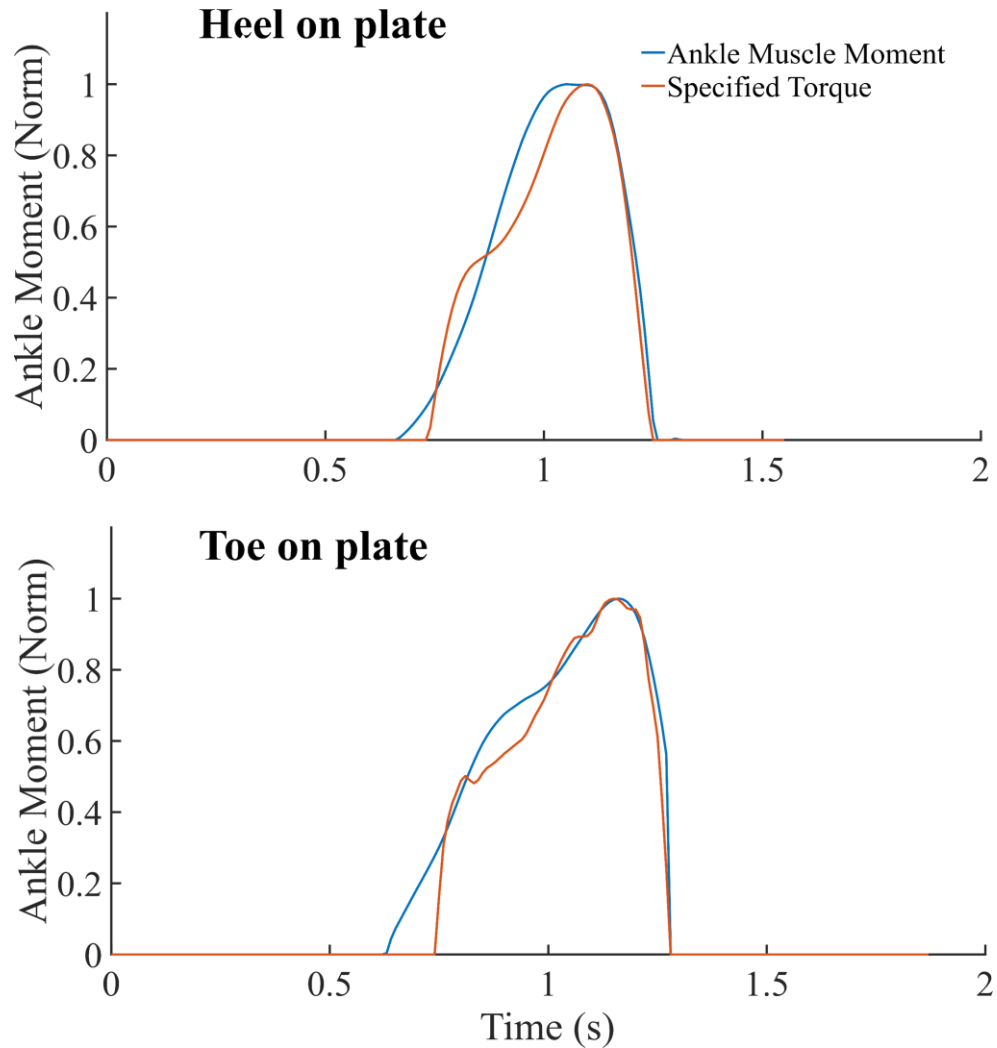


Figure 13. Plots depicting the comparison between the prescribed torque and biological ankle plantarflexor moment for walking over a hard plate with pressure under the midfoot.

I.5. Conclusion

This study demonstrates the ability of our closed-loop ankle exoskeleton controller to accurately adapt assistance across a wide variety of walking conditions without the need for walking condition classification or real-time assessment of muscle activity. Our results from the validation experiment in 6 unimpaired individuals suggest that the foot-sensor-based ankle estimation scheme

Table 6. UNEVEN TERRAIN TESTING RESULTS

Walking Condition	Accuracy %	Correlation Coefficient (R)
Foot on foam	88.2 ± 2.5	0.95 ± 0.02
Heel on board	90.0 ± 7.0	0.95 ± 0.06
Toe on board	91.5 ± 2.5	0.97 ± 0.02

Single subject testing results in participant #3. Results averaged over 3 trials.

was effective for estimating the desired moment during level, 5° incline/decline, stair, and turn walking. While our clinical feasibility testing demonstrates feasibility of use in individuals with CP, additional testing is needed to validate this control system on individuals with different walking disabilities, including those caused by stroke or incomplete spinal cord injury. Future work should more extensively assess how this closed-loop control scheme affects human performance during these locomotor conditions and explore the potential of this exoskeleton controller to facilitate improved real-world mobility for individuals with and without neuromuscular disorders.

II. A Low-Profile Hip Exoskeleton for Pathological Gait Assistance: Design and Pilot Testing

II.1. Introduction

Lower-limb Robotic hip exoskeletons are primarily designed for improving gait function in vulnerable populations, such as the elderly or people with neurological disorders, and for augmenting unimpaired walking or running performance [41]. Many large muscle groups drive hip movement [42], [43]. By providing assistive torque at the hip joint, hip exoskeletons may prove useful for improving mobility by reducing the energy cost of walking [44], [45]. Cerebral palsy (CP), the most common child-onset movement disorder, often leads to excessive hip flexion during walking, elevated energy cost of transport, and hip disorders [46], [47]. Recently, studies have investigated the use of wearable robotic devices to improve walking function in individuals with CP [48], [49], with only one study investigating the use of a hip-only exoskeleton for gait training [50]. However, for the purpose of improving mobility, we are not aware of any study that has demonstrated that untethered hip exoskeleton assistance may improve gait biomechanics and energy cost while walking with the device in this patient population.

When designing hip exoskeletons, device mass, fit and comfort are essential factors that influence whether a device can provide an energy cost benefit. The mass of existing hip exoskeletons ranges from 2.8 – 7.6 kg, and some have demonstrated the ability to reduce the metabolic cost of transport during walking in unimpaired individuals. For example, the hip exoskeleton's from HONDA [51] and Samsung Institute of Technology have a mass of 2.8 kg [52]. The Soft Exosuit, designed by Harvard Biodesign Lab [53], the PH-EXOS [54], and the Lightweight Active Pelvis Orthosis [55], have masses of 7.57, 3.5, 4.2 kg respectively. A limitation of existing hip exoskeleton studies is that most included only male participants. The pelvis geometry is complex and anthropometric gender difference exist, including a wider hip to

waist ratio that can affect arm swing [56]. Nearly all hip exoskeletons have been designed by, and tested in, the adult male population [52], [57], [58]; only a small number of female subjects have been reported in the literature [59], [60]. Therefore, there may be a need for more research on hip exoskeletons that are designed to work well on female anatomy and in children.

Providing beneficial hip exoskeleton assistance to the user during walking is dependent upon an effective high-level control strategy. A common approach is the prescription of a predetermined desired torque trajectory for different tasks, including walking, running, and stair climbing [52], [54]. Impedance/admittance control is a frequently used hip exoskeleton control strategy in which the device helps the user to complete a movement by considering the interaction torque between the wearer and the exoskeleton [59]. Electromyography (EMG) signals have been used to control hip devices as a link between the exoskeleton and gait cycle phases, and a measurement of user motion intention [61]. Another approach is oscillator-based control, which utilizes the periodic nature of walking [55], [62]. Most research on hip exoskeletons has focused on level ground [45]. For the few studies reporting incline or stair walking, different torque patterns were prescribed for the different grades [63]. Few studies have reported a single control strategy that is adaptive and effective across different terrains and walking patterns (typical or pathological) [64].

An overarching goal of our research is to design effective wearable robotic solutions to improve mobility of individuals with CP. The purpose of the present study was to design a novel autonomous hip exoskeleton with a user-adaptive control strategy capable of reducing the energy cost of level and incline walking in individuals with and without walking impairment. Our specific goals were to (1) validate our control strategy by comparing the hip assistance torque profile to the biological hip moment during level ground and incline walking, (2) demonstrate the ability of our system to reduce the energy cost of level and incline walking in unimpaired individuals, and (3)



Figure 14 . Pictures of our hip exoskeleton.

complete a pilot/feasibility experiment of hip exoskeleton assistance during level walking in CP. The primary contributions of this paper include the (a) design and validation of a novel low-profile cable-driven hip exoskeleton, (b) demonstrated effectiveness of an adaptive proportional hip joint moment control strategy across two terrains, and (c) the first initial evidence on the ability of hip assistance to improve assisted walking performance in CP.

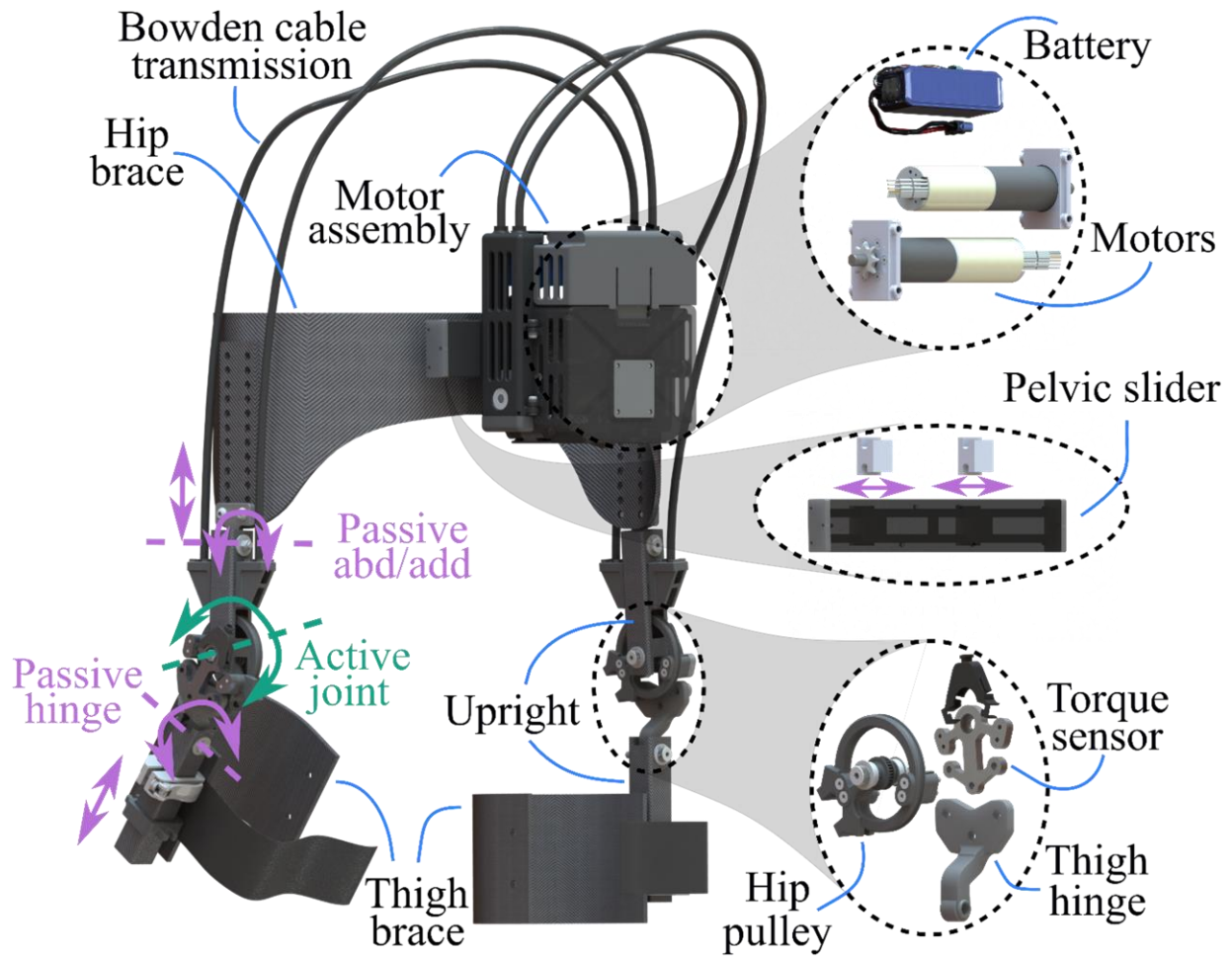


Figure 15. 3D CAD model of the hip exoskeleton components. Purple arrows show the passive DOFs and the green arrow shows the active joint

II.2. Methods

II. 2. 1. Electro-Mechanical Design

We designed a lightweight, low-profile, and untethered hip exoskeleton to provide hip flexion and extension assistance during level and incline walking. The main mechanical design goals were to create a system that (1) provided a relevant magnitude of assistance in a lightweight package, (2) minimized the outward protrusion from the pelvis and thigh to allow natural arm swing,

Table 7. PARTICIPANT INFORMATION

Participant	Condition	Gender	Age (yrs)	Weight (Kg)	Hight (m)	Setpoint (Nm)		Speed (m/s)
						<i>Extension</i>	<i>Flexion</i>	
P1	Unimpaired	Female	31	62	168	6	4	1
P2	Unimpaired	Female	29	55	155	5	3	0.9
P3	Unimpaired	Female	24	51	160	6	4	1.2
P4	Cerebral Palsy	Female	26	49	121	5	4	0.3

particularly in females, and (3) was adjustable and able to accommodate a broad range of anatomies.

Our design, presented here, included a motor assembly, pelvic braces, Bowden cable transmission, and thigh assemblies (Figure 14). To provide active flexion-extension assistance, DC motors actuated cables connected to a bi-directional pulley located at each hip center of rotation. The design also included two additional passive degrees of freedom in the form of abduction/adduction hinges, one below and one above the hip joint, to accommodate out of plane lower-limb motion during walking, including hip adduction, abduction, and circumduction. The total mass of our hip exoskeleton was 2.1 kg, including the 910 mAh battery capable of providing up to 45 minutes of assistance. The majority of the added mass was centered on the low back near the whole-body center of mass to minimize the energetic burden of load carriage [25] (Table I). The pelvic brace, thigh cuffs, and uprights were made of carbon fiber to reduce weight while adding structural rigidity.

The waist assembly consisted of two carbon fiber pelvic braces attached to a horizontal slider to enable hip circumference adjustability. The hip joint assembly and the thigh cuffs were connected to the exoskeleton with vertical adjustability to accommodate different pelvis and thigh lengths. The maximum sagittal plane outward protrusion of the device from the side of the pelvis, hip, or thigh was 5 cm.

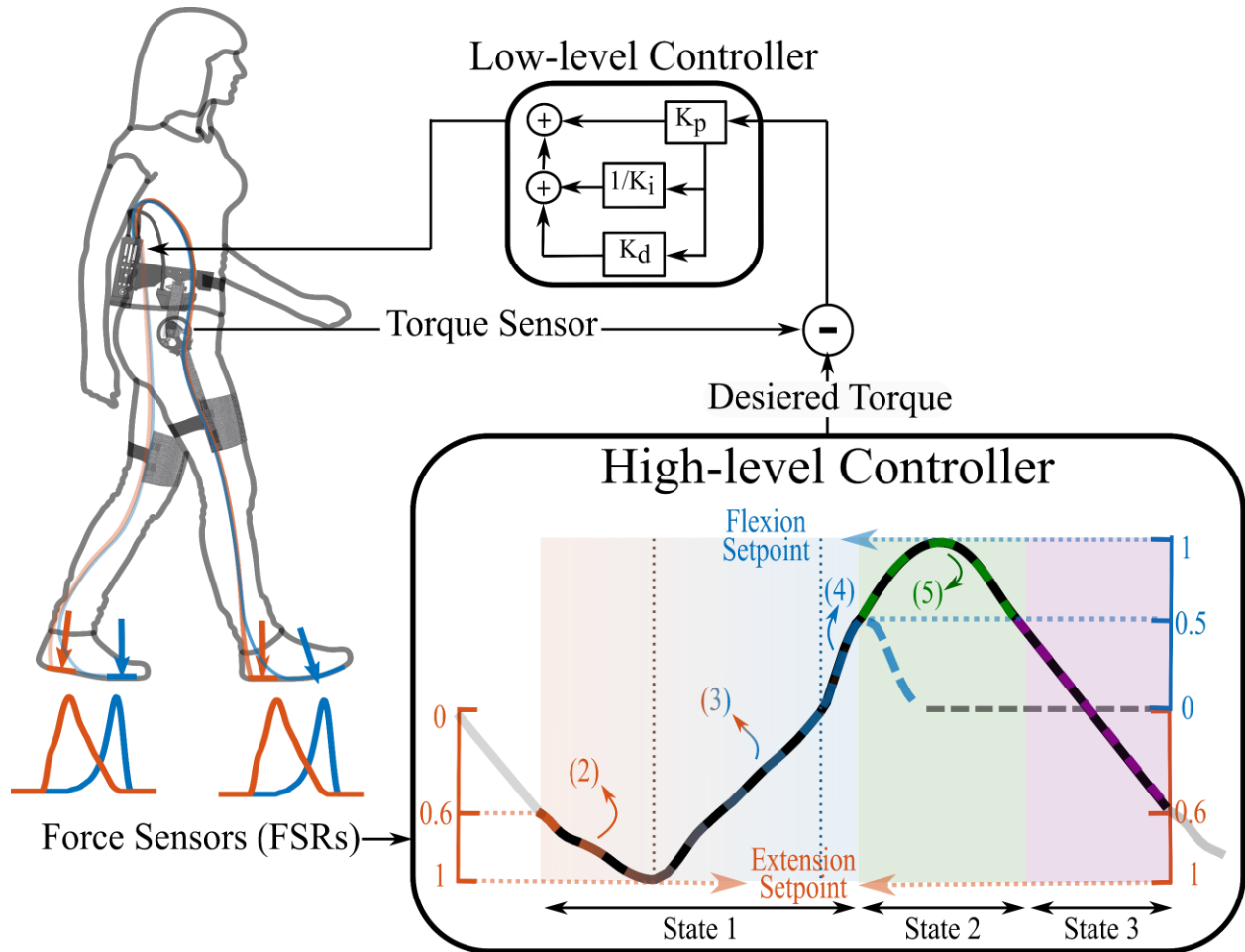


Figure 16. Schematics of our hip exoskeleton control strategy.

The motor assembly included an electrical module with custom printed circuit board, microcontroller (Teensy 3.6), a Bluetooth module, motor drivers, signal conditioners; two brushless DC motors (Maxon EC-4pole, 24 V, 90 W, 89:1 gearbox); and interchangeable lithium polymer battery (E-Flite 22.2 V, 910 mAh). Each motor's output shaft connected to a chain and sprocket that subsequently interfaced with the Bowden cables that terminated at the hip joint pulley. The transmission system gear reduction was 3:1, which, combined with the 89:1 planetary gear box, resulted in a total system reduction of 267:1. This gear reduction allowed for a maximum static torque of 12 Nm. A custom torque sensor was used at the hip joint for closed-loop low-level motor control.

II. 2. 2. Control Overview and Theory

We designed a high-level control system to provide autonomous hip flexion and extension assistance. The main controller design goals were to create a system that was able to respond to user intention and automatically adapt to normal and pathological gait patterns and different terrains. Our approach was to provide assistance proportional to the biological hip joint moment that was estimated in real-time. We utilized embedded heel and fore-foot sensors to estimate the biological hip joint moment during stance phase (Figure 16). During swing phase and the stance-swing transition, we developed equations to match the biological moment as a function of the stance phase moment and time. A low-level proportional-derivative (PD) torque-feedback controller was used to track the high-level desired torque signal.

Operation of the controller involved establishing flexion and extension setpoints for each user based on their body mass and walking speed, and a 5-stride baseline walking period to calibrate the sensors. The user-adaptive input into the controller was based on the relative measurement of force sensitive resistors (FSRs) placed under the forefoot and heel, as in

$$f_s(FSR) = FSR_{forefoot,relative} - 4 \times FSR_{heel,relative} \quad (1)$$

where $FSR_{forefoot,relative}$ and $FSR_{heel,relative}$ was the real time FSR reading divided by its maximum value during the baseline walking calibration. The FSR readings were also used to inform a finite state machine that dictated the desired torque signal.

State 1—Stance

During early stance, which started when the heel was on the ground and ended when f_s was negative and the derivative of f_s became positive, the exoskeleton provided extension assistance starting from 60% of the extension setpoint, as in

$$f_s(FSR) = 0.6 \times Setpoint_{extension} + 0.4 \times Setpoint_{flexion} \times f_s \quad (2)$$

where $\tau_{s,1}$ was the desired torque in state 1. $Setpoint_{extension}$ and $Setpoint_{flexion}$ were the extension and flexion setpoints, respectively.

While f_s was negative, the exoskeleton provided extension assistance as in Equation (3), and when f_s was positive, the exoskeleton provided flexion assistance, as in Equation (4)

$$\tau_{s,1} = Setpoint_{extension} \times f_s, \quad f_s < 0 \quad (3)$$

$$\tau_{s,1} = 0.5 \times Setpoint_{flexion} \times f_s, \quad f_s \geq 0 \quad (4)$$

State 2—Stance-Swing Transition

State 2 designated the stance to swing transition. This state included late stance, which started when f_s was positive and the derivative of f_s transitioned from positive to negative and ended at 30% of the moving average of the swing phase duration. The desired torque in this state was governed by the parabolic function defined in Equation (5).

$$\tau_{s,1} = (0.5 + 0.5 \times (\alpha(t_2 - t)/(t - \beta))) \times Setpoint_{flexion} \quad (5)$$

where α and β are tuning variables and t is the amount of time in the state 2 divided by the previous average of state 2 total time. The desired torque in this state started at 50% of the flexion setpoint, reached the full flexion setpoint at the peak of the parabolic equation, and then reduced to 50% of the flexion setpoint at the end of the state.

State 3—Late Swing

State 3 was the remaining 70% of the swing phase. The desired torque during this phase was in the shape of a linear transition starting from 50% of the flexion setpoint and ending at 60% of the extension setpoint.

II. 2. 3. High-Level Controller Validation

We sought to validate the ability of our high-level exoskeleton controller to prescribe hip torque that was proportional to the biological hip joint moment. Validation was completed in 3 unimpaired female participants (Table 8) during level and 5° incline walking on a force-measuring treadmill (Bertec). An 8-camera motion capture system (Vicon) was used to record marker trajectories simultaneously with the ground reaction forces. The study was approved by the Institutional Review Board of Northern Arizona University (NAU) under protocol #986744.

II. 2. 4. Low-Level Controller Validation

To evaluate the performance of our low-level PD controller and mechanical rigidity of the hip joint assembly, and pelvis and thigh attachments, we completed a separate torque tracking experiment with Participant 1 walking at 0.75 m/s, 1 m/s, and 1.25 m/s. We tested the ability of our hip exoskeleton to provide 8 Nm of extension assistance and 5 Nm of flexion assistance (Figure. 3). These setpoints were selected based on prior reports of relevant torque magnitudes during [55].

II. 2. 5. Unimpaired Walking Performance Validation

Utilizing the same participants from the controller validation experiment, we validated the relevance of our proportional hip moment controller by measuring the metabolic cost of transport during walking with and without the exoskeleton on the treadmill (level and 5° incline) at each participant's preferred speed. Oxygen and carbon dioxide levels were recorded using a wearable metabolic system (Cosmed K5). Prior to the walking trials, we recorded standing rested basal metabolic rate for 2 minutes. Each walking trial lasted for 5-minutes. Net metabolic rate was computed and compared between shod (no device) and exoskeleton-assisted walking as in [49].

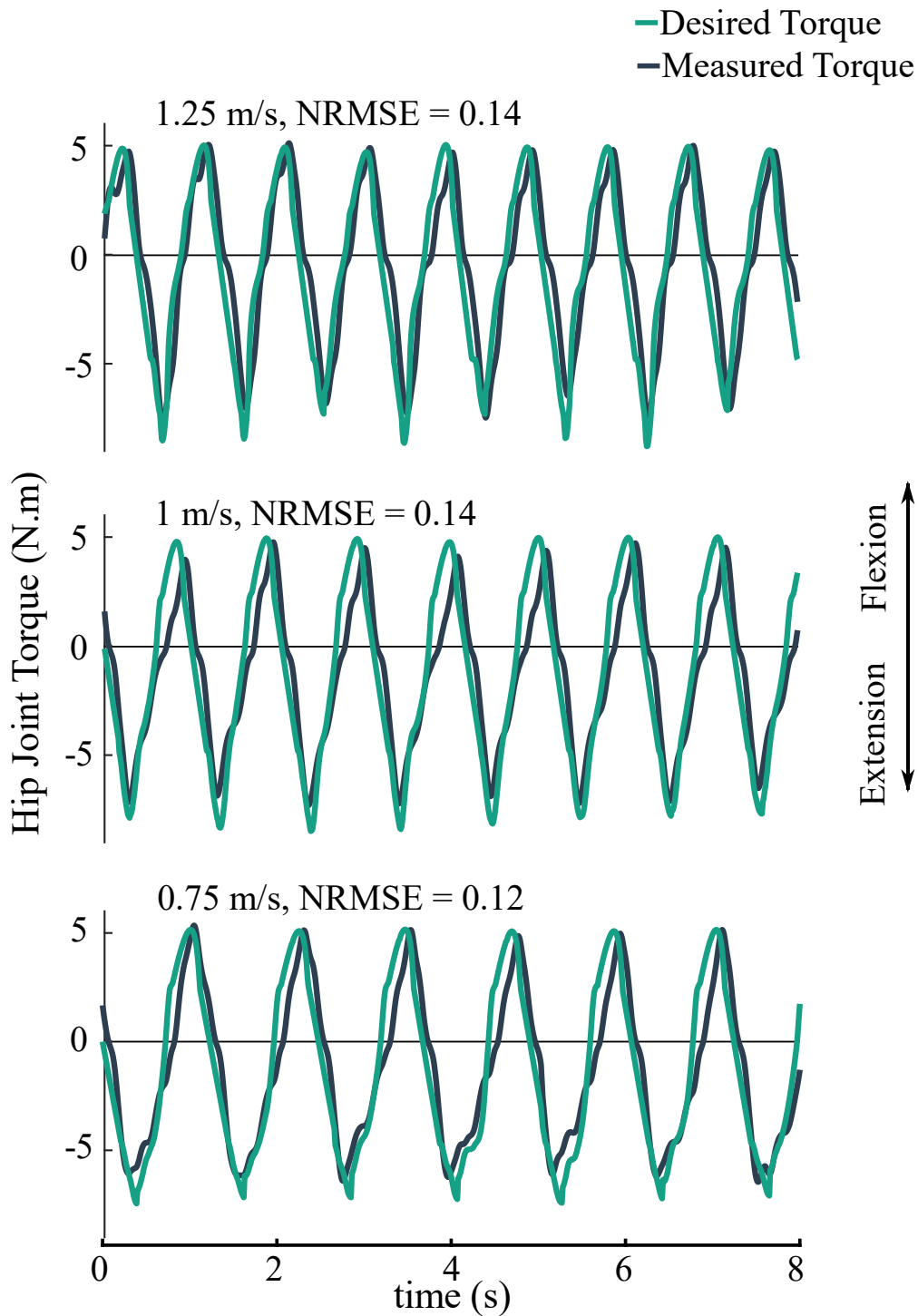


Figure 17 . Desired torque and torque sensor data of one unimpaired participant in real time during walking over treadmill at different speeds with 8 Nm extension and 5 Nm flexion

II. 2. 6. Unimpaired Walking Performance Validation

We performed clinical feasibility testing of our hip exoskeleton with a 24-year-old female with significant walking impairment from CP (Gross Motor Function Classification System (GMFCS)

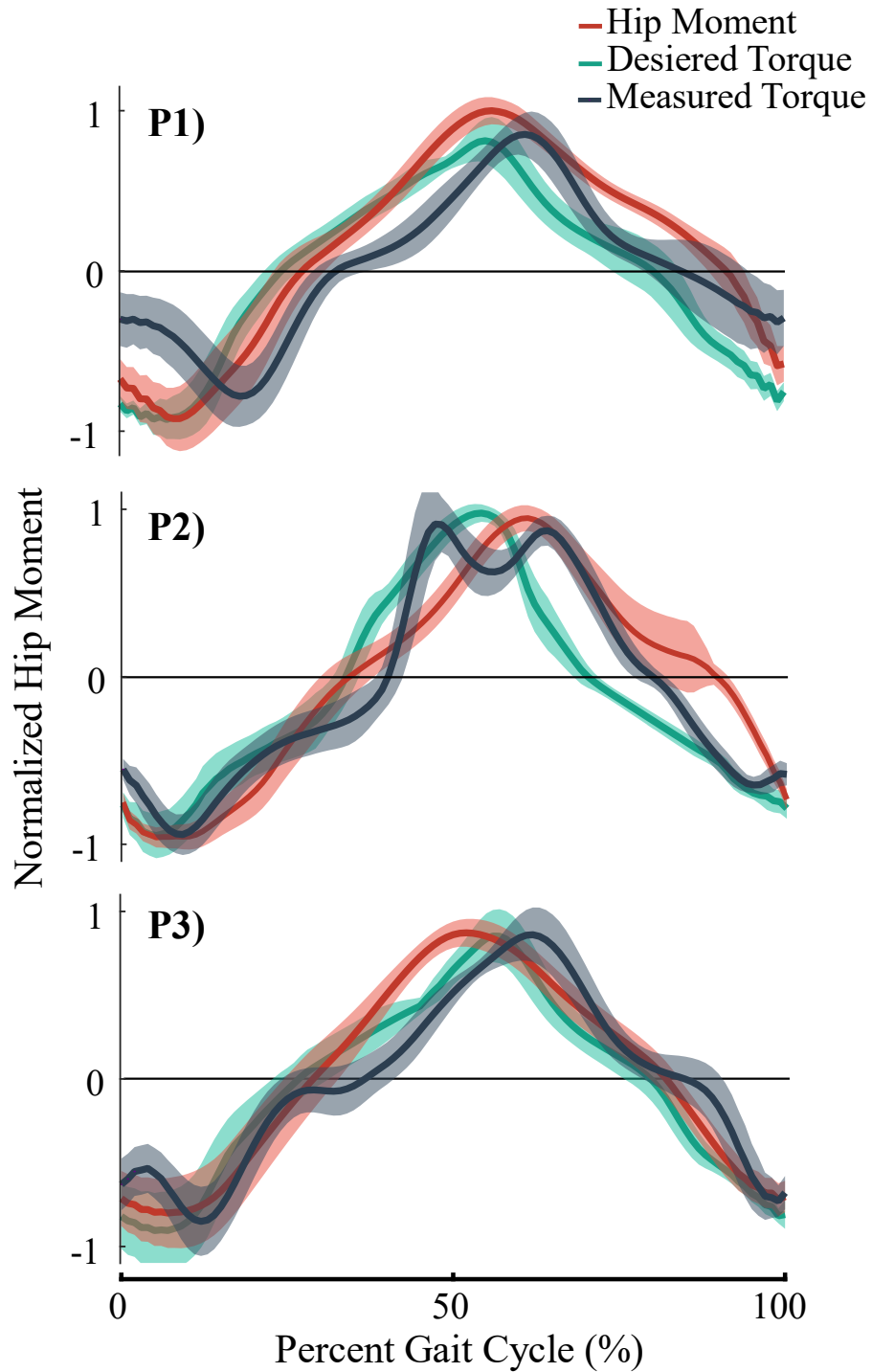


Figure 18 . Desired torque and torque sensor data of three unimpaired participants in real time during walking level ground.

Level III). Following a 5-minute acclimation session, the participant completed treadmill walking trials at her preferred speed with and without the hip exoskeleton. During these trials, we recorded EMG of the Rectus Femoris and Semitendinosus muscles, ground reaction forces, marker

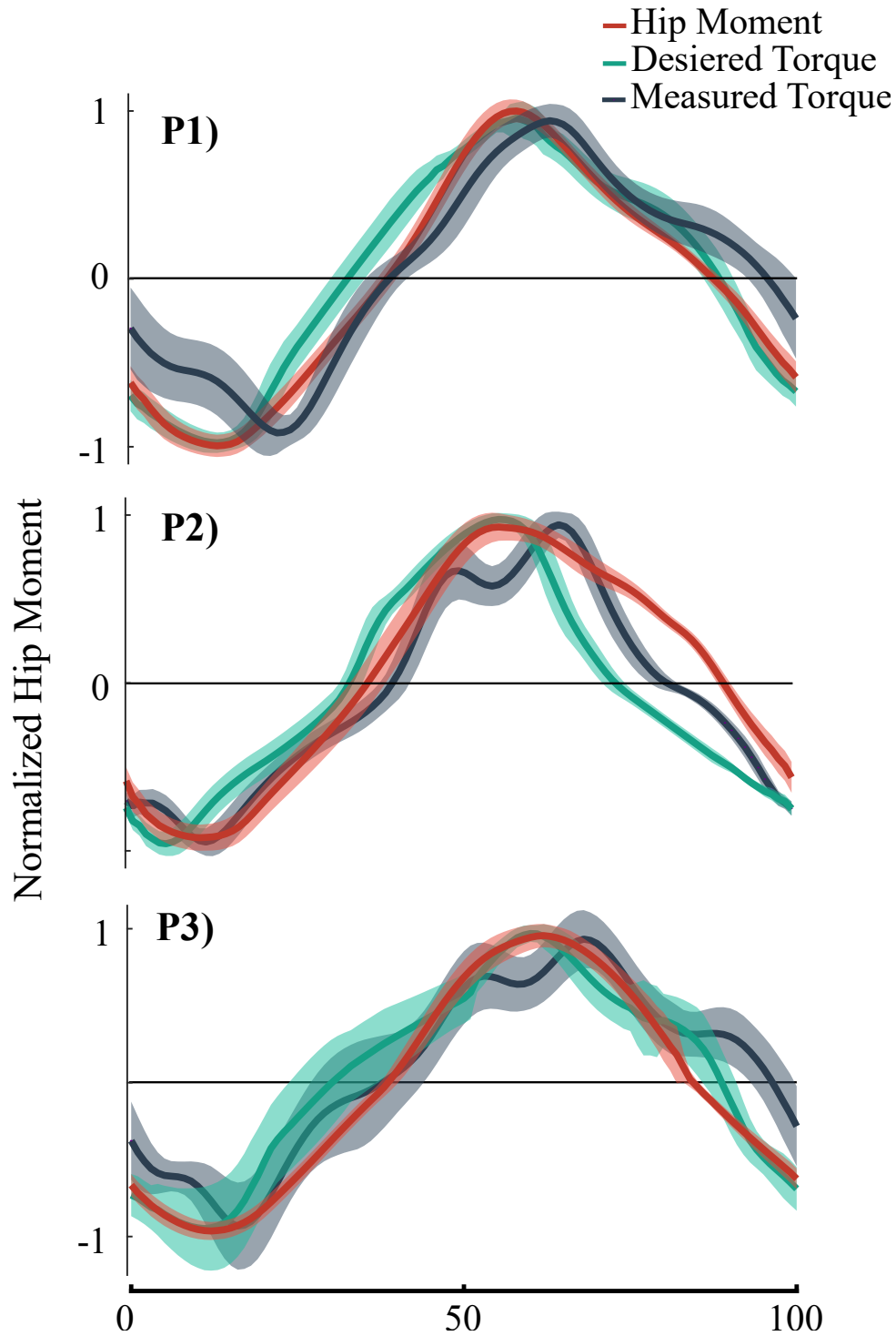


Figure 19 . Desired torque and torque sensor data of three unimpaired participants in real time during walking level ground

trajectories, and metabolic energy consumption as reported above in the unimpaired walking methods section.

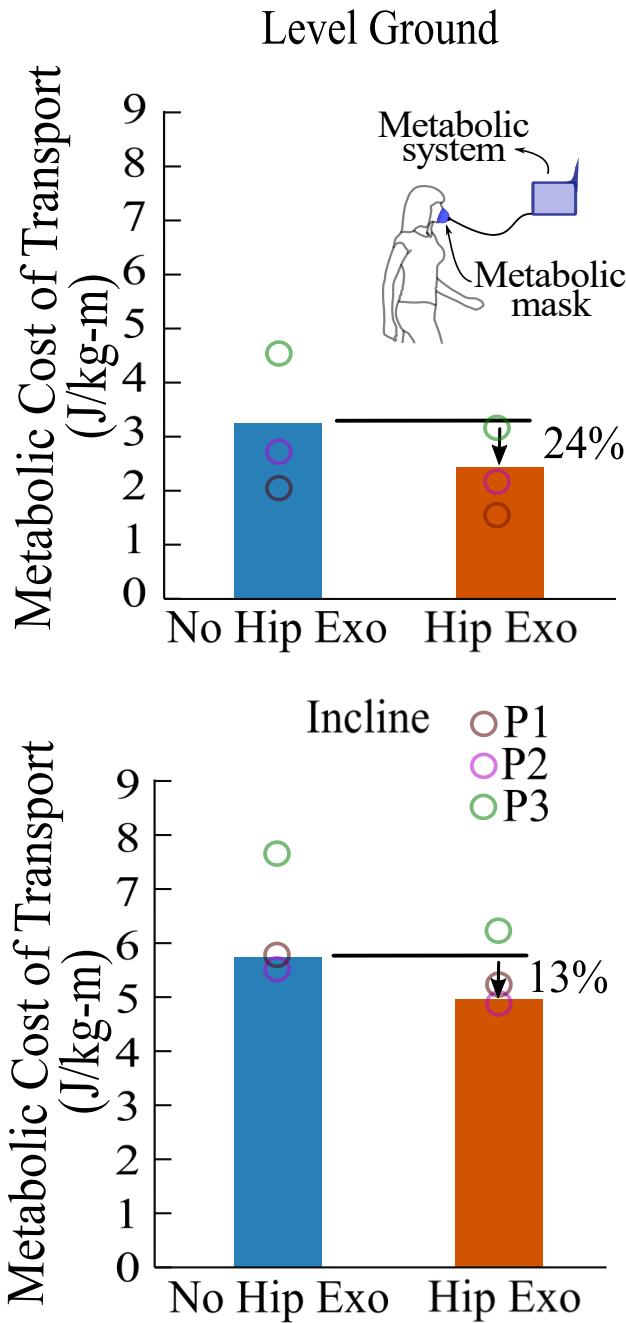


Figure 20. Average metabolic energy consumption reduction of 3 unimpaired subjects during level and incline walking at their preferred speed.

II. 2. 7. Data Processing

After scaling a musculoskeletal model to the anthropometrics of each participant in OpenSim 3.3, we computed joint angles and biological moments during each assisted walking trial using OpenSim's Inverse Kinematics and Inverse Dynamics analyses, respectively. We computed Root

Table 8. HIGH-LEVEL CONTROLLER ACCURACY

Participant	RMSE (%)		R ²		VAF	
	Level	Incline	Level	Incline	Level	Incline
P1	32	20	0.77	0.90	0.74	0.89
P2	32	34	0.70	0.70	0.68	0.67
P3	17	27	0.92	0.83	0.92	0.83
CP	25	-	0.85	-	0.84	-
Mean	26±7	27±7	0.81±0.09	0.81±0.10	0.80±0.11	0.80±0.11

Root Mean Square Error (RSME), coefficient of determination (R2), and Variance Accounted For (VAF) between biological hip moment and desired torque of the hip Exoskeleton.

Mean Square Error (RMSE), coefficient of determination (R2), and Variance Accounted For (VAF) between the normalized biological moment and the desired torque (Table III). Kinematic, kinetic, and EMG data were segmented, normalized to percent gait cycle and averaged. Metabolic data were averaged over last 2 minutes of walking.

II.3. Results

All of our participants safely completed each walking trial without any adverse events.

II. 3. 1. High-Level Controller Validation

The mean RMSE between the estimated hip moment (i.e., the desired torque signal) and the biological hip moment computed from inverse dynamics for all participants was 26% for level walking and 27% for incline walking (Table 7). The mean coefficient of determination (R²) and variance accounted for (VAF) between the estimated hip moment and the measured biological hip moment for all participants were 0.81 and 0.80, respectively, for both level and incline walking.

II. 3. 2. Low-Level Controller Validation

The mean RSME between the desired torque and the torque measured from the torque sensor at the exoskeleton's hip joint was less than 2 Nm across the three walking speeds and tested

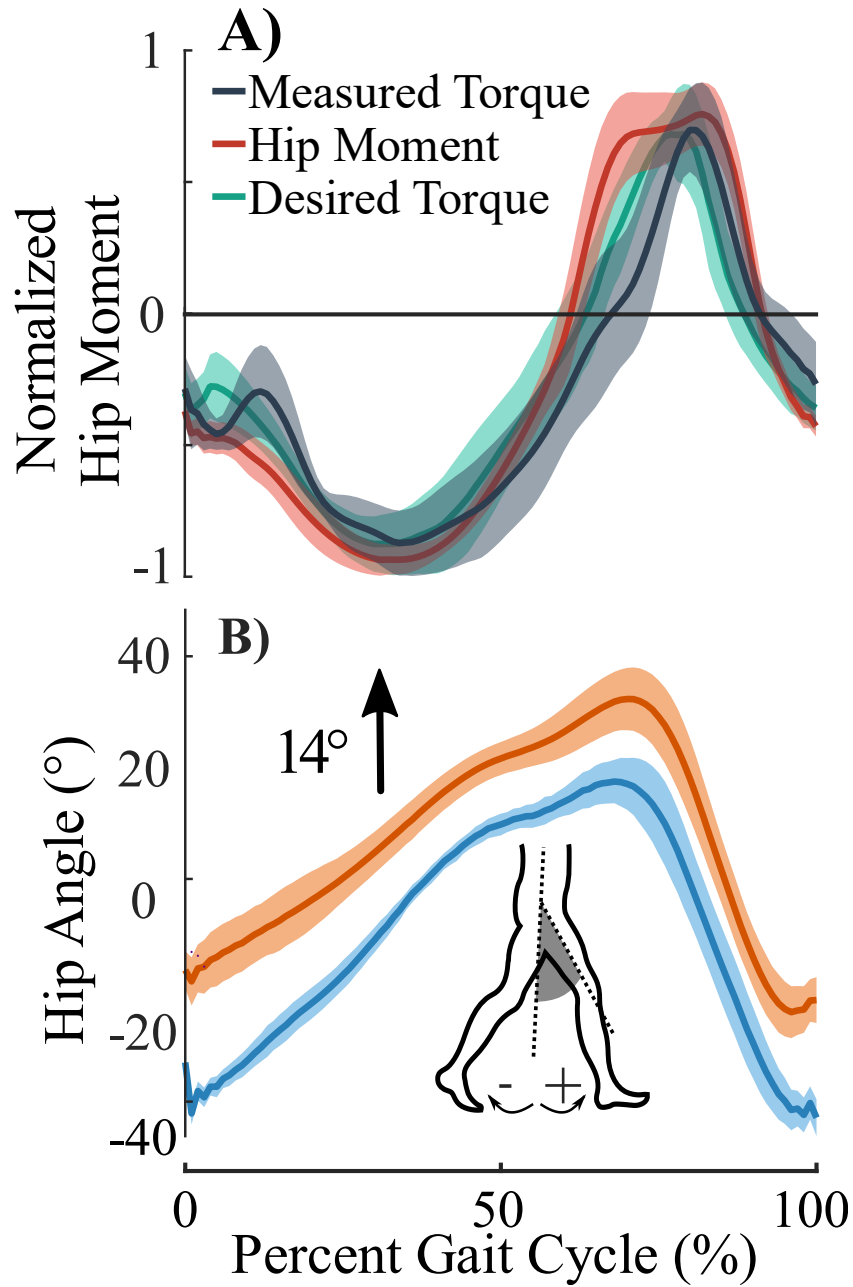


Figure 21. Data of one CP subject at her preferred speed during level walking: A) Biological moment, desired torque and torque sensor data average versus percent gait. B) Average of hip joint angle.

setpoints (Table 8). The average Normalized Root Mean Square Error (NRSME) for an extension setpoint of 8 Nm and flexion setpoint of 5 Nm across the different speeds was 0.13.

II. 3. 3. Walking Performance Outcomes

Our hip exoskeleton reduced the metabolic cost of transport during level and incline walking by $24 \pm 5\%$ and $13 \pm 5\%$, respectively, for unimpaired individuals compared to walking without the device (Figure 20). The hip exoskeleton reduced the metabolic cost of transport for the individual with CP by 15% compared to walking without the device (Figure 21 and 22). Hip exoskeleton assistance reduced excessive hip flexion in the participant with CP by 14° compared to walking without the device; rectus femoris muscle activity decreased by 23%, while semitendinosus muscle activity decreased by 46%.

II.4. Discussion

The overarching objective of this work was to design and test a low-profile and adaptable hip exoskeleton for improving mobility in individuals with and without walking impairment. Our prototype exoskeleton fulfilled our design goals by reliably providing 5-8 Nm of flexion-extension assistance while adding just 2.1 kg to the user. We confirmed that our low-profile pulley and cable transmission system (<5 cm of outward protrusion from the pelvis and thigh) allowed for natural arm swing, even in females. Built-in adjustability accommodated a range of anatomies. A mean NRSME of 0.13 between the desired and measured torque, assessed across the typical range of walking speeds (0.75-1 m/s), provided confidence in the electromechanical performance of the system. We are unable to compare our torque tracking results to other devices because we were unable to locate any prior study in the literature reporting this measure.

We fulfilled our first goal of validating an adaptive proportional hip moment control strategy by demonstrating that the hip assistance torque profile closely followed the biological hip moment during level ground and incline walking. Our high-level control strategy was able to predict the real-time biological hip moment across all participants (unimpaired and CP) with 27% error and

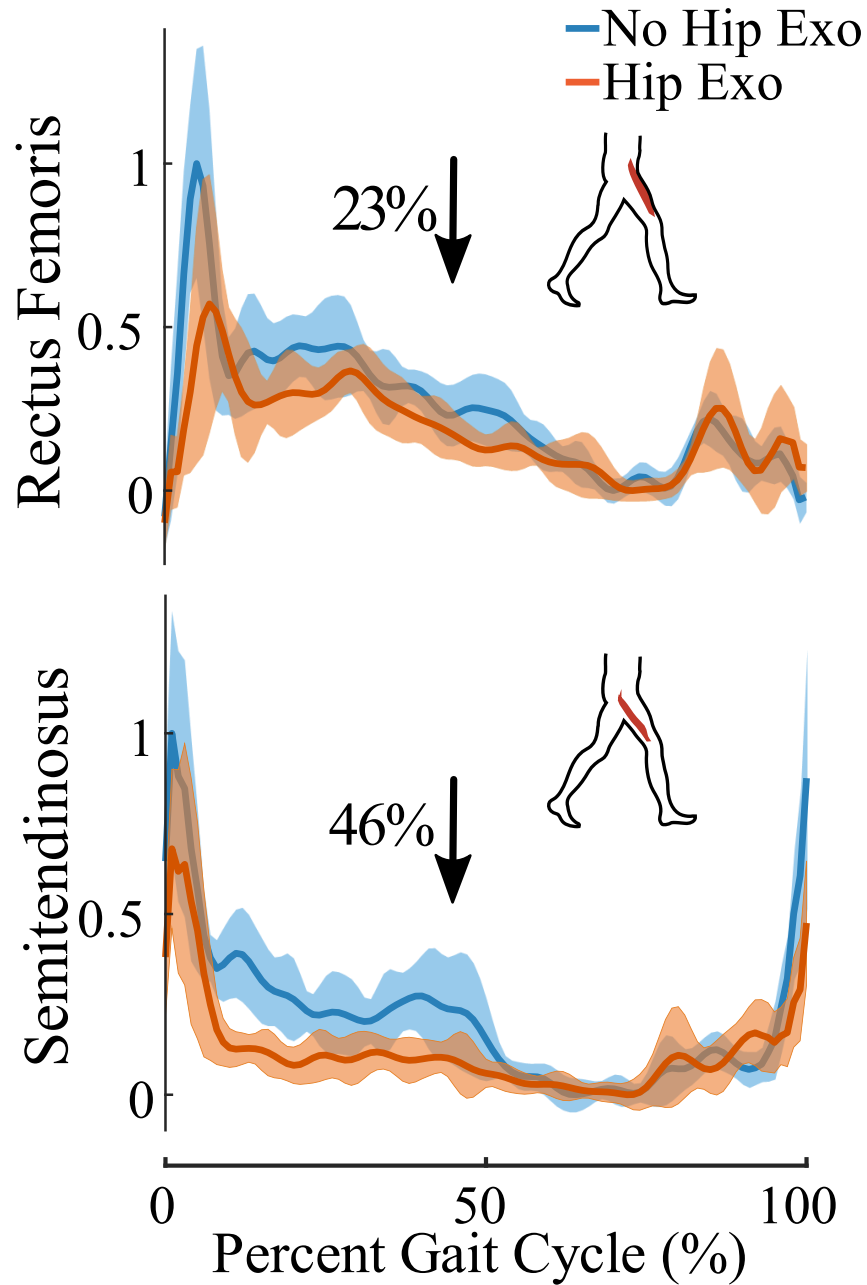


Figure 22. normalized EMG of rectus femoris and semitendinosus of one CP subject at her preferred speed during level walking

high relationship ($R^2 = 0.81$, and $VAF = 0.80$) on both level and incline terrains. While our results should be interpreted with caution because our sample size was very small, we fulfilled our second goal by demonstrating the ability of our system to reduce the energy cost of level and incline walking in unimpaired individuals. Adaptive hip extension and flexion assistance resulted in a

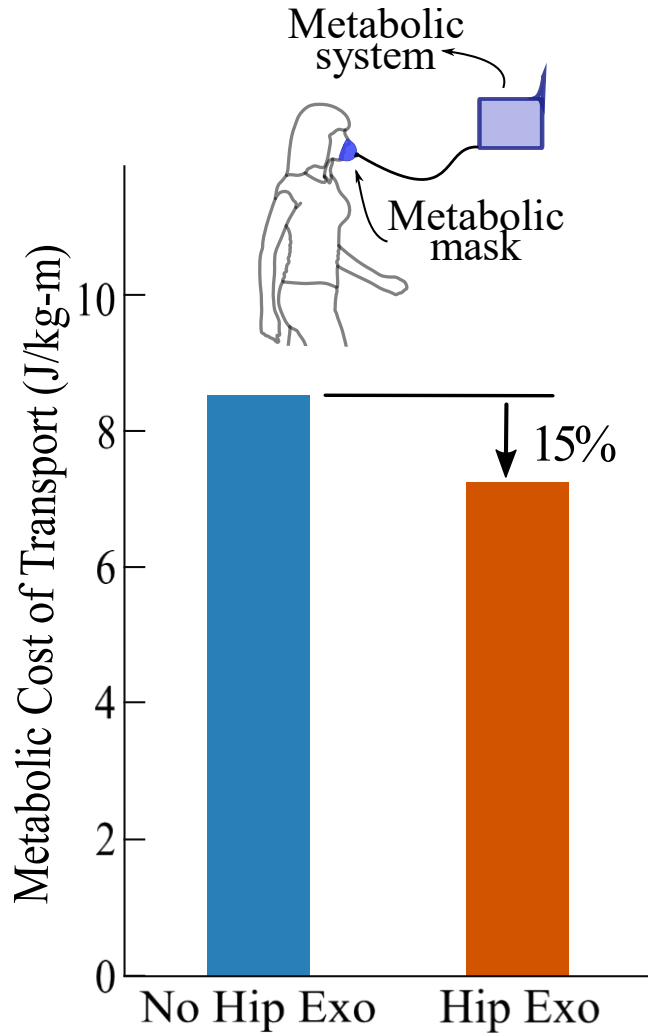


Figure 23. metabolic energy consumption of one CP subject at her preferred speed during level walking on 10 gait cycles with and without hip exoskeleton.

24% reduction in energy cost of level walking and a 13% reduction in energy cost of incline walking. For level walking our results were similar to the greatest previously reported reduction from a hip exoskeleton (19.8% [45]). Again, however, while we observed consistent improvement across both terrains, our results need confirmation in a larger cohort. One potential explanation for the observed reduced effectiveness of hip assistance during incline walking is that incline walking may decrease demand placed on the hip joint and increase the demand placed on the ankle joint.

We fulfilled our third goal of completing a pilot feasibility experiment of hip exoskeleton assistance during level walking in CP. Hip assistance helped our participant with CP walk in a more upright pattern, and reduced hip flexor and extensor muscle activity by 23% and 46%, respectively. This culminated in a 15% improvement in the energy cost of level walking for this participant. To the best of our knowledge, this study is the first to report findings on the potential for improved walking performance while using an untethered robotic exoskeleton in CP. While much additional research is needed, our findings suggest that hip exoskeleton assistance may be a beneficial mobility aid for this patient population.

III. Developing a Synergistic Control Strategy for Knee and Ankle Exoskeleton Assistance

III.1. Introduction

Many studies have been conducted to design exoskeletons in order to assist impaired walking [65], [49]. However, no viable options are available for individuals with moderate-to-severe neuromuscular impairment, like from cerebral palsy (CP), but who are able to walk in some capacity [66]. Commercial full-body exoskeletons, like the EksoGT from Ekso Bionics, are likely too big, bulky, and slow to help a child with some walking ability. At the same time, light-duty, single joint exoskeletons may not provide enough assistance for patients with severe CP to walk independently. Therefore, our goal is to design a device that fits in the middle: a lightweight multi-joint exoskeleton where each joint works in coordination with one other.

Given the fact that human locomotion is a complicated task [67], analyzing the biomechanics of lower extremity joints and estimating the joint moment during human walking is challenging. One of the critical needs of estimating real-time joint moments is in designing and controlling assistive devices for unpaired individuals and individuals with impaired mobility. Powered assistive devices with complex control strategies and multiple input variables make the system vulnerable to uncertainties of input variables [68]. However, Existing methods require multiple sensors to provide an accurate joint moment estimation and are too complex to be incorporated in the control system of an assistive device.

Human joint moment can be predicted using artificial intelligence by proposing joint moment prediction models based on prior knowledge about biomechanics of human joints and response data from experiments [69]–[72]. The forward dynamics approach, which applies measured real-time muscle activity to a musculoskeletal model, is also a common way to estimate

joint moments during locomotion [73]–[76]. However, these methods are limited when applying to assistive devices for people with impaired function because the users do not have a normal muscle activation pattern, which is often required to calculate the desired assistance needed for a specific movement. Reducing the noise of the muscle EMG signal and improving measurement accuracy is another challenge, making these approaches less optimal for assistive devices.

The inverse dynamics method, which requires motion and force information of a movement, is another approach to calculate joint moments during an activity. Although this approach does not require EMG processing, it requires a lot of calculation, making real-time application difficult [71]. Another limitation is the measurement of ground reaction force (GRF) - the most common way of measuring GRF using stationary force plates especially limits the application of this approach because such stationary devices restrict the application of this method. Liu and his colleagues proposed a mobile force plate that uses three triaxial gyroscopes, accelerometers, and force sensors under the ball of the foot and under the heel [77]. They used 18 sensors (9 for each foot) to estimate vertical and horizontal ground reaction forces using complicated mathematical calculations with 10.6% and 13.5% errors. Another study estimated GRF using pressure insoles under the foot. Despite the fact that the portable system allows for more activities, calculating GRF in that study is computationally expensive [78], [79].

Our first objective was to develop a simple real-time knee as well as ankle joint moment prediction model and verify our model by comparing the predicted joint moment with that of estimated by Opensim[®]. Our second objective was to use the model to create an adaptive control strategy capable of providing synergistic ankle and knee assistance based on real-time joint moment estimation. We validated our coordinated controller by comparing the metabolic cost of

transportation and ankle as well as knee joint angles with a reference controller by testing on an unimpaired individual.

III.2. Method

We developed a strategy to control a light ankle-knee exoskeleton based on the calculated biomechanical moment of the respective joints. We used Force Sensitive Resistors (FSRs) to estimate ground reaction forces. The ankle and knee joint moments were calculated using inverse dynamics equations.

III. 2. 1. *Ground Reaction Forces*

There are two regions under the foot that are contacting the ground: the ball of the foot and heel. The mid-foot is not touching any surface because of the arch [14], [15]. Therefore, we calculate the vertical ground reaction force as follow:

$$G_y = N_{forefoot} + N_{heel} \quad (1)$$

Where $N_{forefoot}$ and N_{heel} are the normal force applying to the forefoot and heel from the ground. Assuming the foot is not slipping during stance but rolling on ground, the ground reaction force in the x direction (G_x) is a function of G_y and rolling friction coefficient (f_r) [80], [81].

$$G_x = G_y \times f_r \quad (2)$$

By rearranging equation 2, we estimated f_r by dividing the G_x by G_y from the force plate. Based on f_r and the direction of body force on the ground (Figure 24). To simplify our estimation, we assume f_r as a constant number, with a sign change almost in the mid-stance, we have:

$$G_x = (N_{forefoot} - N_{heel}) \times f_r \quad (3)$$

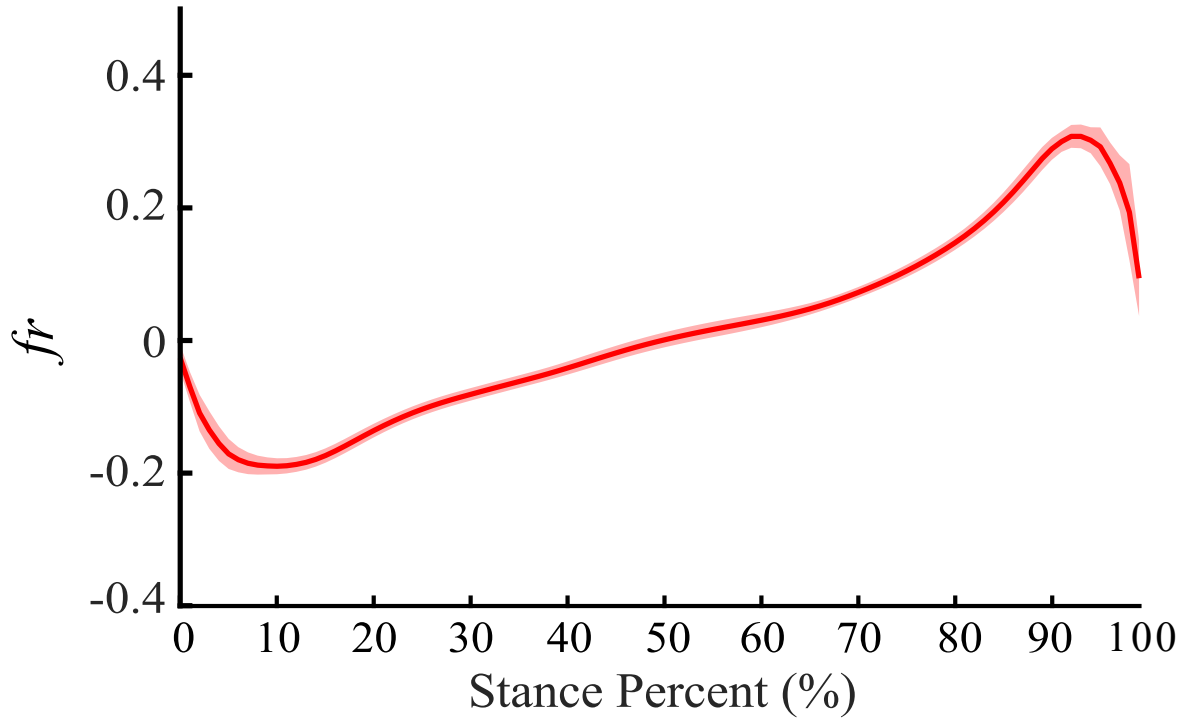


Figure 24. Rolling friction coefficient of unimpaired individual during level walking with preferred speed on 5 gait cycles.

To calculate $N_{forefoot}$ and N_{heel} we placed two FlexiForce™ A502 force sensitive resistors (FSRs) under the foot: one ($FSR_{forefoot}$) under the ball of the foot, and another under the heel (FSR_{heel}). To calibrate the FSRs we compare the reading of FSRs with subject's weigh, during a standing baseline, and the correction factor will be multiplied to FSR reading.

Therefore, the estimated vertical and horizontal ground reaction forces are estimated as follow:

$$G_y = FSR_{forefoot} + FSR_{heel} \quad (4)$$

$$G_x = f_r(FSR_{forefoot} - FSR_{heel}) \quad (5)$$

Where the $FSR_{forefoot}$ and FSR_{heel} are the FSR reading times correction factor related to the FSR sensor under the forefoot and heel.

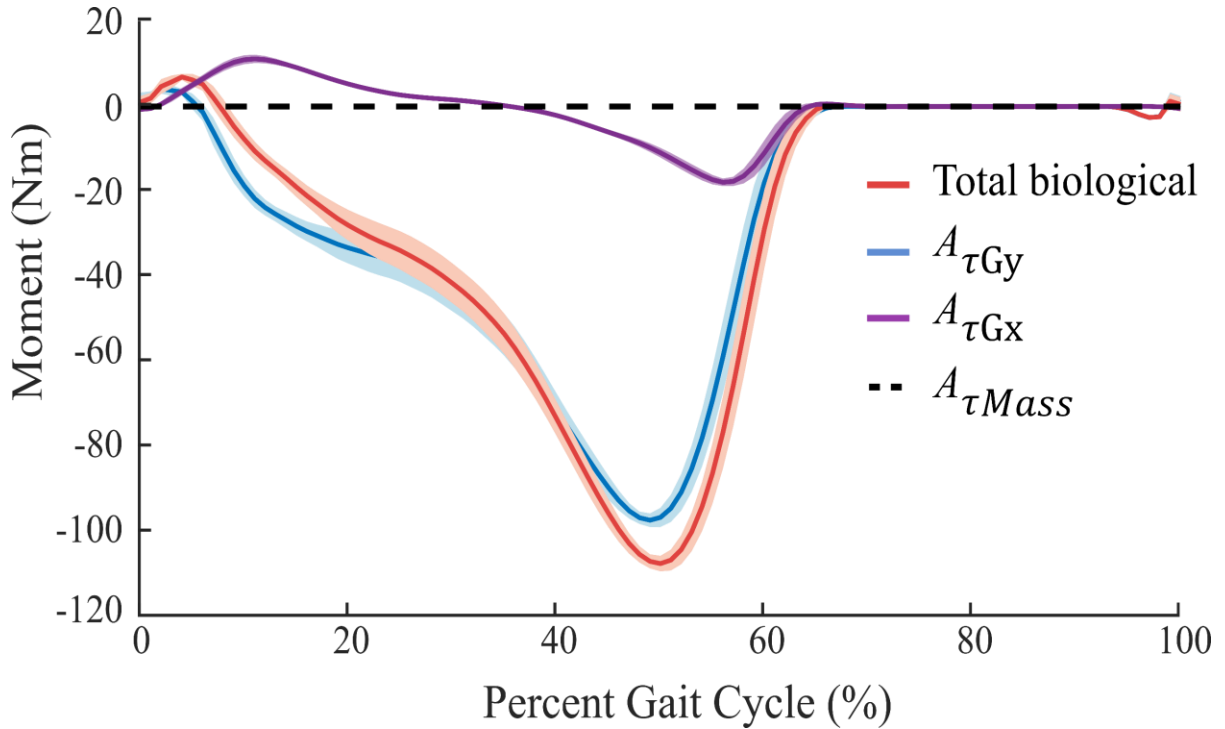


Figure 25. Contribution of mass, horizontal, and vertical ground reaction force to the ankle moment.

III. 2. 2. Ankle Moment Estimation

Based on inverse dynamics equations, ankle joint torque is estimated using the following equation:

$$A_{\tau} = I_f \ddot{\gamma} - (G_x \times MA_{A_{G_x}}) - (G_y \times MA_{A_{G_y}}) \quad (6)$$

Where I_f is the moment of inertia of the foot and $\ddot{\gamma}$ is the angular acceleration of the foot. $MA_{A_{G_x}}$ and $MA_{A_{G_y}}$ are the ankle joint moment arm of G_x and G_y , or vertical and horizontal distance between the foot Center of Pressure (COP) and the ankle joint.

By analyzing the gait biomechanics data of 9 unimpaired individuals, we evaluated the contribution of each term to the resultant ankle moment and found that the I_f and G_y contributed <0.001% and < 3% to the ankle moment, respectively (Figure 25), and are neglectable. Vertical ground reaction force plays the most significant role in ankle plantar flexion torque, $97.27 \pm 0.59\%$.

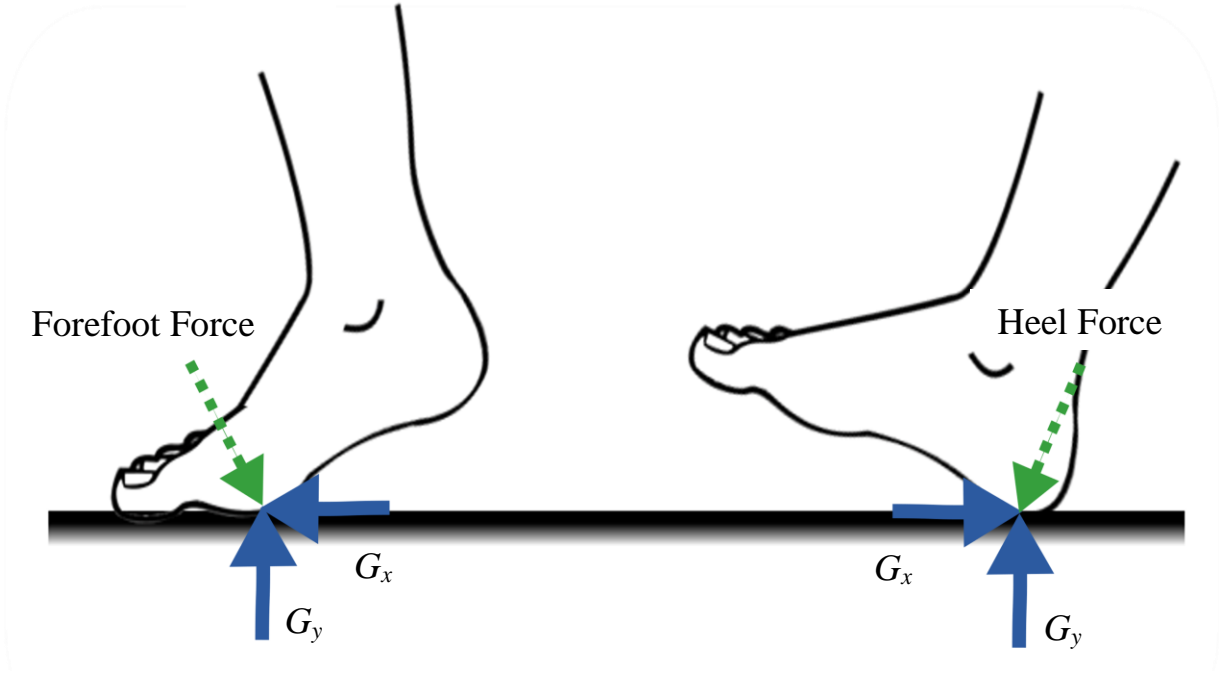


Figure 26. Schematic of ground reaction force and foot force to the ground during level ground walking.

As stated, the vertical ground reaction force mainly applies to the heel and the forefoot. When the heel is over the ground, the ankle moment arm of vertical ground reaction force, $MA_{A_y,heel}$, is negative, as a result, ankle torque, A_τ , is positive which means the ankle should provide dorsiflexion to reach equilibrium. When the forefoot is over the ground, moment arm of vertical ground reaction force, $MA_{A_y,forefoot}$, is positive, therefore, A_τ is negative, and the ankle should provide plantar flexion to reach equilibrium (Figure 26). Hence, the ankle plantarflexion moment can be estimated by the following equation:

$$A_{\tau,p} = -N_{forefoot} \times MA_{A_{G_y},forefoot} \quad (7)$$

To estimate the relative ankle moment, real-time ankle moment estimation was divided by its maximum value during baseline:

$$A_{\tau,p,rel} = \frac{-N_{forefoot} \times MA_{AG_y,forefoot}}{-N_{forefoot,max} \times MA_{AG_y,forefoot,max}} \quad (8)$$

$MA_{AG_y,forefoot}$ changes about 5% during the stance phase. As a result, we assumed $\frac{MA_{AG_y,forefoot}}{MA_{AG_y,forefoot,max}}$ is close to 1. To estimate the normal found reaction force to the forefoot, we placed a FSR under the forefoot of the subject. The following equation shows the final estimation of relative ankle plantar flexion:

$$A_{\tau,p,rel} = \frac{FSR_{forefoot}}{FSR_{forefoot,max}} \quad (9)$$

III. 2. 3. Knee Moment Estimation

In this study, We focused on knee extension moment versus knee flexion moment because gravity will cause knee flexion, as a result of knee joint structure, during walking. In order to support the body weight of an impaired user, the assistive device should provide knee extension assistance during the stance phase. Here we proposed a simple model to estimate knee extension during the stance phase.

Similar to the ankle joint, three sources contribute to sagittal plane knee moment, and they are (1) horizontal ground reaction force, $K_{\tau_{G_x}}$, (2) vertical ground reaction force, $K_{\tau_{G_y}}$, and (3) the shank segment mass and mass of inertia, $K_{\tau_{Mass}}$. The contribution of each source is calculated using the following equations:

$$K_{\tau_{G_x}} = G_x \left(l_s \sin\theta + MA_{AG_x} \right) = G_x \times MA_{K_{G_x}} \quad (10)$$

$$K_{\tau_{G_y}} = G_y \left(l_s \cos\theta + MA_{AG_y} \right) = G_y \times MA_{K_{G_y}} \quad (11)$$

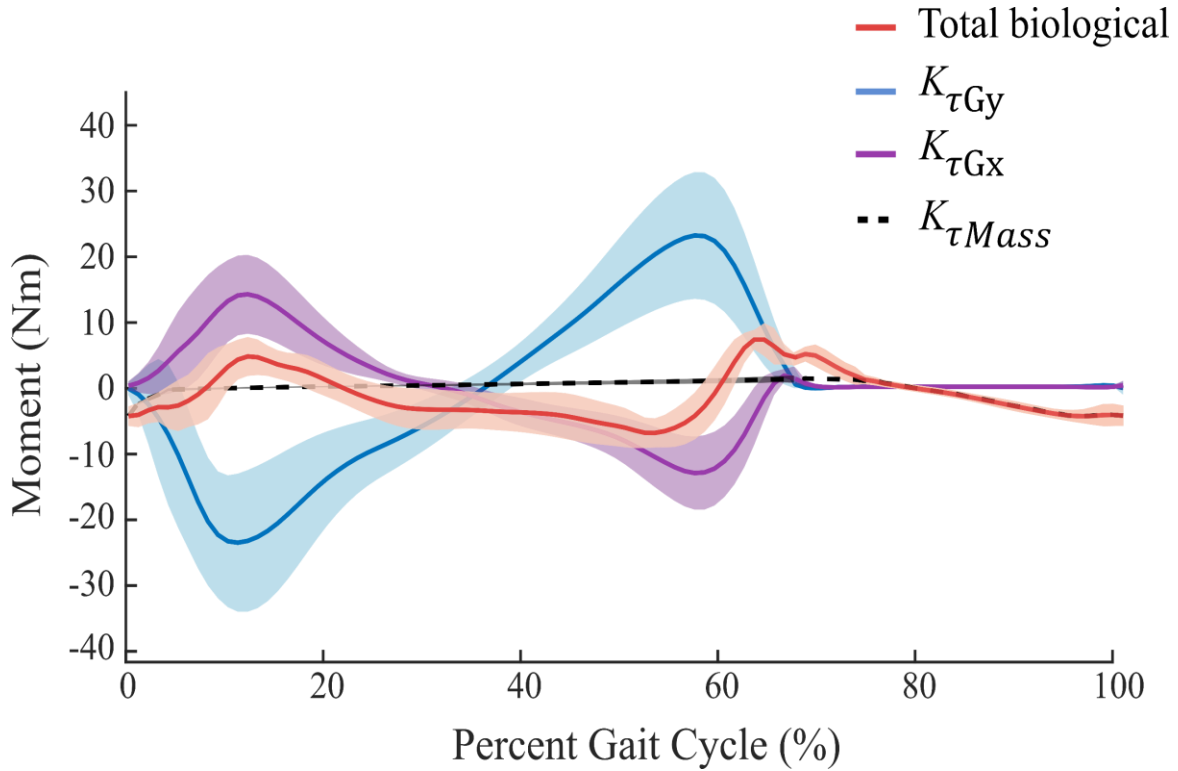


Figure 27. Contribution of mass, horizontal, and vertical ground reaction force to the knee moment.

$$K_{\tau_{Mass}} = I_s \ddot{\theta} + m_s l_{s_c} \left[\sin\theta (l_s - l_{s_c}) (\ddot{\theta} \sin\theta + \dot{\theta}^2 \cos\theta) - \cos\theta (g + (l_s - l_{s_c}) (\ddot{\theta} \cos\theta - \dot{\theta}^2 \sin\theta)) \right] \quad (12)$$

which l_s is the length of the shank, l_{s_c} is the distance between knee joint and shank center of mass, θ is the shank angle relative to the ground, m_s and l_s are the mass and length of the shank segment, respectively. Contribution of $K_{\tau_{mass}}$ in the knee joint moment is neglectable ($1.12 \pm \text{SD}\%$). Figure 27 shows the moment contribution of each source in the knee moment during unimpaired walking. As it is shown in the figure 3-A, the moment caused by G_x has a similar pattern to the biological knee moment. Based on this analysis, we proposed that the knee extension moment, $K_{\tau,e}$, during stance phase can be estimated as follow:

$$K_{\tau} = G_x \times MA_{K_{G_x}} \quad (13)$$

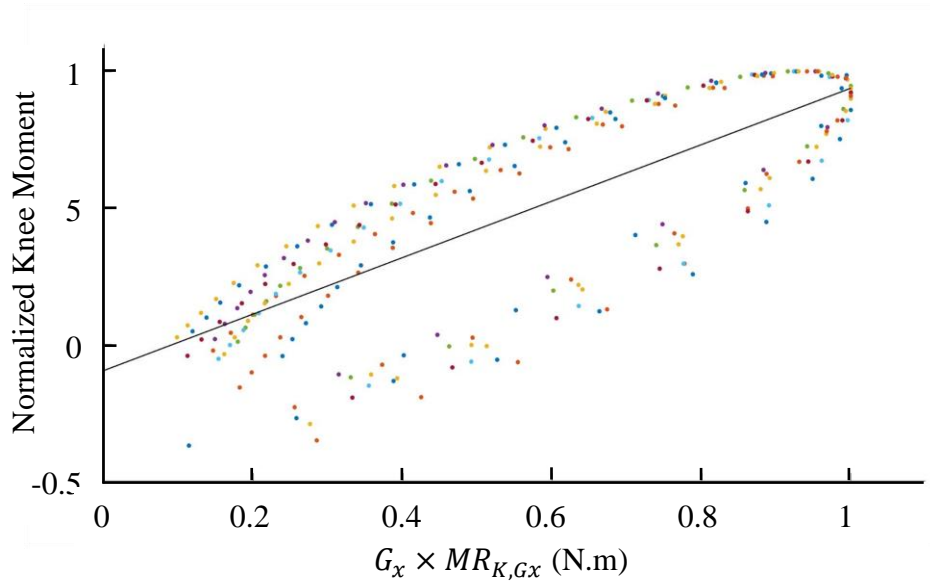


Figure 28. Scatter plot of knee moment versus $G_x \times MA_{K_{G_x}}$.

Figure 28 shows the correlation coefficient of this model is 0.63. Relative knee moment can be estimated by dividing real-time knee moment estimation by its maximum during baseline:

$$K_{\tau,rel} = \frac{G_x \times MA_{K_{G_x}}}{G_{x,max} \times MA_{K_{G_x},max}} \quad (14)$$

Figure 29 also shows that $MA_{K_{G_x}}$ is almost constant during stance phase, about 4 mm change during stance, that means in order to estimate the relative knee extension moment, $K_{\tau,e,rel}$,

$\frac{\mu \times MA_{K_{G_x}}}{\mu \times MA_{K_{G_x},max}}$ is close to 1. Using equation (5), we have

$$K_{\tau,rel} = \frac{FSR_{heel} - FSR_{forefoot}}{(FSR_{heel} - FSR_{forefoot})_{max}} \quad (15)$$

To estimate relative flexion knee moment, we only used the positive element of equation 15, as follow:

$$K_{\tau,f,rel} = \frac{FSR_{heel}}{FSR_{heel,max}} \quad (16)$$

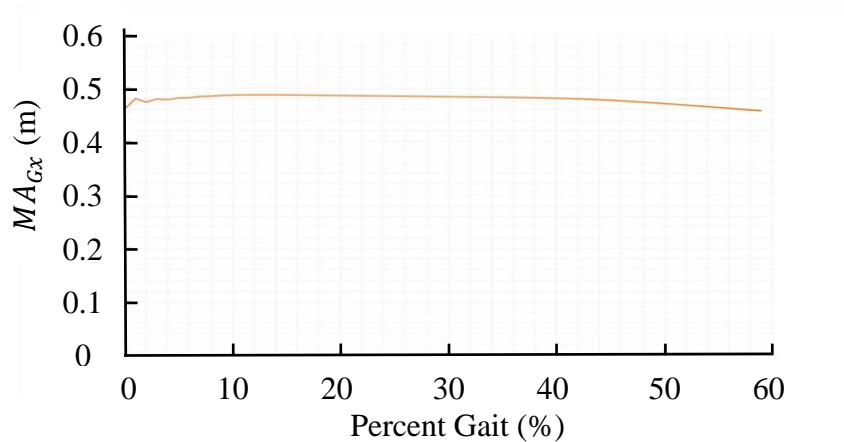


Figure 29. $MA_{K_{Gx}}$ over gait cycle during level ground walking.

III. 2. 4. Experiment Design

Our design, presented here, included a motor assembly, Bowden cable transmission, thigh cuffs, shank cuffs, and foot assemblies (Figure 30) shows the ankle-knee exoskeleton designed in the biomechanics lab at NAU. Motor assembly was worn on the torso, close to the wearer's body center of mass, to reduce the effect of its weight on the energy consumption of the wearer. Knee extension and ankle plantarflexion torque were transferred from four brushless DC motors through Bowden cables to pulleys mounted on ankle and knee assemblies. The ankle and knee joints of the exoskeleton operated as sagittal-plane revolute joints allowing ankle plantar flexion and dorsiflexion as well as knee flexion/extension.

III. 2. 5. Experiment Design

The magnitude of the desired moment was set based on the user's preference. An unimpaired subject was asked to walk over a treadmill while wearing our ankle-knee exoskeleton with (1) zero assistance, (2) the reference controller, and (3) the coordinated controller. The reference controller was on-off assistance, providing knee assistance during the stance phase and ankle assistance

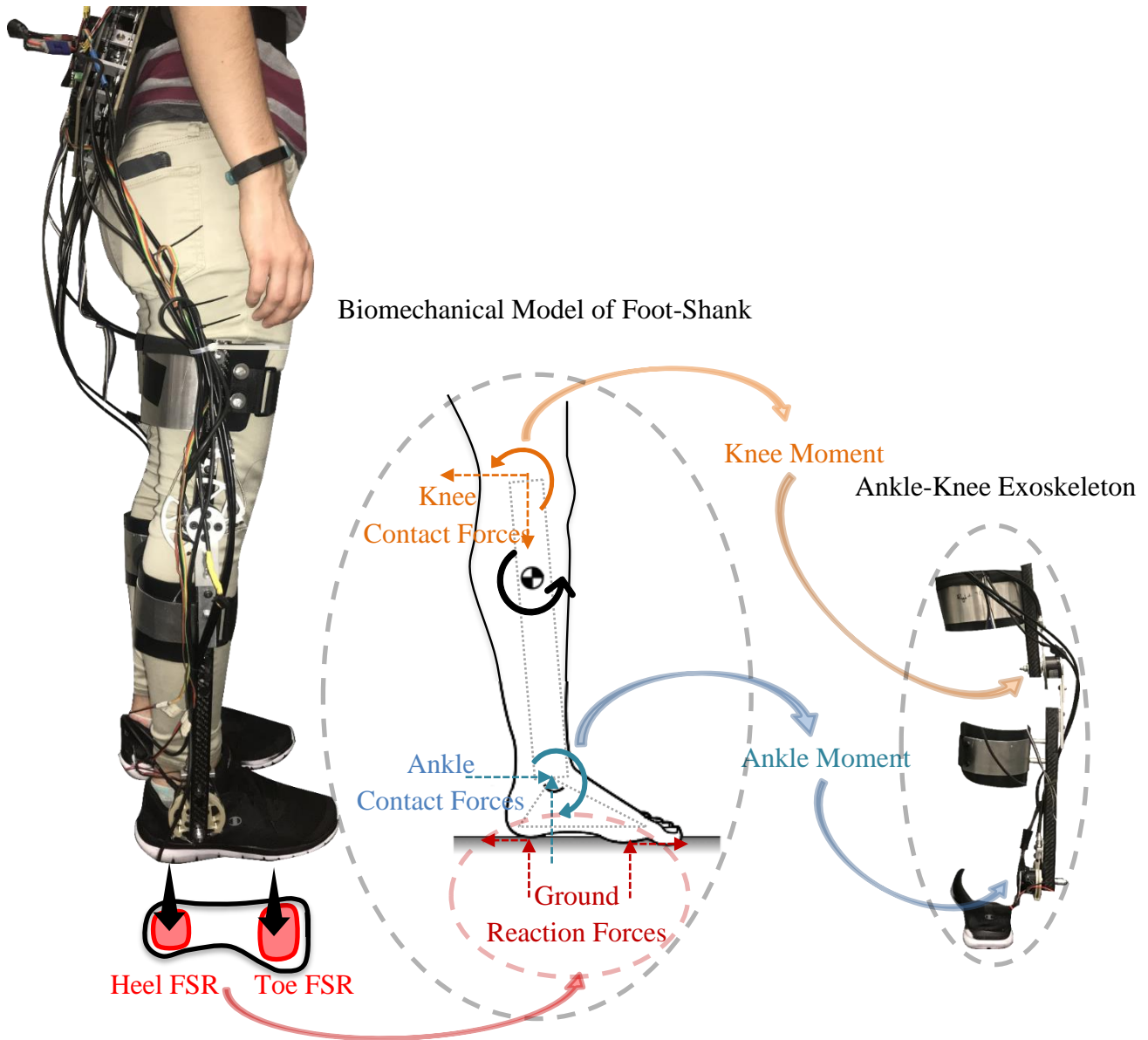


Figure 30. The schematic of our biomechanical model of foot-shank, the control strategy based on this model, and the ankle-knee exoskeleton designed in NAU Biomechatronic Lab.

during the mid-late stance phase. The coordinated controller is the ankle-knee controller in which the desired torque of ankle and knee joints was based on the estimated relative ankle plantar flexion and knee extension moments, using equations (9) and (15).

The motor assembly includes a custom printed circuit board, Bluetooth module, microcontroller (Teensy 3.6), four motor drivers, four brushless DC motors (Maxon EC-4pole, 24 V, 90 W, 89:1

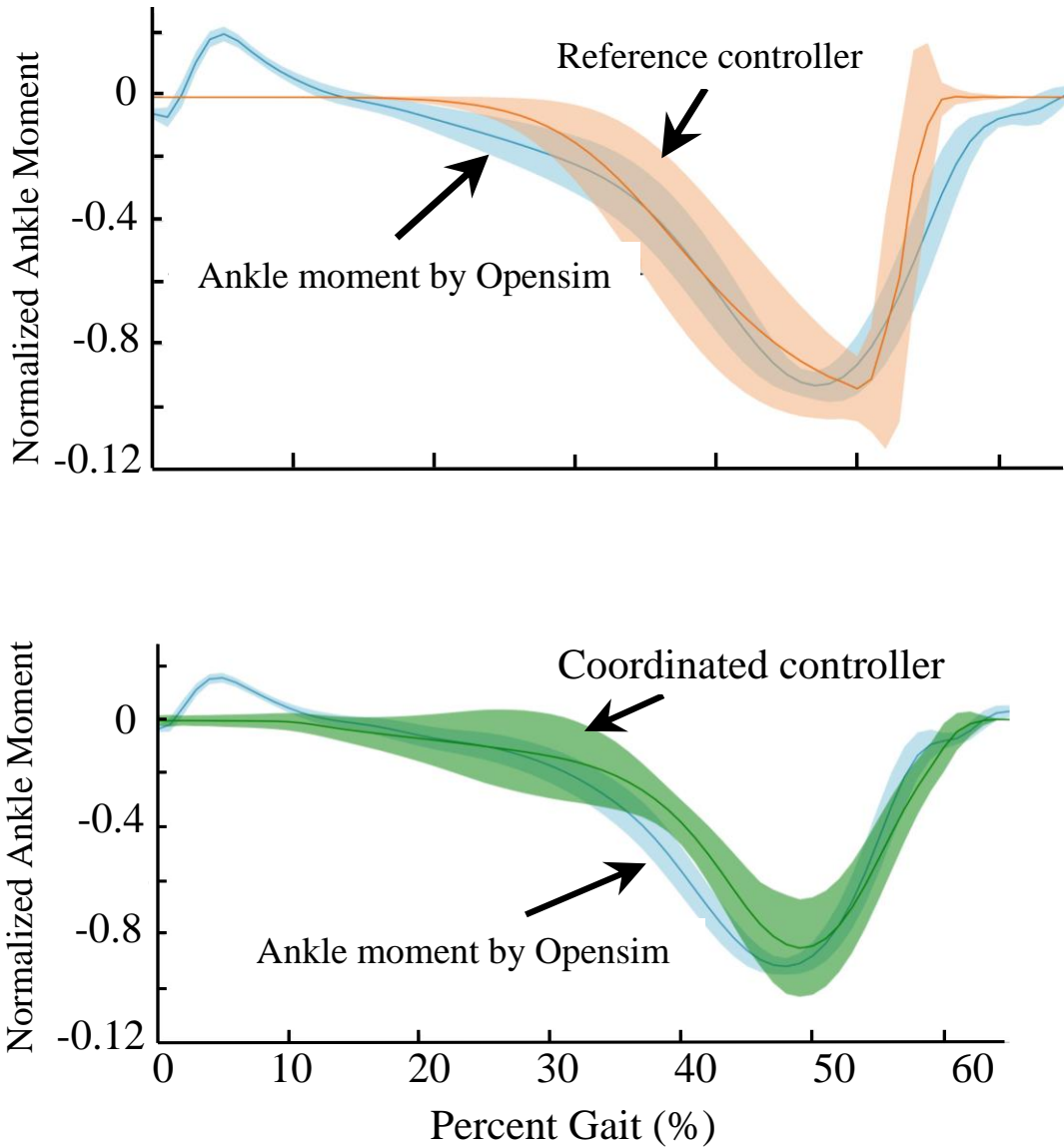


Figure 31. Normalized ankle joint moment estimated by Opensim in compare to the coordinated controller and a reference controller during stance phase.

gearbox), one interchangeable lithium polymer battery, and four torque sensors at the knee and ankle joints. The low-level controller for both reference and coordinated controller was the PID controller.

III.1. Results and Discussion

The one participant of the study safely completed each walking trial without any adverse events.

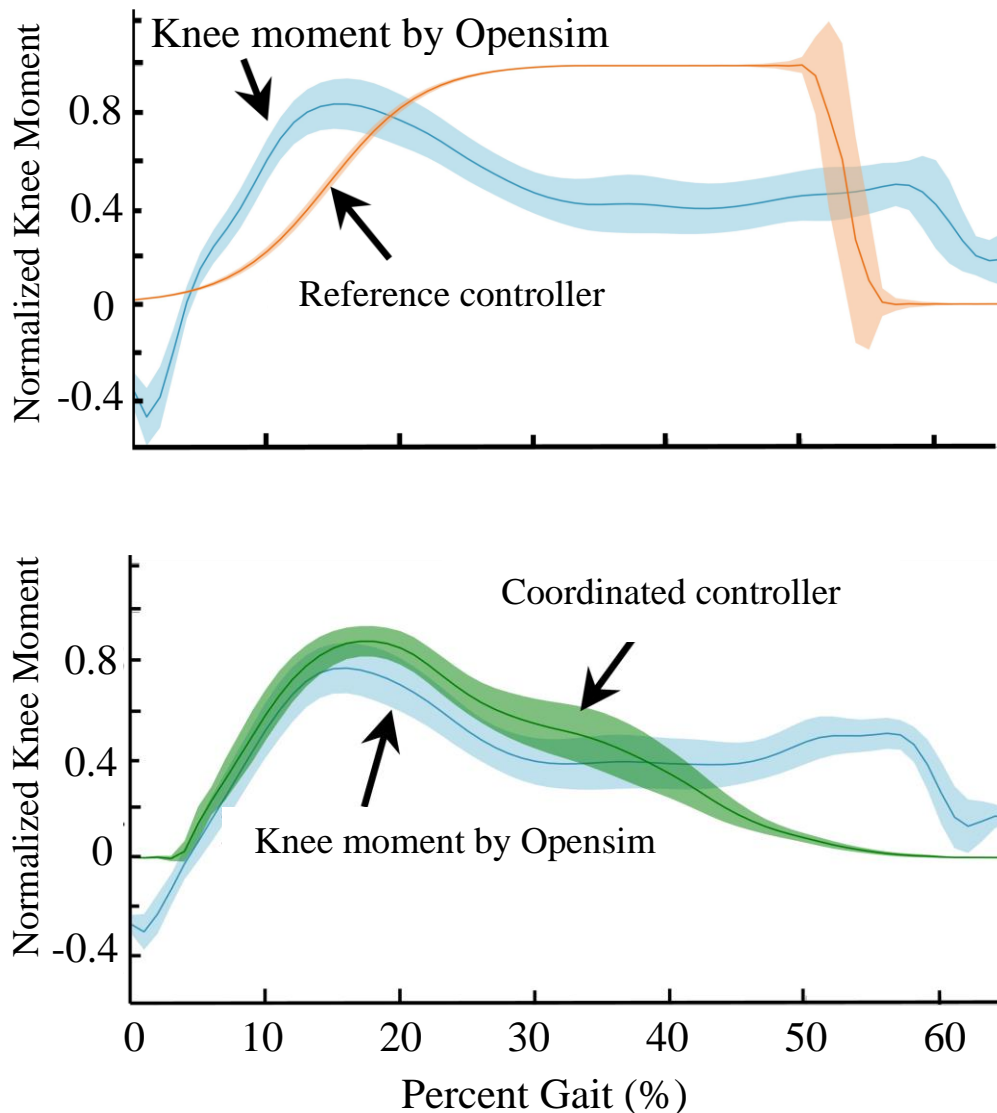


Figure 32. Normalized knee joint moment estimated by Opensim in compare to the coordinated controller and a reference controller during stance phase.

Statistical indices (R^2 of 0.91 and 0.45, as well as root mean square of 0.10 and 0.24 for ankle and knee, respectively) show that our model could predict the ankle plantarflexion moment and stance phase knee moment with reasonable accuracy (Table 9).

The assistance provided by our coordinated control strategy reduced the metabolic cost of walking 11.6%, while the reference controller only reduced it by 1.1% relative to zero moment assistance.

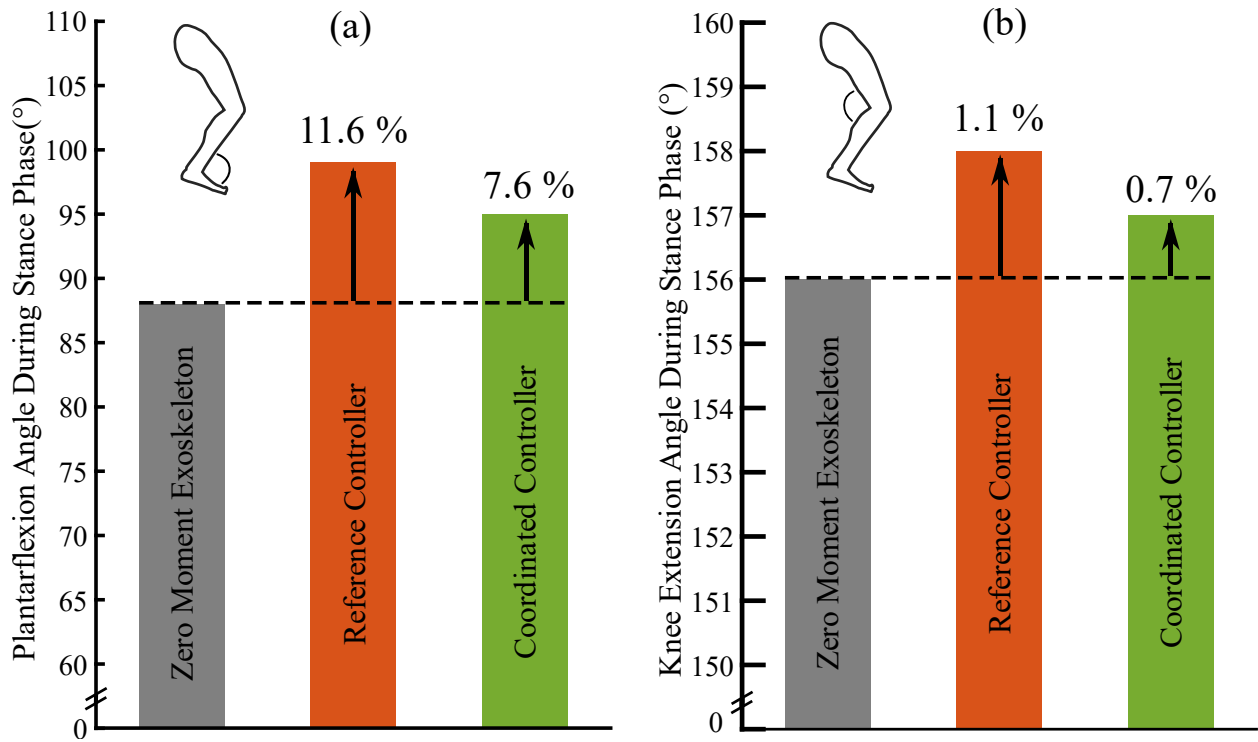


Figure 33. Maximum (a) plantarflexion ankle and (b) knee extension angle during stance phase for zero moment, reference controller and coordinated controller assistance.

Our novel control strategy increased the ankle plantar flexion and knee extension angle of the unimpaired subject during the stance about 7.6% and 0.7%, respectively, which is less than the increased angles in the case of walking with the reference controller (11.6% and 1.1%). It means that our coordinated controller decreased the unimpaired individual’s cost of walking without affecting remarkably on her walking pattern.

Table 9. COORDINATED CONTROLLER ACCURACY

	<i>RMSE</i>	<i>R²</i>	<i>VAF</i>
Ankle Plantarflexion	0.12	0.86	0.73
Knee Extension	0.14	0.61	0.23

Root Mean Square Error (RSME), coefficient of determination (R^2), and Variance Accounted For

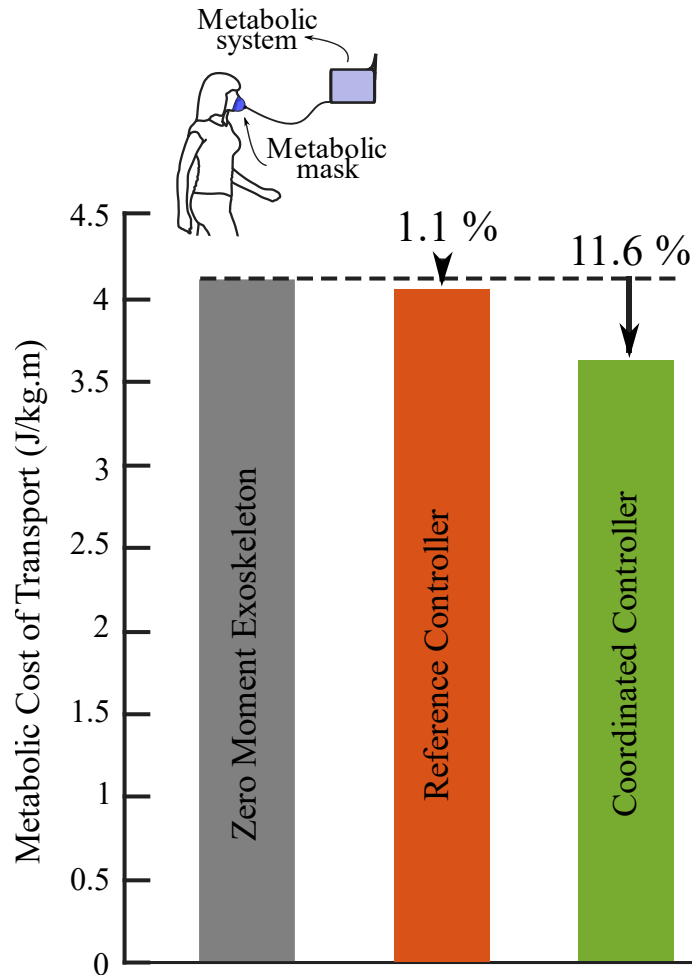


Figure 34. Metabolic cost of walking for zero moment, reference controller and coordinated controller assistance.

There have been many studies on control strategies for exoskeletons for patients with CP to overcome their walking restriction, but there is a dearth of research on an exoskeletons adaptive-coordinated control strategy for individuals with severe CP, and therefore much research is needed in this area. The ultimate goal of this research is to design a coordinated control strategy suitable for assisting individuals with severe CP.

IV. Simulating Ankle Torque during Walking Using a new Bioinspired Muscle Model with Application for Controlling a Powered Exoskeleton

IV.1. Introduction

Human-like motion is a primary goal for many robotic assistive devices. Emulating the strategy of the human neuromuscular system may aid the control of such powered devices, yet many challenges remain. The ankle joint plays an important role in human walking and locomotion [82], and the ankle plantar flexors contribute to gait performance by providing vertical support and forward progression of the body [83], [84]. Many active and passive ankle exoskeletons have been developed over the last five decades with good results, but they face many challenges that limit general use and commercialization [82]. Requirements for lower weight and affordability of passive ankle prostheses are not the only limitations. The complexity of control and electronics has also limited the manufacture of exoskeletons with active ankle actuation [85]. As a result, no powered ankle orthoses are currently available for purchase. Commercialized exoskeletons have only passive ankles. The passive orthoses and prostheses can emulate the behavior of the human ankle during low-speed walking, but in normal and high-speed walking, they cannot provide additional energy for powered plantar flexion [86].

Control strategies of the ankle joint of assistive devices that have been studied over the last decades can be organized into five groups: (1) control based on following a path (trajectory-tracking controller) [87]–[90], (2) control using lumped models (variable impedance control) [91]–[93], (3) muscle-model-oriented control [94]–[96], (4) control based on biosignals [97]–[100] or human-robot interaction data [101]–[103], (5) other strategies like functional electrical stimulation [104], [105], on-off control [106] etc. Emulating the strategy of the human neuromuscular system, group (3), may aid the control of robotic assistive devices, yet many challenges remain. Muscle-

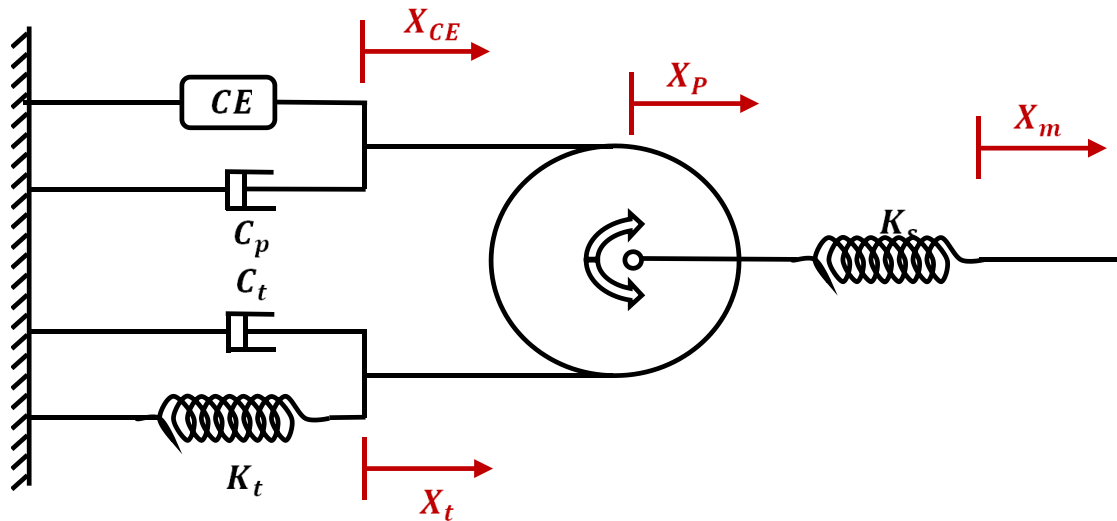


Figure 35. Schematic of the Winding Filament Muscle (WFM) model. The contractile element (CE) represents the myosin cross-bridges, the actin filament is represented by a pulley, the titin protein is represented by a spring-damper element, and the tendon is represented by a spring in series with the pulley.

model-oriented control of powered assistive devices helps these devices mimic human musculoskeletal system behaviors.

Among all muscle models, Hill type models are the most commonly used for controlling assistive devices [107]. The Hill muscle model represents muscle function through two simple elements, and often fails to accurately predict muscle force in different situations [108]. Nishikawa et al. developed a novel “winding filament” hypothesis for muscle contraction (Figure 35) that incorporates a role for the giant titin protein in active muscle [109]. In this study, we investigated the potential for using the winding filament model (WFM) of muscle to predict the net muscle moment of the ankle. The long-term goal is to use this model to improve ankle control of a commercial powered exoskeleton.

IV.2. Method

As biological tissues, muscle and tendon exhibit time dependent properties. However, Hill-type muscle models do not contain any time-dependent properties, suggesting that Hill models cannot

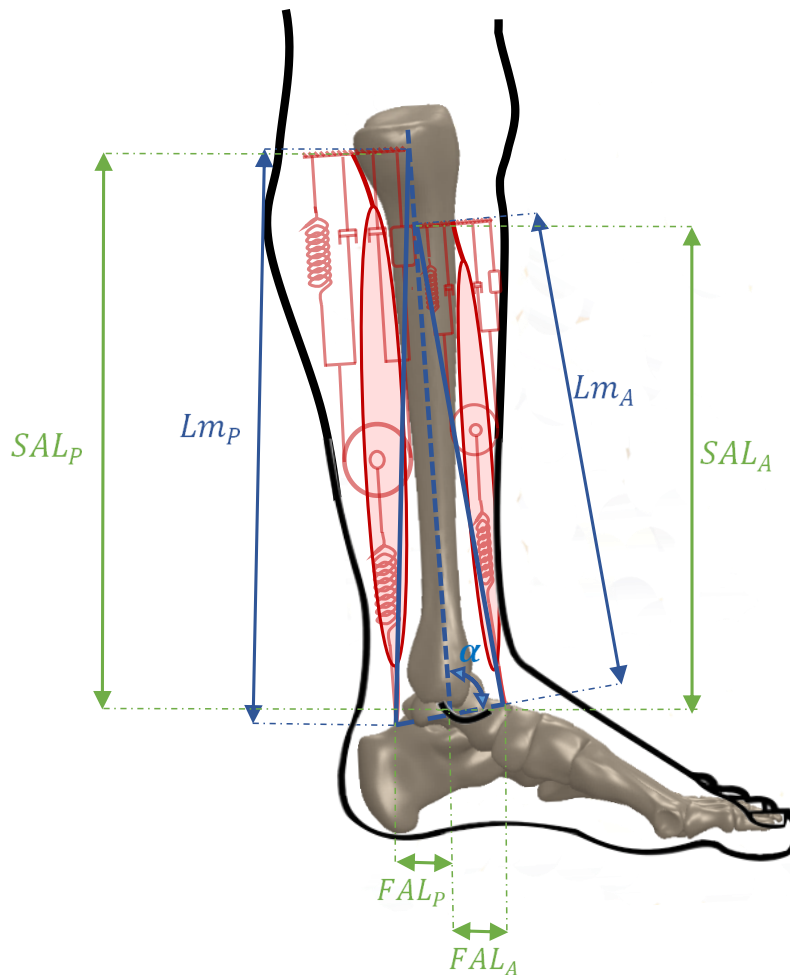


Figure 36. The bio-inspired WFH algorithm uses a pair of antagonistic virtual muscles (m_A = anterior muscles and m_P = posterior muscle) to control ankle torque. Lm_A and Lm_P represent the lengths of the anterior and posterior muscles, respectively.

accurately predict muscle function when time-dependent properties of muscle play a significant role in motion. In contrast, the winding filament hypothesis incorporates time-dependent tissue behavior and may be more capable of capturing human-like actuation [110].

IV. 2. 1. The Winding Filament Muscle Model

Many previous studies have used muscle models to emulate musculoskeletal behavior during various tasks in order to develop a control strategy for prosthetic devices [95], [96], [107], [111].

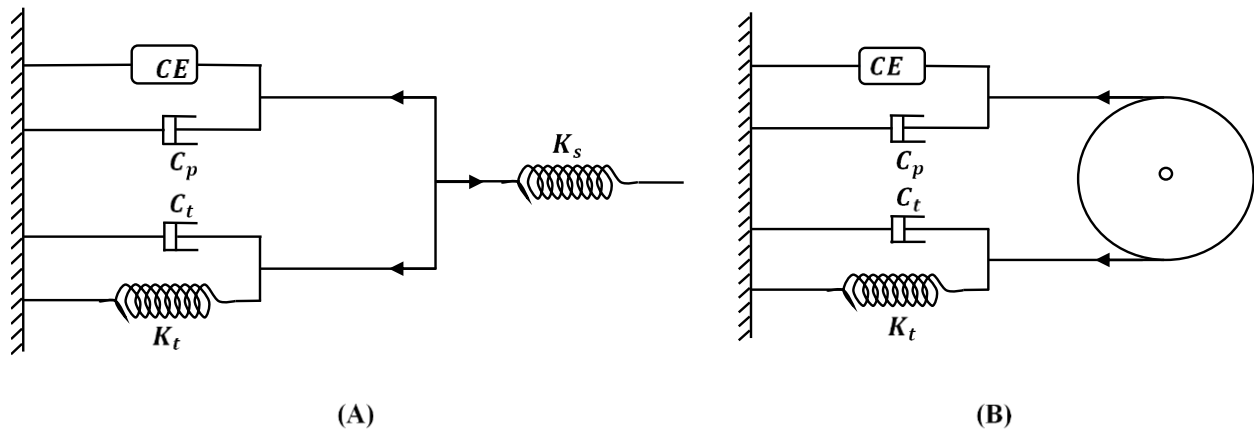


Figure 37. (A) Translational Balance, (B) Rotational Balance.

Most of those studies used the Hill muscle model that does not take into account the history dependent properties of muscle, and more importantly, relies on muscle activation—evaluated by EMG—data which, in most cases, are missing for persons with spinal cord injury. Thus, Hill-type muscle models are typically incapable of being used to control exoskeleton devices for patients with high-level disabilities.

To address these problems associated with controllers based on Hill-type muscle models, we used the Winding Filament Model (WFM) of muscle. The WFM (Figure 35) uses springs and dampers arranged around a pulley representing the actin filaments to describe the activation-dependent material properties of muscle. Activation rotates the pulley in the counter-clockwise direction, whereas imposed forces translate the pulley. Forces on each side of the pulley are balanced in each time step, so that pulley rotation and translation are not completely independent in order to emulate the history dependent properties of muscle.

The WFM contains 6 elements: two spring, two dampers, one pulley and one contractile element. The contractile element (CE) represents myosin crossbridges, and the damper parallel to the myosin (C_p) represents the muscle force-velocity relationship. The damper and spring in

parallel yields an element representing the viscoelastic behavior of the titin protein. The pulley represents actin filaments, and it can rotate freely. There is also a spring in series with the pulley that represents the elasticity of tendon and other series elastic elements. Although the damping coefficients and spring stiffness of different elements of the model may not be constant [10], this simplifying assumption is required to reduce the calculation processes for the algorithm.

The WFM produces an acceptable prediction of muscle force using either square-wave [112] or simple bell-shaped activation, which shows that it is proposed in a way that could predict muscle behavior mostly based on muscle length and not muscle activation [112]. These important results show that the WFM makes it possible to use a muscle-model-based control strategy to control exoskeletons for totally disabled patients, without requiring their missing muscle activation data.

The force generated by the titin protein consists of a spring force (F_{ts}) and a damper force (F_{td}):

$$F_{ts} + F_{td} = K_t \times X_t(t) + C_t \times \dot{X}_t(t) = F_t \quad (1)$$

$$F_{ts} + F_{td} = K_t \times X_t(t) + C_t \times \dot{X}_t(t) = F_t \quad (2)$$

X_t is the titin position with respect to the resting position of the titin protein. The net force of titin will be:

$$F_{ts} + F_{td} = K_t \times X_t(t) + C_t \times \dot{X}_t(t) = F_t \quad (3)$$

The CE generates force, which is defined as maximum isometric force (P_0) multiplied by muscle activation (Act) at certain percent gait (PG). The net force produced by the contractile element and the parallel damper is:

$$P_0 \times Act(PG(t)) + C_{ce} \times \dot{X}_{ce}(t) = F_{ce} \quad (4)$$

The net force of titin will be:

$$F_{ts} + F_{td} = K_t \times X_t(t) + C_t \times \dot{X}_t(t) = F_t \quad (5)$$

Based on the static assumption, the forces around the pulley are in equilibrium at every instant in time. Based on the rotational balance about the pulley we have:

$$F_t = F_{ce} \quad (6)$$

By making Equation (3) equal to Equation (4), the \dot{X}_{ce} and \dot{X}_t will be:

$$\dot{X}_{ceI}(t) = \frac{\dot{X}_t(t) \times C_t + X_t(t) \times K_t - F_{ce}}{C_{ce}} \quad (7)$$

$$\dot{X}_{tI}(t) = \frac{\dot{X}_{ce}(t) \times C_{ce} + F_{ce} - X_t \times K_t}{C_t} \quad (8)$$

Based on translational balance, we have:

$$F_t + F_{ce} = K_{ss} \times (X_m(t) - X_p(t)) \quad (9)$$

By making Equation (3) equal to Equation (4), the \dot{X}_{ce} and \dot{X}_t will be:

$$\dot{X}_{ceII}(t) = \frac{(X_m(t) - X_p(t)) \times K_s - X_t \times K_t - \dot{X}_t \times C_t - F_{ce}}{C_{ce}} \quad (10)$$

$$\dot{X}_{tII}(t) = \frac{(X_m(t) - X_p(t)) \times K_s - X_t \times K_t - \dot{X}_{ce} \times C_{ce} - F_{ce}}{C_t} \quad (11)$$

Based on superposition of rotational balance and translational balance (Figure 26), \dot{X}_{ce} and \dot{X}_t are defined as:

$$\dot{X}_{ce}(t) = \frac{(X_m(t) - X_p(t)) \times K_s - 2F_{ce}}{C_{ce}} \quad (12)$$

$$\dot{X}_t(t) = \frac{(X_m(t) - X_p(t)) \times K_s - 2X_t \times K_t}{C_t} \quad (13)$$

Using Equation (12) and Equation (13), the velocity of the pulley center of mass will be:

Table 10. WFM MODE PARAMETERS, USING PARTICLE SWARM OPTIMIZATION

<i>Parameters</i>	<i>Symbol</i>	<i>Value</i>	<i>Unit</i>	<i>Source</i>
Peak isometric force	$P_{o_A}^1$	1484.03	N	PSO ³ , [112], [113] ⁴
	$P_{o_P}^2$	2344.77	N	PSO, [112], [113]
Series spring constant	K_{s_A}	1999.99	N/cm	PSO, [112], [113]
	K_{s_P}	650.07	N/cm	PSO, [112], [113]
Titin spring constant	K_{t_A}	129.66	N/cm	PSO, [112]
	K_{t_P}	456.26	N/cm	PSO, [112]
Titin damper coefficient	C_{t_A}	10.26	N.s/cm	PSO
	C_{t_P}	937.51	N.s/cm	PSO
CE damper coefficient	C_{ce_A}	498.55	N.s/cm	PSO, [112]
	C_{ce_P}	230.67	N.s/cm	PSO, [112]
Shank Attachment Length	SAL_A	29.00	cm	[113]
	SAL_P	33.00	cm	[113]
Foot Attachment Length	FAL_A	4.00	cm	[119]
	FAL_P	5.50	cm	[114]

A: anterior muscle, P: Posterior muscle, ¹Particle Swarm Optimization, ⁴Range of parameters was set based on literature.

$$\dot{X}_p(t) = \dot{X}_{ce}(t) + \dot{X}_t(t) \quad (14)$$

X_p can be calculated as the derivative of \dot{X}_p . X_m , is the position of the end of the muscle, calculated from the geometry and ankle angle. Finally, the muscle force, F_m , will be:

$$F_m(t) = K_s \times (X_m - X_p) \quad (15)$$

The mass of the muscle and non-conservative forces are neglected in the derivations.

IV. 2. 2. Model Configuration and Implementation

The WFM control algorithm incorporates a pair of virtual muscles (Figure 35) that emulate the human shank muscles: a tibialis anterior muscle (Lm_A) contracts to produce ankle dorsiflexion,

Table 11. THE ROOT MEAN SQUARE ERROR BETWEEN BIOLOGICAL MOMENT AND WFM.

Type of data	Train	Train	Train	Train	Test	Test	Test	Test
Subject number	1-F*	2-F	3-M*	4-M	1-F	2-F	3-M	4-F
RMSE	118.95	167.23	213.85	119.08	102.16	110.88	163.59	139.67

*F stands for Female subject, and M stands for Male subject.

and a posterior muscle (Lm_p), based on the soleus and gastrocnemius, contracts to produce ankle plantarflexion.

The parameters of the WFM for each virtual muscle were found using Particle Swarm Optimization (PSO) in MATLAB[®] 2018. The shank attachment length and foot moment arm were estimated based on literature [113], [114]. The lower and upper bounds of the unknowns were estimated based on the literature: the peak isometric force (P_o) [113], [115], [116], series spring constant (K_s), titin spring constant and damper coefficient (K_t and C_t) [113] [117], and CE damper coefficient (C_{ce}) [112]. The model parameters were found by optimizing the calculated ankle joint torque over training data from 4 healthy subjects during walking over treadmill at a speed of 1.2 m/s. The data were from Lerner's study [118]. The WFM model parameters are presented in Table 10. The optimization was done using the walking data of four healthy subjects (two male and two female) as training data, and then we test the results of optimization on another four subjects (one male and three female). The walking speed of all the subjects were 125 (m/s).

IV.3. Result and Discussion

The control of an exoskeleton should be designed generally for all populations, so the activation of muscles should be defined generally too. In this case, we designed a general shape for activation that is a function of gait cycle time. The result of the optimization shows that the best activation curve that fits for the training walking data of four subjects has the maximum activation of 0.05

for anterior virtual muscle, and 0.1 for posterior one. Based on the result of optimization, the maximum force of the muscle was calculated 5 times of subject's body weight in kilogram. The RMSE between WFM torque and Inverse Dynamics in OpenSim for test and train data are presented in Table 11.

The purpose of this study was evaluating two general activation curves that best fit the torque output of WFM model to the ID in OpenSim. It is expected that the RMSE of the WFM modeling be large, since it is a general model that should work for every different person with different pattern of walking. The important result of this study is that the test data have the same amount of RSME as the train data—the mean of RSME for train subject is 154.78, and for test subject 129.07. Comparing the RMSE of test and train data indicates that our model can predict the ankle joint torque of all populations with the same amount of error, which is acceptable for an exoskeleton.

V. Conclusions and Future Work

We sought to design and evaluate four adaptive control strategies for a lightweight ankle exoskeleton, a lightweight hip exoskeleton, a unilateral ankle-knee exoskeleton, and the ankle of a commercialized exoskeleton based on various biomechanical and biological methods. We also sought to enhance our understanding of the effect of adaptive assistance strategies on improving the gait of unimpaired individuals and individuals with impaired mobilities. In the first three studies, the goal was to design control strategies that were adaptive to different terrains and non-pathological and pathological walking patterns with the ultimate goal of improving the mobility of impaired individuals with some independent walking capacity. In the final study, we sought to design a bio-inspired control strategy for the ankle joint of a commercially-available exoskeleton for individuals without independent walking capacity.

In chapter one of this dissertation, we presented the development of an adaptive control system of an ankle exoskeleton. Additionally, our study evaluated the ability of the proposed control strategy to accurately adapt to level, incline, and decline walking, each at multiple speeds; stair ascent; stair descent; and 90° turning while walking over-ground. Validation experiments on six unimpaired individuals and four individuals with CP are presented in this chapter to confirm the ability of the proposed control strategy to accurately estimate the biological ankle moment in real-time. The results indicated that the proposed control strategies were able to assist unimpaired and impaired individuals during walking on different terrains and improved the metabolic cost of walking. Results from the validation experiment showed that the suggested approach effectively estimated the desired moment during walking over various terrains. Future investigation on evaluating the performance of our ankle-moment adaptive estimation scheme on real-world mobility for individuals with and without neuromuscular disorders is required.

Chapter two presented the design and test of a low-profile hip exoskeleton and validation of the high-level controller during walking on level ground and incline to evaluate its effect on improving mobility of unimpaired and impaired individuals. The validation of the presented control strategy was demonstrated by comparing the hip assistance torque profile with the biological hip moment. The results of the clinical feasibility test indicated the effectiveness of our hip assistance on energy consumption during walking for individuals with and without walking impairments. Future work on this project will consist of further studies on clinical participants with larger sample sizes to further assess the presented study's practical benefits and confirm the generalizability of the current findings.

Chapter three discussed the development and initial evaluation of a coordinated control strategy of a unilateral ankle-knee exoskeleton based on biomechanics and inverse dynamics of human walking over level ground. Initially, efforts to obtain a simplified model of ankle and knee joint moment online estimation were presented. A pilot experiment was then conducted to evaluate the feasibility of the proposed control strategy in improving metabolic cost and kinematics of walking of an unimpaired subject. The proposed coordinated control strategy improves the primary outcomes compared to both on-off assistance and no assistance. Future research will consist of conducting experiments with larger sample sizes and on individuals with pathological gait. Additionally, evaluating the proposed control strategy on more varied terrain remains as future work.

Chapter four examined the potential for a bio-inspired model to predict ankle joint and improve ankle control of a commercial powered exoskeleton. First, the real-time ankle moment estimation model is developed, and optimization is conducted using MATLAB particle swarm optimization toolbox to evaluate the model's parameters. The proposed model was evaluated on walking data

of four subjects, and the results showed the model could predict ankle moment accurately. Future work will include implementing an ankle control strategy based on the proposed model on a commercialized exoskeleton for further evaluation of the benefits of this research.

In conclusion, the overarching goal was to design exoskeleton assistance strategies that were (1) able to adapt to different walking patterns and real-world terrains without classification or prescription, and (2) practical for use in real-world settings. We developed and validated ankle and hip assistive control strategies on unimpaired and impaired individuals with CP to evaluate the adaptivity of the assistive strategy on different patterns of walking and different impairment levels. We also examined the adaptive ankle exoskeleton controller on across many different terrains to evaluate the adaptivity of our generalized proportional ankle moment assistive strategy . The hip exoskeleton controller was evaluated over incline and level ground to examine adaptivity over these conditions; further evaluation is needed on other common terrains encountered during daily-life activities, such as stair ascent/descent and incline. Similarly, the ankle-knee exoskeleton controller described in chapter two needs further evaluation on the adaptivity of the proposed coordinated ankle-knee assistance strategy on different terrains and walking patterns. Chapter four of this dissertation proposed a novel bio-inspired control strategy for the ankle joint of a full-body exoskeleton intending to assist individuals with no independent walking ability. One of the advantages of the proposed assistance strategy was that it did not acquire EMG input, unlike conventional muscle model control strategies, which may make this approach suitable for individuals deficient muscle activity patterns. Evaluating adaptivity on different walking speeds and terrains requires further evaluation and experiment. Future work will involve larger cohorts to address the limitation of small sample sizes. Further evaluation of a variety of terrains is considered a future study for both unilateral ankle-knee exoskeleton and hip exoskeleton.

References

- [1] S. Lee *et al.*, “Autonomous multi-joint soft exosuit with augmentation-power-based control parameter tuning reduces energy cost of loaded walking,” *J. Neuroeng. Rehabil.*, vol. 15, no. 1, p. 66, 2018.
- [2] F. A. Panizzolo *et al.*, “A biologically-inspired multi-joint soft exosuit that can reduce the energy cost of loaded walking,” *J. Neuroeng. Rehabil.*, vol. 13, no. 1, p. 43, 2016.
- [3] M. M. Alemi, J. Geissinger, A. A. Simon, S. E. Chang, and A. T. Asbeck, “A passive exoskeleton reduces peak and mean EMG during symmetric and asymmetric lifting,” *J. Electromyogr. Kinesiol.*, vol. 47, pp. 25–34, 2019.
- [4] M. F. Abel *et al.*, “The ReWalk powered exoskeleton to restore ambulatory function to individuals with thoracic-level motor-complete spinal cord injury,” *J Pediatr Orthop*, vol. 6, no. 11, pp. 333–340, 2012.
- [5] R. Griffin *et al.*, “Stepping Forward with Exoskeletons: Team IHMC’s Design and Approach in the 2016 Cybathlon,” *IEEE Robot. Autom. Mag.*, vol. 24, no. 4, pp. 66–74, 2017.
- [6] T. Vouga, R. Baud, J. Fasola, M. Bouri, and H. Bleuler, “TWIICE - A lightweight lower-limb exoskeleton for complete paraplegics,” in *IEEE International Conference on Rehabilitation Robotics*, 2017, pp. 1639–1645.
- [7] E. M. McCain *et al.*, “Mechanics and energetics of post-stroke walking aided by a powered ankle exoskeleton with speed-adaptive myoelectric control,” *J. Neuroeng. Rehabil.*, 2019.
- [8] T. Yan, M. Cempini, C. M. Oddo, and N. Vitiello, “Review of assistive strategies in powered lower-limb orthoses and exoskeletons,” *Rob. Auton. Syst.*, vol. 64, pp. 120–136, 2015.
- [9] S. Kim and J. Bae, “Force-Mode Control of Rotary Series Elastic Actuators in a Lower Extremity Exoskeleton Using Model-Inverse Time Delay Control,” *IEEE/ASME Trans. Mechatronics*, vol. 22, no. 3, pp. 1392–1400, 2017.
- [10] L. Zhou, W. Chen, J. Wang, S. Bai, H. Yu, and Y. Zhang, “A Novel Precision Measuring Parallel Mechanism for the Closed-Loop Control of a Biologically Inspired Lower Limb Exoskeleton,” *IEEE/ASME Trans. Mechatronics*, vol. 23, no. 6, pp. 2693–2703, 2018.
- [11] Ü. Önen, F. M. Botsalı, M. Kalyoncu, M. Tınkır, N. Yılmaz, and Y. Şahin, “Design and Actuator Selection of a Lower Extremity Exoskeleton,” *IEEE/ASME Trans. Mechatronics*, vol. 19, no. 2, pp. 623–632, 2014.
- [12] T. P. Huang, K. A. Shorter, P. G. Adamczyk, and A. D. Kuo, “Mechanical and energetic consequences of reduced ankle plantar-flexion in human walking,” *J. Exp. Biol.*, vol. 218, no. Pt 22, pp. 3541–3550, Nov. 2015.
- [13] J. Zhang *et al.*, “Human-in-the-loop optimization of exoskeleton assistance during walking,” *Science (80-.)*, vol. 356, no. 6344, pp. 1280 LP – 1284, Jun. 2017.
- [14] S. H. Collins, M. B. Wiggin, and G. S. Sawicki, “Reducing the energy cost of human walking using an unpowered exoskeleton,” *Nature*, vol. 522, no. 7555, pp. 212–215, 2015.
- [15] Z. F. Lerner *et al.*, “An untethered ankle exoskeleton improves walking economy in a pilot study of individuals with cerebral palsy,” *IEEE Trans. Neural Syst. Rehabil. Eng.*, vol. 26, no. 10, pp. 1985–1993, 2018.
- [16] P. Antonellis, S. Galle, D. De Clercq, and P. Malcolm, “Altering gait variability with an ankle exoskeleton,” *PLoS One*, vol. 13, no. 10, p. e0205088, 2018.

- [17] G. S. Sawicki and D. P. Ferris, “Mechanics and energetics of level walking with powered ankle exoskeletons,” *J. Exp. Biol.*, vol. 211, no. Pt 9, pp. 1402–1413, May 2008.
- [18] I. McCarthy, T. Suzuki, N. Tyler, and C. Holloway, “Mobility in the built environment: Age-related changes in gait characteristics when walking on complex terrain,” *Heal. Aging Res.*, 2016.
- [19] M. R. Tucker *et al.*, “Control strategies for active lower extremity prosthetics and orthotics: a review,” *J. Neuroeng. Rehabil.*, vol. 12, p. 1, Jan. 2015.
- [20] V. Monaco *et al.*, “An ecologically-controlled exoskeleton can improve balance recovery after slippage,” *Sci. Rep.*, 2017.
- [21] M. Windrich, M. Grimmer, O. Christ, S. Rinderknecht, and P. Beckerle, “Active lower limb prosthetics: a systematic review of design issues and solutions,” *Biomed. Eng. Online*, vol. 15, no. Suppl 3, p. 140, Dec. 2016.
- [22] J. R. Koller, C. D. Remy, and D. P. Ferris, “Biomechanics and energetics of walking in powered ankle exoskeletons using myoelectric control versus mechanically intrinsic control,” *J. Neuroeng. Rehabil.*, vol. 15, no. 1, p. 42, 2018.
- [23] H. Huang, T. A. Kuiken, and R. D. Lipschutz, “A strategy for identifying locomotion modes using surface electromyography,” *IEEE Trans. Biomed. Eng.*, vol. 56, no. 1, pp. 65–73, Jan. 2009.
- [24] B. L. Davies and M. J. Kurz, “Children with cerebral palsy have greater stochastic features present in the variability of their gait kinematics,” *Res. Dev. Disabil.*, vol. 34, no. 11, pp. 3648–3653, 2013.
- [25] Z. F. Lerner, T. A. Harvey, and J. L. Lawson, “A Battery-Powered Ankle Exoskeleton Improves Gait Mechanics in a Feasibility Study of Individuals with Cerebral Palsy,” *Ann. Biomed. Eng.*, vol. 47, no. 6, 2019.
- [26] K. Rasske, D. G. Thelen, and J. R. Franz, “Variation in the human Achilles tendon moment arm during walking,” *Comput. Methods Biomech. Biomed. Engin.*, 2017.
- [27] F. Di Nardo, A. Mengarelli, E. Maranesi, L. Burattini, and S. Fioretti, “Assessment of the ankle muscle co-contraction during normal gait: A surface electromyography study,” *J. Electromyogr. Kinesiol.*, 2015.
- [28] T. L. Wickiewicz, R. R. Roy, P. L. Powell, and V. R. Edgerton, “Muscle architecture of the human lower limb,” *Clin. Orthop. Relat. Res.*, no. 179, pp. 275–283, Oct. 1983.
- [29] A. P. Hills, E. M. Hennig, M. McDonald, and O. Bar-Or, “Plantar pressure differences between obese and non-obese adults: a biomechanical analysis,” *Int. J. Obes. Relat. Metab. Disord. J. Int. Assoc. Study Obes.*, vol. 25, no. 11, pp. 1674–1679, Nov. 2001.
- [30] E. J. Luger, M. Nissan, A. Karpf, E. L. Steinberg, and S. Dekel, “Patterns of weight distribution under the metatarsal heads,” *J. Bone Joint Surg. Br.*, vol. 81, no. 2, pp. 199–202, Mar. 1999.
- [31] D. Quintero, D. J. Villarreal, D. J. Lambert, S. Kapp, and R. D. Gregg, “Continuous-Phase Control of a Powered Knee–Ankle Prosthesis: Amputee Experiments Across Speeds and Inclines,” *IEEE Trans. Robot.*, vol. 34, no. 3, pp. 686–701, 2018.
- [32] Z. F. Lerner, D. L. Damiano, and T. C. Bulea, “A lower-extremity exoskeleton improves knee extension in children with crouch gait from cerebral palsy,” *Sci. Transl. Med.*, vol. 9, no. 404, Aug. 2017.
- [33] M. F. Abel and D. L. Damiano, “Strategies for increasing walking speed in diplegic cerebral palsy,” *J. Pediatr. Orthop.*, vol. 16, no. 6, pp. 753–758, 1996.
- [34] D. L. Kowalk, J. A. Duncan, and C. L. Vaughan, “Abduction-adduction moments at the

- knee during stair ascent and descent,” *J. Biomech.*, vol. 29, no. 3, pp. 383–388, 1996.
- [35] G. Orekhov, Y. Fang, J. Luque, and Z. F. Lerner, “Ankle Exoskeleton Assistance Can Improve Over-Ground Walking Economy in Individuals with Cerebral Palsy,” *IEEE Trans. Neural Syst. Rehabil. Eng.*, vol. 28, no. 2, pp. 461–467, 2020.
- [36] S. L. Delp *et al.*, “OpenSim: Open-Source Software to Create and Analyze Dynamic Simulations of Movement,” *IEEE Trans. Biomed. Eng.*, vol. 54, no. 11, pp. 1940–1950, 2007.
- [37] L. M. Mooney and H. M. Herr, “Biomechanical walking mechanisms underlying the metabolic reduction caused by an autonomous exoskeleton,” *J. Neuroeng. Rehabil.*, 2016.
- [38] M. M. Mukaka, “Statistics corner: A guide to appropriate use of correlation coefficient in medical research.,” *Malawi Med. J.*, vol. 24, no. 3, pp. 69–71, Sep. 2012.
- [39] G. M. Gasparri, J. Luque, and Z. F. Lerner, “Proportional Joint-Moment Control for Instantaneously Adaptive Ankle Exoskeleton Assistance,” *IEEE Trans. Neural Syst. Rehabil. Eng.*, vol. 27, no. 4, pp. 751–759, 2019.
- [40] Z. F. Lerner, D. L. Damiano, and T. C. Bulea, “Estimating the Mechanical Behavior of the Knee Joint during Crouch Gait: Implications for Real-Time Motor Control of Robotic Knee Orthoses,” *IEEE Trans. Neural Syst. Rehabil. Eng.*, vol. 24, no. 6, 2016.
- [41] B. Chen, B. Zi, L. Qin, and Q. Pan, “State-of-the-art research in robotic hip exoskeletons: A general review,” *J. Orthop. Transl.*, vol. 20, pp. 4–13, 2020.
- [42] E. A. ANDERSSON, J. NILSSON, and A. THORSTENSSON, “Intramuscular EMG from the hip flexor muscles during human locomotion,” *Acta Physiol. Scand.*, vol. 161, no. 3, pp. 361–370, Oct. 1997.
- [43] P. William and R. Warwick, *Gray’s Anatomy*. New York, 1980.
- [44] W. Chen, S. Wu, T. Zhou, and C. Xiong, “On the biological mechanics and energetics of the hip joint muscle-tendon system assisted by passive hip exoskeleton.,” *Bioinspir. Biomim.*, vol. 14, no. 1, p. 16012, Dec. 2018.
- [45] G. S. Sawicki, O. N. Beck, I. Kang, and A. J. Young, “The exoskeleton expansion: improving walking and running economy,” *J. Neuroeng. Rehabil.*, vol. 17, no. 1, p. 25, 2020.
- [46] D. R. Patel, M. Neelakantan, K. Pandher, and J. Merrick, “Cerebral palsy in children: a clinical overview,” *Transl. Pediatr.*, vol. 9, no. Suppl 1, pp. S125–S135, Feb. 2020.
- [47] I. Hodgkinson, M. L. Jindrich, P. Duhaut, J. P. Vadot, G. Metton, and C. Bérard, “Hip pain in 234 non-ambulatory adolescents and young adults with cerebral palsy: a cross-sectional multicentre study.,” *Dev. Med. Child Neurol.*, vol. 43, no. 12, pp. 806–808, Dec. 2001.
- [48] Z. F. Lerner, D. L. Damiano, and T. C. Bulea, “A lower-extremity exoskeleton improves knee extension in children with crouch gait from cerebral palsy,” *Sci. Transl. Med.*, vol. 9, no. 404, Aug. 2017.
- [49] G. Orekhov, Y. Fang, J. Luque, and Z. F. Lerner, “Ankle Exoskeleton Assistance Can Improve Over-Ground Walking Economy in Individuals With Cerebral Palsy,” *IEEE Trans. Neural Syst. Rehabil. Eng.*, vol. 28, no. 2, pp. 461–467, 2020.
- [50] L. R. Bunge *et al.*, “Effectiveness of powered exoskeleton use on gait in individuals with cerebral palsy: A systematic review,” *PLoS One*, vol. 16, no. 5, p. e0252193, May 2021.
- [51] C. Buesing *et al.*, “Effects of a wearable exoskeleton stride management assist system (SMA®) on spatiotemporal gait characteristics in individuals after stroke: a randomized controlled trial.,” *J. Neuroeng. Rehabil.*, vol. 12, p. 69, Aug. 2015.
- [52] Y. Lee *et al.*, “A flexible exoskeleton for hip assistance,” in *2017 IEEE/RSJ International*

- Conference on Intelligent Robots and Systems (IROS)*, 2017, pp. 1058–1063.
- [53] A. T. Asbeck, K. Schmidt, and C. J. Walsh, “Soft exosuit for hip assistance,” *Rob. Auton. Syst.*, vol. 73, pp. 102–110, 2015.
- [54] Q. Wu, X. Wang, F. Du, and X. Zhang, “Design and Control of a Powered Hip Exoskeleton for Walking Assistance Regular Paper,” *Int. J. Adv. Robot. Syst.*, 2015.
- [55] F. Giovacchini *et al.*, “A light-weight active orthosis for hip movement assistance,” *Rob. Auton. Syst.*, vol. 73, pp. 123–134, 2015.
- [56] D. Singh, “Adaptive significance of female physical attractiveness: role of waist-to-hip ratio.,” *J. Pers. Soc. Psychol.*, vol. 65, no. 2, pp. 293–307, Aug. 1993.
- [57] B. Lim *et al.*, “Delayed Output Feedback Control for Gait Assistance With a Robotic Hip Exoskeleton,” *IEEE Trans. Robot.*, vol. 35, no. 4, pp. 1055–1062, 2019.
- [58] K. Seo, J. Lee, Y. Lee, T. Ha, and Y. Shim, “Fully autonomous hip exoskeleton saves metabolic cost of walking,” in *2016 IEEE International Conference on Robotics and Automation (ICRA)*, 2016, pp. 4628–4635.
- [59] D.-S. Kim *et al.*, “A wearable hip-assist robot reduces the cardiopulmonary metabolic energy expenditure during stair ascent in elderly adults: a pilot cross-sectional study.,” *BMC Geriatr.*, vol. 18, no. 1, p. 230, Sep. 2018.
- [60] H.-J. Lee *et al.*, “A Wearable Hip Assist Robot Can Improve Gait Function and Cardiopulmonary Metabolic Efficiency in Elderly Adults.,” *IEEE Trans. neural Syst. Rehabil. Eng. a Publ. IEEE Eng. Med. Biol. Soc.*, vol. 25, no. 9, pp. 1549–1557, Sep. 2017.
- [61] L. Grazi *et al.*, “Gastrocnemius myoelectric control of a robotic hip exoskeleton,” in *2015 37th Annual International Conference of the IEEE Engineering in Medicine and Biology Society (EMBC)*, 2015, pp. 3881–3884.
- [62] J. Masood, J. Ortiz, J. Fernández, L. A. Mateos, and D. G. Caldwell, “Mechanical design and analysis of light weight hip joint Parallel Elastic Actuator for industrial exoskeleton,” in *2016 6th IEEE International Conference on Biomedical Robotics and Biomechanics (BioRob)*, 2016, pp. 631–636.
- [63] K. Seo, J. Lee, and Y. J. Park, “Autonomous hip exoskeleton saves metabolic cost of walking uphill,” in *2017 International Conference on Rehabilitation Robotics (ICORR)*, 2017, pp. 246–251.
- [64] S. S. P. A. Bishe, T. Nguyen, Y. Fang, and Z. F. Lerner, “Adaptive Ankle Exoskeleton Control: Validation Across Diverse Walking Conditions,” *IEEE Trans. Med. Robot. Bionics*, vol. 3, no. 3, pp. 801–812, 2021.
- [65] D. S. Miomir Vukobratović, Branislav Arso Borovac, Dušan Surla, *Biped Locomotion: Dynamics, Stability, Control and Application - Miomir Vukobratovic, Branislav Borovac, Dusan Surla, Dragan Stokic - Google Books*. Springer-Verlag, 1990.
- [66] A. Joseph, “Robotic Exoskeletons Show Promise As Tool to Help Kids with Cerebral Palsy Walk Easier - Scientific American.” [Online]. Available: <https://www.scientificamerican.com/article/robotic-exoskeletons-show-promise-as-tool-to-help-kids-with-cerebral-palsy-walk-easier/>. [Accessed: 16-Nov-2019].
- [67] M. C. Carrozza, S. Micera, and J. L. Pons, Eds., *Wearable Robotics: Challenges and Trends*. Springer International Publishing, 2019.
- [68] J. Rosen and P. W. Ferguson, Eds., *Wearable Robotics: Systems and Applications*. Mara Conner, 2020.
- [69] L. Wang and T. S. Buchanan, “Prediction of joint moments using a neural network model of muscle activations from EMG signals,” *IEEE Trans. Neural Syst. Rehabil. Eng.*, vol. 10,

- no. 1, pp. 30–37, 2002.
- [70] T. Uchiyama, T. Bessho, and K. Akazawa, “Static torque–angle relation of human elbow joint estimated with artificial neural network technique,” *J. Biomech.*, vol. 31, no. 6, pp. 545–554, 1998.
- [71] M. M. Ardestani *et al.*, “Human lower extremity joint moment prediction: A wavelet neural network approach,” *Expert Syst. Appl.*, vol. 41, no. 9, pp. 4422–4433, 2014.
- [72] J.-J. Luh, G.-C. Chang, C.-K. Cheng, J.-S. Lai, and T.-S. Kuo, “Isokinetic elbow joint torques estimation from surface EMG and joint kinematic data: using an artificial neural network model,” *J. Electromyogr. Kinesiol.*, vol. 9, no. 3, pp. 173–183, 1999.
- [73] L.-C. TSAI, P. M. COLLETTI, and C. M. POWERS, “Magnetic Resonance Imaging–Measured Muscle Parameters Improved Knee Moment Prediction of an EMG-Driven Model,” *Med. Sci. Sport. Exerc.*, vol. 44, no. 2, 2012.
- [74] J. CHEN, X. ZHANG, L. GU, and C. NELSON, “ESTIMATING MUSCLE FORCES AND KNEE JOINT TORQUE USING SURFACE ELECTROMYOGRAPHY: A MUSCULOSKELETAL BIOMECHANICAL MODEL,” *J. Mech. Med. Biol.*, vol. 17, no. 04, p. 1750069, Mar. 2017.
- [75] M. Sartori, M. Reggiani, D. Farina, and D. G. Lloyd, “EMG-driven forward-dynamic estimation of muscle force and joint moment about multiple degrees of freedom in the human lower extremity,” *PLoS One*, vol. 7, no. 12, 2012.
- [76] Q. Ding, X. Zhao, A. Xiong, and J. Han, “A Novel Motion Estimate Method of Human Joint with EMG-Driven Model,” in *2011 5th International Conference on Bioinformatics and Biomedical Engineering*, 2011, pp. 1–5.
- [77] T. Liu, Y. Inoue, K. Shibata, and K. Shiojima, “A Mobile Force Plate and Three-Dimensional Motion Analysis System for Three-Dimensional Gait Assessment,” *IEEE Sens. J.*, vol. 12, no. 5, pp. 1461–1467, 2012.
- [78] A. Forner Cordero, H. J. F. M. Koopman, and F. C. T. van der Helm, “Use of pressure insoles to calculate the complete ground reaction forces,” *J. Biomech.*, vol. 37, no. 9, pp. 1427–1432, Sep. 2004.
- [79] D. A. Jacobs and D. P. Ferris, “Estimation of ground reaction forces and ankle moment with multiple, low-cost sensors,” *J. Neuroeng. Rehabil.*, vol. 12, p. 90, Oct. 2015.
- [80] S. K. Clark, “A BRIEF-HISTORY OF TIRE ROLLING RESISTANCE,” in *RUBBER CHEMISTRY AND TECHNOLOGY*, 1983, vol. 56, no. 2, pp. 494–495.
- [81] H. B. Pacejka, “Chapter 9 - Short Wavelength Intermediate Frequency Tire Model,” H. B. Pacejka, Ed. Oxford: Butterworth-Heinemann, 2012, pp. 403–474.
- [82] R. Jiménez-Fabián and O. Verlinden, “Review of control algorithms for robotic ankle systems in lower-limb orthoses, prostheses, and exoskeletons,” *Med. Eng. Phys.*, vol. 34, no. 4, pp. 397–408, 2012.
- [83] R. R. Neptune, S. A. Kautz, and F. E. Zajac, “Contributions of the individual ankle plantar flexors to support, forward progression and swing initiation during walking,” *J. Biomech.*, vol. 34, no. 11, pp. 1387–1398, Nov. 2001.
- [84] S. Nadeau, D. Gravel, A. B. Arsénault, and D. Bourbonnais, “Plantarflexor weakness as a limiting factor of gait speed in stroke subjects and the compensating role of hip flexors,” *Clin. Biomech.*, vol. 14, no. 2, pp. 125–135, Feb. 1999.
- [85] A. M. Dollar and H. Herr, “Lower Extremity Exoskeletons and Active Orthoses: Challenges and State-of-the-Art,” *IEEE Trans. Robot.*, vol. 24, no. 1, pp. 144–158, 2008.

- [86] M. Lars, *Sagittal plane characterization of normal human ankle function across a range of walking gait speeds*. 2018.
- [87] A. M. Oymagil, J. K. Hitt, T. Sugar, and J. Fleeger, "Control of a Regenerative Braking Powered Ankle Foot Orthosis," in *2007 IEEE 10th International Conference on Rehabilitation Robotics*, 2007, pp. 28–34.
- [88] J. Hitt, A. M. Oymagil, T. Sugar, K. Hollander, A. Boehler, and J. Fleeger, "Dynamically Controlled Ankle-Foot Orthosis (DCO) with Regenerative Kinetics: Incrementally Attaining User Portability," in *Proceedings 2007 IEEE International Conference on Robotics and Automation*, 2007, pp. 1541–1546.
- [89] M. A. Holgate, A. W. Bohler, and T. G. Suga, "Control algorithms for ankle robots: A reflection on the state-of-the-art and presentation of two novel algorithms," in *2008 2nd IEEE RAS & EMBS International Conference on Biomedical Robotics and Biomechatronics*, 2008, pp. 97–102.
- [90] R. Lu, Z. Li, C. Su, and A. Xue, "Development and Learning Control of a Human Limb With a Rehabilitation Exoskeleton," *IEEE Trans. Ind. Electron.*, vol. 61, no. 7, pp. 3776–3785, 2014.
- [91] K. W. Hollander and T. G. Sugar, "A Robust Control Concept for Robotic Ankle Gait Assistance," in *2007 IEEE 10th International Conference on Rehabilitation Robotics*, 2007, pp. 119–123.
- [92] F. Sup, A. Bohara, and M. Goldfarb, "Design and Control of a Powered Transfemoral Prosthesis," *Int. J. Rob. Res.*, vol. 27, no. 2, pp. 263–273, Feb. 2008.
- [93] H. NAITO, Y. AKAZAWA, K. TAGAYA, T. MATSUMOTO, and M. TANAKA, "An Ankle-Foot Orthosis with a Variable-Resistance Ankle Joint Using a Magnetorheological-Fluid Rotary Damper," *J. Biomech. Sci. Eng.*, vol. 4, pp. 182–191, Jan. 2009.
- [94] M. F. Eilenberg, H. Geyer, and H. Herr, "Control of a Powered Ankle-Foot Prosthesis Based on a Neuromuscular Model," *IEEE Trans. Neural Syst. Rehabil. Eng.*, vol. 18, no. 2, pp. 164–173, 2010.
- [95] D. Ao, R. Song, and J. Gao, "Movement Performance of Human-Robot Cooperation Control Based on EMG-Driven Hill-Type and Proportional Models for an Ankle Power-Assist Exoskeleton Robot.," *IEEE Trans. Neural Syst. Rehabil. Eng.*, vol. 25, no. 8, pp. 1125–1134, Aug. 2017.
- [96] N. Thatte and H. Geyer, "Toward Balance Recovery With Leg Prostheses Using Neuromuscular Model Control.," *IEEE Trans. Biomed. Eng.*, vol. 63, no. 5, pp. 904–913, May 2016.
- [97] D. P. Ferris, J. M. Czerniecki, and B. Hannaford, "An ankle-foot orthosis powered by artificial pneumatic muscles," *J. Appl. Biomech.*, vol. 21, no. 2, pp. 189–197, May 2005.
- [98] S. Au, M. Berniker, and H. Herr, "Powered ankle-foot prosthesis to assist level-ground and stair-descent gaits.," *Neural Netw.*, vol. 21, no. 4, pp. 654–666, May 2008.
- [99] H. Kawamoto and Y. Sankai, "Power Assist System HAL-3 for Gait Disorder Person," in *Proceedings of the 8th International Conference on Computers Helping People with Special Needs*, 2002, pp. 196–203.
- [100] C. Fleischer, C. Reinicke, and G. Hommel, "Predicting the intended motion with EMG signals for an exoskeleton orthosis controller," in *2005 IEEE/RSJ International Conference on Intelligent Robots and Systems*, 2005, pp. 2029–2034.
- [101] H. A. Varol and M. Goldfarb, "Real-time Intent Recognition for a Powered Knee and Ankle Transfemoral Prosthesis," in *2007 IEEE 10th International Conference on Rehabilitation*

- Robotics*, 2007, pp. 16–23.
- [102] H. A. Varol, F. Sup, and M. Goldfarb, “Powered Sit-to-Stand and Assistive Stand-to-Sit Framework for a Powered Transfemoral Prosthesis.,” *IEEE Int. Conf. Rehabil. Robot.*, vol. 5209582, pp. 645–651, 2009.
- [103] H. Kazerooni, *The Berkeley Lower Extremity Exoskeleton Project*, vol. 21. 2004.
- [104] D. Popovic and T. Sinkjær, “Improved Control for Functional Electrical Stimulation to Restore Walking,” *Hong Kong Physiother. J.*, vol. 18, no. 1, pp. 12–20, 2000.
- [105] N. Costa and D. G. Caldwell, “Control of a Biomimetic ‘Soft-actuated’ 10DoF Lower Body Exoskeleton,” in *The First IEEE/RAS-EMBS International Conference on Biomedical Robotics and Biomechatronics, 2006. BioRob 2006.*, 2006, pp. 495–501.
- [106] K. E. Gordon, G. S. Sawicki, and D. P. Ferris, “Mechanical performance of artificial pneumatic muscles to power an ankle-foot orthosis.,” *J. Biomech.*, vol. 39, no. 10, pp. 1832–1841, 2006.
- [107] J. Rosen, M. B. Fuchs, and M. Arcan, “Performances of hill-type and neural network muscle models - Toward a myosignal-based exoskeleton,” *Comput. Biomed. Res.*, vol. 32, no. 5, pp. 415–439, 1999.
- [108] G. I. Zahalak, “A distribution-moment approximation for kinetic theories of muscular contraction,” *Math. Biosci.*, vol. 55, no. 1–2, pp. 89–114, 1981.
- [109] K. C. Nishikawa, J. A. Monroy, T. E. Uyeno, S. H. Yeo, D. K. Pai, and S. L. Lindstedt, “Is titin a ‘winding filament’? A new twist on muscle contraction,” *Proc. R. Soc. B Biol. Sci.*, vol. 279, no. 1730, pp. 981–990, 2012.
- [110] K. C. Nishikawa, J. A. Monroy, T. E. Uyeno, S. H. Yeo, D. K. Pai, and S. L. Lindstedt, “Is titin a ‘winding filament’? A new twist on muscle contraction.,” *Proceedings. Biol. Sci.*, vol. 279, no. 1730, pp. 981–90, Mar. 2012.
- [111] S. K. Au, P. Bonato, and H. Herr, “An EMG-position controlled system for an active ankle-foot prosthesis: an initial experimental study,” in *9th International Conference on Rehabilitation Robotics, 2005. ICORR 2005.*, 2005, pp. 375–379.
- [112] U. Tahir *et al.*, “Case Study: A Bio-Inspired Control Algorithm for a Robotic Foot-Ankle Prosthesis Provides Adaptive Control of Level Walking and Stair Ascent ,” *Frontiers in Robotics and AI* , vol. 5. p. 36, 2018.
- [113] E. M. Arnold, S. R. Ward, R. L. Lieber, and S. L. Delp, “A model of the lower limb for analysis of human movement.,” *Ann. Biomed. Eng.*, vol. 38, no. 2, pp. 269–279, Feb. 2010.
- [114] J. R. Baxter, T. A. Novack, H. Van Werkhoven, D. R. Pennell, and S. J. Piazza, “Ankle joint mechanics and foot proportions differ between human sprinters and non-sprinters.,” *Proceedings. Biol. Sci.*, vol. 279, no. 1735, pp. 2018–2024, May 2012.
- [115] H. Hoppeler and M. Flück, “Normal mammalian skeletal muscle and its phenotypic plasticity,” *J. Exp. Biol.*, vol. 205, no. 15, pp. 2143 LP – 2152, Aug. 2002.
- [116] T. Fukunaga *et al.*, “Physiological cross-sectional area of human leg muscles based on magnetic resonance imaging.,” *J. Orthop. Res.*, vol. 10, no. 6, pp. 928–934, Nov. 1992.
- [117] C. N. Maganaris and J. P. Paul, “In vivo human tendon mechanical properties.,” *J. Physiol.*, vol. 521 Pt 1, pp. 307–313, Nov. 1999.
- [118] D. J. Haight, Z. F. Lerner, W. J. Board, and R. C. Browning, “A comparison of slow, uphill and fast, level walking on lower extremity biomechanics and tibiofemoral joint loading in obese and nonobese adults.,” *J. Orthop. Res.*, vol. 32, no. 2, pp. 324–330, Feb. 2014.
- [119] C. N. Maganaris, V. Baltzopoulos, and A. J. Sargeant, “Changes in the tibialis anterior tendon moment arm from rest to maximum isometric dorsiflexion: in vivo obfile:///G:/My

Drive/WFM/Some papers/S0268003399000182.riservations in man,” *Clin. Biomech.*, vol. 14, no. 9, pp. 661–666, 1999.